Lawrence Berkeley National Laboratory
Recent Work

Title
Electronic Processes in Uniaxially Stressed p-Type Germanium

Permalink
https://escholarship.org/uc/item/7z38v6th

Author
Dubon Jr., O.D.

Publication Date
1996-02-06

eScholarship.org Powered by the California Digital Library
University of California

LBL-38287
UC-404

Lawrence Berkeley Laboratory
UNIVERSITY OF CALIFORNIA

Engineering Division

Electronic Processes in Uniaxially Stressed *p*-Type Germanium

O.D. Dubon, Jr.
(Ph.D. Thesis)

February 1996

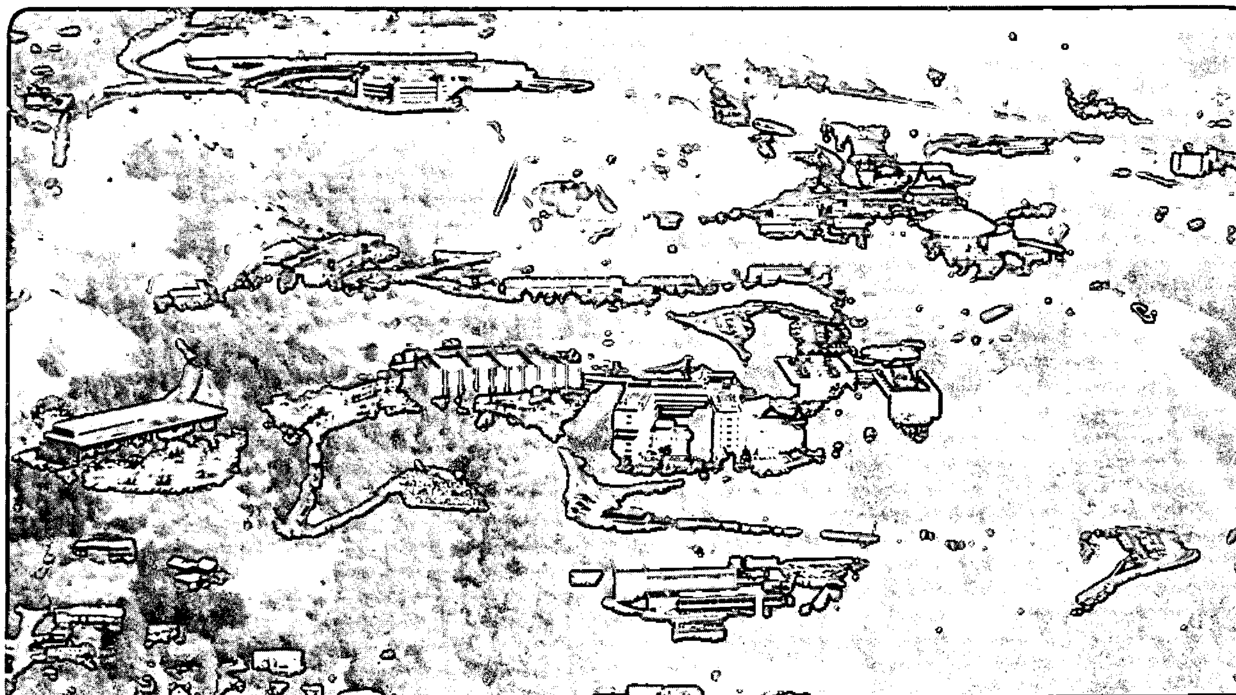

REFERENCE COPY
Does Not
Circulate
Bldg. 50 Library.
LBL-38287
Copy 1

Prepared for the U.S. Department of Energy under Contract Number DE-AC03-76SF00098

DISCLAIMER

This document was prepared as an account of work sponsored by the United States Government. While this document is believed to contain correct information, neither the United States Government nor any agency thereof, nor the Regents of the University of California, nor any of their employees, makes any warranty, express or implied, or assumes any legal responsibility for the accuracy, completeness, or usefulness of any information, apparatus, product, or process disclosed, or represents that its use would not infringe privately owned rights. Reference herein to any specific commercial product, process, or service by its trade name, trademark, manufacturer, or otherwise, does not necessarily constitute or imply its endorsement, recommendation, or favoring by the United States Government or any agency thereof, or the Regents of the University of California. The views and opinions of authors expressed herein do not necessarily state or reflect those of the United States Government or any agency thereof or the Regents of the University of California.

LBL-38287
UC-404

Electronic Processes in Uniaxially Stressed *p*-Type Germanium

Oscar Danilo Dubon, Jr.

Department of Engineering
University of California, Berkeley

and

Engineering Division
Ernest Orlando Lawrence Berkeley National Laboratory
University of California
Berkeley, California 94720

February 1996

This work was supported by the Director, Office of Energy Research, Office of Basic Energy Sciences, Materials Sciences Division, of the U.S. Department of Energy under Contract No. DE-AC03-76SF00098.

Electronic Processes in Uniaxially Stressed *p*-Type Germanium

by

Oscar Danilo Dubon, Jr.

B.S. (University of California at Los Angeles) 1989

M.S. (University of California at Berkeley) 1992

A dissertation submitted in partial satisfaction of the
requirements for the degree of
Doctor of Philosophy
in
Engineering-
Materials Science and Mineral Engineering
in the
GRADUATE DIVISION
of the
UNIVERSITY of CALIFORNIA at BERKELEY

Committee in Charge:

Professor Eugene E. Haller, Chair
Professor Eicke R. Weber
Professor Peter Y. Yu

1996

Electronic Processes in Uniaxially Stressed *p*-Type Germanium

Copyright © 1996

by

Oscar Danilo Dubon, Jr.

The U.S. Department of Energy has the right to use this document
for any purpose whatsoever including the right to reproduce
all or any part thereof

Abstract

Electronic Processes in Uniaxially Stressed *p*-type Germanium

by

Oscar Danilo Dubon, Jr.

Doctor of Philosophy in Engineering-

Materials Science and Mineral Engineering

University of California at Berkeley

Professor Eugene E. Haller, Chair

The effect of uniaxial stress on acceptor-related electronic processes in germanium single crystals doped with Ga, Be, and Cu have been studied by Hall and photo-Hall effect measurements in conjunction with infrared spectroscopy. Uniaxial stress perturbs the germanium crystal structure deforming the valence band edge and therefore affecting materials properties that influence hole transport. These include pressure-induced changes in the free hole lifetime and in the electronic structure of multivalent acceptors. Developing a better understanding of these fundamental properties is important in furthering our knowledge of electronic processes in semiconductors affecting the performance of germanium infrared detectors.

The stress dependence of the hole lifetime in p-type germanium single crystals is used as a test for competing models of the non-radiative capture of holes by acceptors. The hole lifetime is a key factor determining detector performance, and it depends on the physical mechanism by which the holes are captured. It is shown by photo-Hall measurements that the hole lifetime in Ga- and Be-doped Ge single crystals increases by over one order of magnitude upon the application of uniaxial stress at liquid helium temperatures. Photo-Hall measurements of Ge:Be crystals have shown a stress-induced change in

the temperature dependence of the hole lifetime as well. These results are consistent with the observed increase of the responsivity of Ge:Ga detectors when uniaxial stress is applied. The data are discussed within the framework of the well known cascade capture model and the recently proposed direct capture model.

The electronic properties of germanium doped with the copper triple acceptor are shown to change dramatically by the application of uniaxial stress. The three-hole nature of the neutral copper ground-state results in a variety of phenomena that are interesting and important. Upon the application of uniaxial stress, the threshold of the photoconductivity response shifts to lower energies achieving a nearly constant value of 17 meV above 4 kbar. A variational calculation shows that this behavior is caused by a change in the copper ground-state configuration from a pseudo Li^0, $(1s)^3$-like to a normal Li^0, $(1s)^2(2s)^1$-like configuration having a stress-insensitive hole binding energy. This ground-state transformation produces a tremendous decrease in the electrical resistivity of many orders of magnitude that is attributed to the stress-induced onset of impurity band conduction due to the extended nature of the *2s*-like electron wavefunctions of the $(1s)^2(2s)^1$ high-pressure configuration. A simple calculation shows that an insulator-metal (Mott-Hubbard-Anderson) transition should occur in uniaxially stressed Ge having a copper concentration in the 10^{15} cm^{-3} range. These results provide a first explanation for the performance of uniaxially stressed, copper-diffused Ge:Ga detectors which display a high conductivity in the absence of a photon signal and consequently have poor sensitivity.

Table of Contents

Acknowledgments

1. Introduction 1

1.1 Impurity states in germanium 3

1.2 Aspects of unstressed and uniaxially stressed p-Ge 4

1.3 Photoconductive detectors: figures of merit 7

2. Uniaxially stressed germanium doped with monovalent acceptors 11

2.1 Capture cross sections in unstressed p-Ge 16

2.2 Capture cross sections in stressed p-Ge: m^* dependence 19

2.2.1 Introduction 19

2.2.2 Experimental approach and results 21

2.3 A second look at the experimental capture cross sections 30

2.4 A final comment Ge:Ga stressed detectors 33

3. Uniaxially stressed germanium doped with divalent acceptors 34

3.1 Characteristics of Be-doped Ge: Be^+ centers 34

3.2 Characteristics of Ge:Be detectors 38

3.3 Hall and photo-Hall measurements of Ge:Be 41

3.4 Analysis of the photo-Hall data 44

3.5 Effective-mass dependence of the capture cross section in Ge:Be 46

3.6 A final comment Ge:Be stressed detectors 48

4. Uniaxially stressed germanium doped with the copper triple acceptor 49
4.1 Copper in germanium 49
4.2 Germanium IR detectors containing copper 51
4.3 Spectroscopy of uniaxially stressed copper doped germanium 55
4.4 Electronic conduction in doped semiconductors 66
4.5 Electronic conduction in uniaxially stressed Cu-doped Ge 69
4.5.1 Experimental approach and results 70
4.5.2 Hopping conduction in Ge:Cu 74
4.5.3 ε_2 conduction in doped semiconductors 77
4.5.4 ε_2 conduction in uniaxially stressed Cu-doped Ge 82
4.5.5 Hall effect measurements of uniaxially stressed Ge:Cu 83
4.5.6 Summary of electrical measurements 92

5. Conclusions 94

6. Future Work 96

7. Appendices 97
Appendix A: Hall effect and photo-Hall effect measurements 97
Appendix B: Aspects of photoconductivity measurements and IR spectroscopy 112

Appendix C: Effective mass approximation for Cu impurities in Ge 119

8. References 127

Acknowledgments

I would like to thank Professor Eugene Haller for his invaluable support and for giving me the opportunity of conducting research on my own terms and the guidance when this was not such a good idea. I would also like to thank Professors Eicke Weber and Peter Yu for reviewing this thesis.

The contribution of many scholars has been significant in my education at Berkeley. I am grateful to Dr. Wladek Walukiewicz for being open to countless discussions not always related to science. I am fortunate to have had the opportunity to work with Professor Leo Falicov, an inspiring figure who is deeply missed. Dr. Ingrid Wilke, Dr. Chumin Wang and Dr. Heinz Fuchs have made significant contributions to portions of the work presented in this thesis. My collaborations with Dr. Erik Bründermann, Angela Linhart, Dr. Gilles Sirmain, and Dr. Lothar Reichertz have yielded many exciting results on p-Ge lasers. More importantly these professional relationships have yielded good friendships.

I am deeply grateful to the graduate students, the postdocs, Stefan, and the staff members with whom I have had the privilege of working. Their thoughtfulness both at a professional and personal level is forever appreciated. I would in particular like to thank Kohei and Amy for their advice, encouragement and friendship and Jeff Beeman for his technical and moral support.

Beyond my colleagues at LBNL, many thanks go to Tim, Mark, John, John, and Carl. I am very grateful to Nancy for being a constant source of inspiration, to Marvin for his patience, and to Lisa for her loving companionship.

Finally, words cannot express the significance of the constant support and encouragement that I have received from my family, especially my parents. It is through their sacrifice and effort that I have been able to pursue my goals.

This work was supported by the Director, Office of Energy Research, Materials Sciences Division, of the U.S. Department of Energy under Contract No. DE-AC03-76SF00098.

1. Introduction

The detection of infrared (IR) radiation (1 μm-1 mm or equivalently 1.2-0.0012 eV) is of great interest to a wide variety of research activities including the characterization of defects in semiconductors, the study of the Earth's atmosphere, and the observation of IR sources in the universe. This has produced a demand for highly sensitive IR detectors and has led to the wide use of semiconductors such as Ge, PbS, and HgCdTe for IR detection due to their photoconductive characteristics. Semiconductors are photoconductors because they can exhibit an increase in electrical conductivity upon absorbing light.

Germanium is a group IV semiconductor. Doped germanium is well suited for the detection of IR radiation (10-200 μm).[1-4] Group III elements such as B, Al, and Ga are single acceptors in Ge and in their neutral state bind a hole with an energy of 11 meV. Neutral double acceptors such as Be, Cd, and Hg bind holes with an energy in the range 25-100 meV depending on the element. Copper is a triple acceptor in Ge and in its neutral state binds holes with an energy of 43.2 meV. At liquid helium temperature essentially all holes are bound by the acceptors since the thermal energy is insufficient to excite them into the valence band. Therefore, if photons with energy equal to or greater than the hole binding energy are incident on a germanium detector, they will produce an increase in the electrical conductivity since holes are photoexcited from a bound acceptor energy state to the valence band. With an external bias these excess holes form a signal current (Figue 1.1).

Uniaxially stressed gallium-doped germanium detectors are unsurpassed in performance for the detection of far infrared (FIR) radiation in the 100-200 μm (6-12 meV) range under low photon backgrounds.[5,6] The

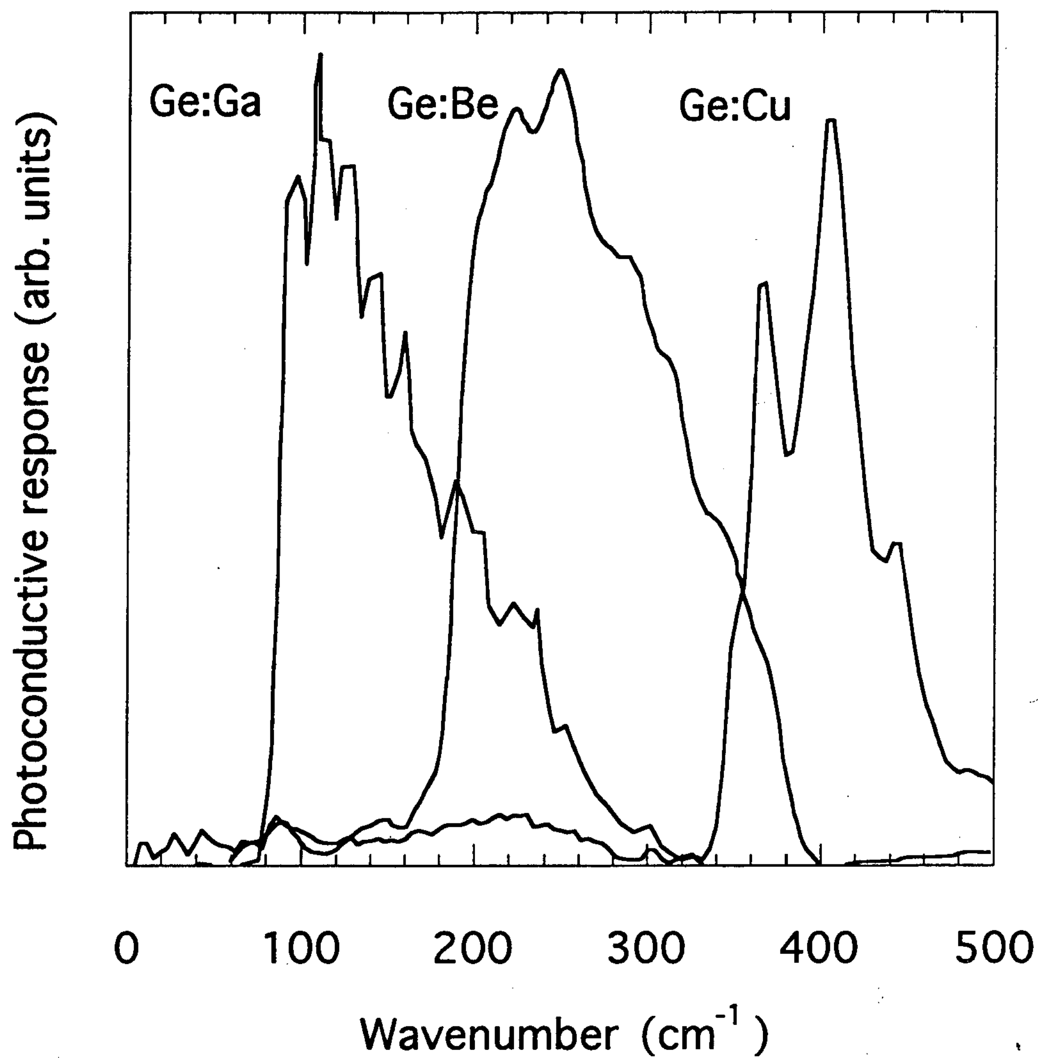

Figure 1.1. Spectral response for Ge:Ga, Ge:Be, Ge:Cu (T=4.2 K and 0.2 mm-thick black polyethylene used as cold filter). Dips in the Ge:Cu spectrum are due to absorption arising from optically active multiphonon modes. Some absorption features are caused by the black polyethylene filter, the mylar beamsplitter, and Fabry-Perot interference within the sample.

application of uniaxial stress perturbs the germanium crystal structure deforming the valence band edge,[7,8] reducing the hole binding energy of group III acceptors from 11 meV to as low as 6 meV,[9,10] and therefore extending the spectral sensitivity of Ge:Ga detectors to lower photon energies.[5,6] Deformation of the valence band affects other materials properties that influence free hole transport and detector performance.[8,9,11,12] In this work I have used standard Hall and photo-Hall effect measurements and infrared spectroscopy to study the effect of uniaxial stress on acceptor-related electronic processes in germanium single crystals doped with Ga, Be and Cu including pressure-induced changes in the free hole lifetime and in the electronic nature of multivalent acceptors. Developing a better understanding of these fundamental properties provides a framework for furthering our knowledge and advancing the technology of stressed detectors.

1.1 Impurity states in germanium

Effective mass theory successfully describes the general spectroscopic nature of shallow impurities in semiconductors.[12,13] Monovalent dopants such as gallium in germanium produce energy states related to the binding of a single charge carrier by a Coulombically attractive center in a dielectric medium. The atomic analog to this system is the hydrogen atom. The binding energy E and Bohr radius a_B associated with the hydrogen atom can be scaled to adequately describe the energies and radii associated with group III acceptors and group V donors in germanium:

$$E = -\frac{13.6\, m_H}{\varepsilon_r^2\, m_0}\ \text{eV} \quad \text{and} \quad a_B = \frac{0.53\, \varepsilon_r\, m_0}{m_H}\ \text{Å}$$

where m_H is the hydrogenic effective mass (equal to $0.2m_0$ in the case of holes in Ge), ε_r is the relative dielectric constant which is equal to 16 for germanium, and m_0 is the free electron mass. The semiconductor dielectric constant

accounts for the screening of the dopant nuclei by the electron cloud of the host atoms while the effective mass accounts for the difference in the motion of charge carriers (electrons and holes) in energy bands versus free space. Such values for Ge yield a binding energy and Bohr radius of 11 meV and 40 Å, respectively.

Double acceptors such as beryllium in germanium also have an atomic analog: the He atom. As in the case of the He atom, approximation techniques must be used to calculate the binding energies of these centers.[14,15] However, such calculations can be and have been made for He whereby only scaling by the effective mass and relative dielectric constant is necessary in order to arrive at adequate values for dopants. This has been performed for Be in Ge; a variational calculation yields a first ionization potential (i.e., hole binding energy by neutral Be) of 24.5 meV compared to the experimentally observed value of 24.8 meV.[14]

Acceptors binding a third hole including Be^+ and copper, a substitutional triple acceptor, do not have a direct atomic analog. The fourfold degeneracy at the valence-band edge of Ge and most other cubic semiconductors allows for the accommodation of up to four holes in the *1s* lowest one-particle level of these acceptors, which would be equivalent in the atomic framework to having electrons with a pseudospin of 3/2. Variational calculations have shown that, indeed, the analog of Be^+ is a pseudo He^- ion having electrons of hypothetical spin 3/2 and a $(1s)^3$ ground-state configuration.

1.2 Aspects of unstressed and uniaxially stressed p-Ge

The application of uniaxial stress breaks the fourfold degeneracy of the valence band edge leaving two, (time-reversal) doubly degenerate, split bands

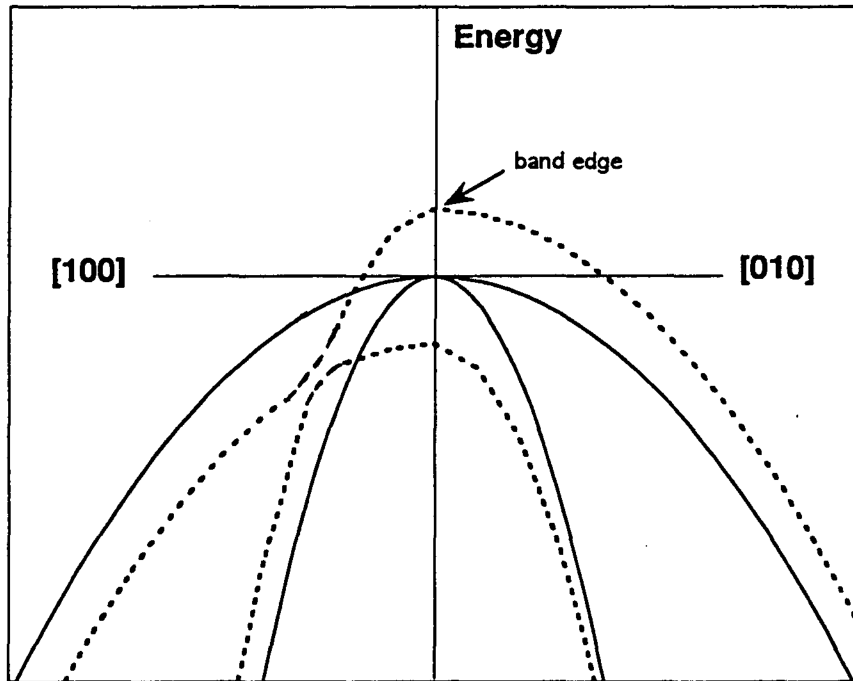

Figure 1.2. Schematic of valence band for zero-stress (solid lines) and uniaxially stressed (dashed lines) conditions. The figure is drawn for compressive stress in the [100] direction. The deformed band which thermally excited holes populated a low T is labeled "band edge." It has a density of states effective mass give by $m^*=(m_{[100]}m_{[010]}m_{[001]})^{1/3}$ where $m_{[100]}=0.046m_0$ and $m_{[010]}=m_{[001]}= 0.011m_0$, and $m^*=0.082m_0$ in the high stress limit.[7,8] The spin-orbit split-off band is not shown. At zero stress its maximum lies about 300 meV below the valence band edge.

in addition to the spin-orbit split-off band which remains doubly degenerate as well (Fig. 1.2). In the limit of high compressive uniaxial stress, the constant energy surface near the band minimum which the holes populate at low temperature is an ellipsoid having an average (density of states) m^* equal to $0.082m_0$ compared to its zero-stress value of $0.36m_0$.[7,16] (Note: the zero-stress values of m^* and m_H differ due to the degeneracy of the heavy- and light-hole bands at the valence band edge.) Therefore, stress can be used to change the magnitude of the hole effective mass as m^* is inversely proportional to the curvature of the valence band at the band minimum. Clearly, a consequence of this is that all properties exhibiting an effective mass dependence will show a pressure dependence. Two major properties are the hole mobility and as already mentioned the ionization energies of acceptors.

The mobility is a measure of the drift velocity v_d that free carriers (electrons and holes) attain upon being subjected to an electric field E:

$$v_d = \mu E \tag{1.1}$$

The magnitude of μ is limited by the different scattering processes that the carriers undergo including scattering by ionized and neutral impurities and by phonons and can generally be approximated by the relation[17]

$$\mu^{-1} \approx (\mu_{ac})^{-1} + (\mu_{ni})^{-1} + (\mu_{ii})^{-1} \tag{1.2}$$

where μ_{ac}, μ_{ni}, and μ_{ii} are the mobilities associated with scattering by acoustic phonons, neutral impurities and ionized impurities, respectively. Optical phonons can also scatter electrons and holes at higher temperatures but do not contribute at detector operating temperatures. Impurity and phonon scattering in semiconductors have been extensively studied and formulations for the different contributions are well established. For p-type Ge at zero stress, $\mu_{ac} \approx 2.4 \times 10^7 T^{-1.5}$, $\mu_{ni} \approx 9 \times 10^{20} (m_H/m_0) N_{ni}^{-1}$ and $\mu_{ii} \approx 1.2 \times 10^{17} T^{1.5} (m_0/m^*) N_{ii}^{-1}$ all in units of cm^2/Vs.[18-20] N_{ni} is the neutral impurity concentration, N_{ii} is the

ionized impurity concentration and the hydrogenic effective mass m_H is equal to $\varepsilon_r^2 m_0 E_A/E_H$ where E_H and E_A are the ionization energies of the hydrogen atom (13.6 eV) and of acceptors, respectively.[20] Because of the effective mass dependence of the various scattering processes, the mobility μ is sensitive to the application of uniaxial stress. Moreover, μ_{ac} is very sensitive to pressure-induced changes of the lattice and consequently shows a complex dependence on the deformation of the valence band edge.[21] The effect of pressure on μ_{ac} can be determined experimentally (Chapter 2).

1.3 Photoconductive detectors: figures of merit

Stressed Ga-doped Ge photoconductive detectors are best suited for the detection of far IR radiation under low photon backgrounds due to not only their spectral sensitivity but also their high responsivities and low noise.[5,6] The responsivity of a detector is defined as the signal output divided by the radiant input power which in terms of experimental measurables refers to the electrical signal that is produced by a flux of incident photons. The output signal and the photon flux can be measured as an electrical current (units of amperes) and incident power (units of watts), respectively; therefore, a typical unit for the responsivity is amperes/watt (A/W).

The responsivity is a function of the applied electric field which may vary from 0.1 V/cm for stressed Ge:Ga detector to 30 V/cm for copper-doped Ge crystals under typical operating conditions.[4,22,23] However, detector performance is ultimately determined by fundamental materials properties, the two major ones being the hole mobility μ and the hole lifetime τ. These parameters determine the signal current of a detector. While μ is a measure of how efficiently a hole travels in the valence band, the hole lifetime reflects the average time between the photoexcitation of a hole into the valence band and

its subsequent capture at an acceptor. The hole lifetime is a key factor determining detector performance. It depends on the physical mechanism by which the holes are captured and the density of ionized impurities that can capture free holes (at which point the holes no longer contribute to the conduction process). The operating temperature of IR Ge detectors is very low (typically ≤4.2 K); consequently, the concentration of ionized acceptors is equal to the concentration of compensating donors since the concentration of thermally ionized acceptors ($\leq 10^5$ cm^{-3}) is much less than the typical donor concentration ($\geq 10^{10}$ cm^{-3}). Therefore, an advantage of Ge as a detector material is the ability to grow Ge crystals with controlled densities of *both* donors and acceptors.[24]

For a detector of a cubic shape with a side dimension of length L, the responsivity R is given by[3,25,26]

$$R = \frac{\text{signal current}}{\text{optical input}} = \frac{q p_{opt} v_d L^2}{\Phi h\nu} \tag{1.3}$$

where q is the electron charge, p_{opt} is the concentration of photoexcited holes, and Φ is the rate at which photons of energy $h\nu$ are incident on the detector. The hole concentration p is equal to the product of the hole lifetime and the hole generation rate, the latter term being equal to $\Phi\eta/L^3$ where η is the quantum efficiency for photon absorption. For a bias voltage V applied across a length L (Fig. 3), the drift velocity is given by $v_d=\mu V/L$, and one arrives at an expression for the responsivity

$$R = \frac{q\eta\tau\mu V}{h\nu L^2}. \tag{1.4}$$

It is clear then that the responsivity is proportional to the product of the hole lifetime and mobility and that any stress-induced changes to these properties will directly affect the performance of the detector.

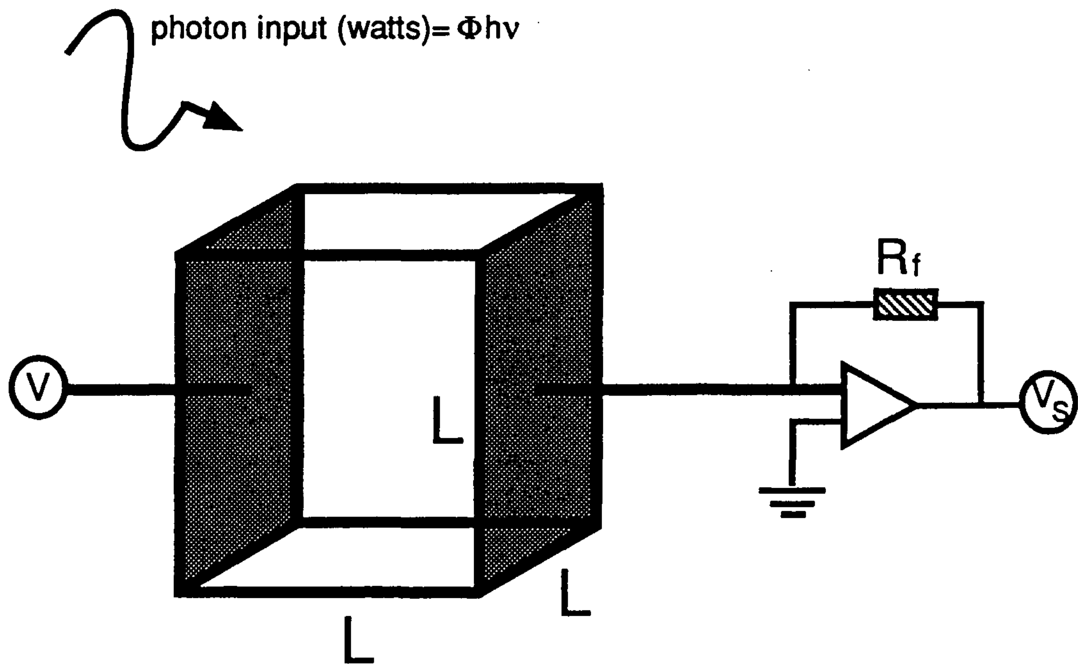

signal current (amps)= $\frac{V_s}{R_f}$

responsivity= $\frac{\text{signal current}}{\text{photon input}}$

Figure 1.3. Schematic of an ideal detector of volume L^3. For an applied bias voltage V and photon incidence Φ, a signal current is produced and is equal to the signal voltage V_s measured divided by the feedback resistor R_f of the amplifier circuit.

The sources of detector noise include Johnson, thermal generation-recombination, and shot noise.[3,26] The total noise is evaluated in terms of the noise equivalent power (NEP), which is defined as the photon power necessary to produce a signal-to-noise ratio of one and is equal to the total noise current divided by the responsivity. Therefore, a typical unit for the NEP is watts or watts/(Hz)$^{1/2}$ when the spectral noise density is used instead of the noise. Because the NEP is inversely proportional to R, it may also exhibit a dependence on τ and μ. However, the NEP cannot be reduced to a simple expression in terms of τ and μ similarly to R as the contributions of the noise terms, i.e., the current fluctuations associated with the various noise phenomena, may themselves show τ and μ dependencies. A further discussion of detector issues can be found elsewhere.[3,25,26] In the remaining sections of this work, I will concentrate on the stress-induced changes in the responsivity as this figure of merit best elucidates the intimate relationship between materials properties and detector performance.

2. Uniaxially stressed germanium doped with monovalent acceptors

The effect of uniaxial stress on acceptor-related properties has been extensively studied and is best understood for the case of monovalent acceptors in Ge.[8,9,27-31] Already since thirty years ago it has been shown that uniaxial compression enhances the hole mobility at low temperature (Fig. 2.1).[9] The hole mobility at low temperature (6 K) increases by as much as a factor of 2.5 in Ge:Al and Ge:In. The stress-induced deformation of the valence band lowers the hole effective mass which in turn changes the rate at which holes are scattered by neutral and ionized acceptors and phonons.

Uniaxial stress in a [100] direction reduces the symmetry of the acceptor lowest one-particle level (from T_d to D_{2d}) producing two, doubly degenerate energy levels. The influence of stress on the hole binding energy by shallow acceptors has also been observed by both Hall effect measurements and infrared spectroscopy (Fig. 2.2).[26,31,32] Moreover, extensive theoretical work has been performed and experimentally verified to show the effect of stress on the both the ground state and bound excited states of acceptors in germanium and silicon (Fig. 2.3).[28-30] These effects have been of great fundamental interest and have served as a basis for the development of far infrared detectors.

Figure 2.4 shows the responsivity of a Ge:Ga detector under stressed and unstressed conditions. The effect of stress is clearly to increase the responsivity for a given applied electric field. In addition, the operating range of applied electric fields is reduced. Such observations cannot be attributed only to the known increase of the hole mobility and the change in the absorption coefficient of Ga acceptors.[11] Its is necessary for the hole lifetime to be highly

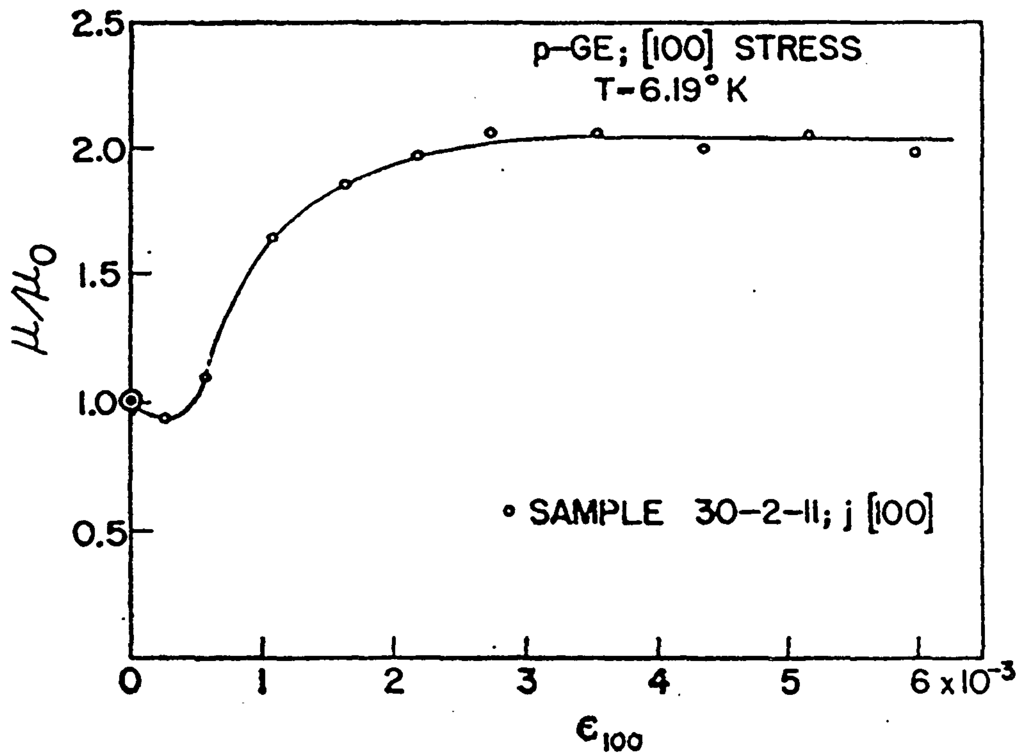

Figure 2.1. Hall mobility of Ge:Al as a function of strain for current parallel to the [100] stress; μ_0=1.5x10^5 cm^2/Vs. A value for ε_{100} of 0.001 corresponds to 1 kbar.[9]

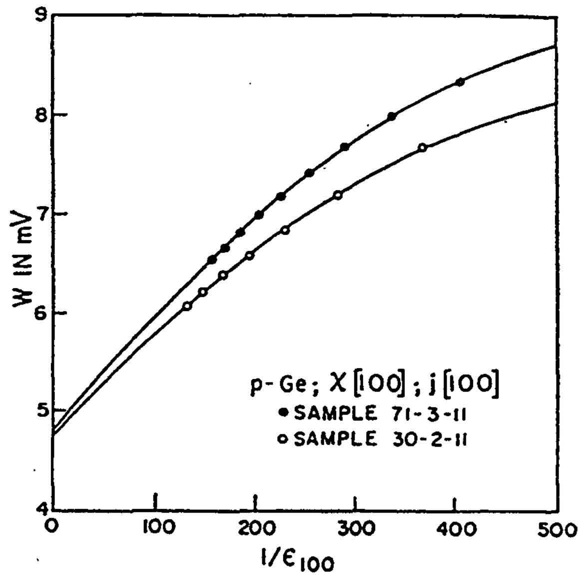

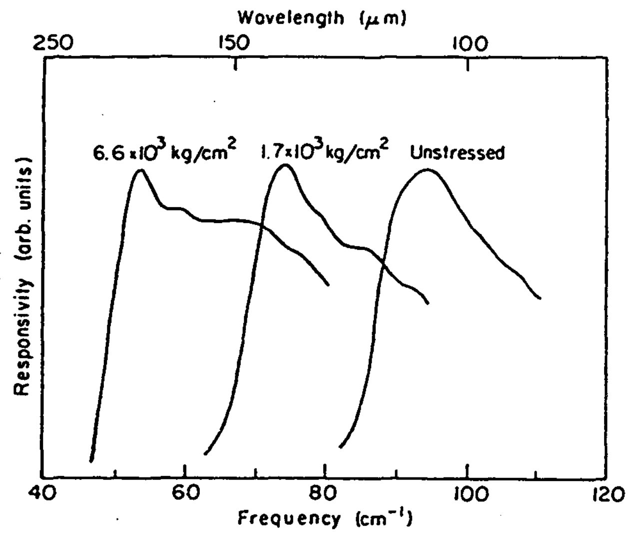

(a) (b)

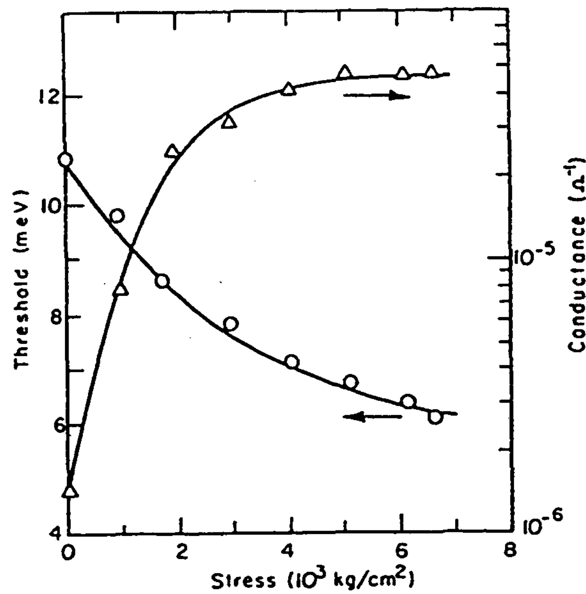

(c)

Figure 2.2. (a) Activation energy W as a function of inverse strain for [100] stress for samples of Al- and In-doped germanium;[9] (b) spectral response of uniaxially stressed Ge:Ga for different values of stress;[5] and (c) stress dependence of the threshold for impurity photoconductivity in Ge:Ga.[5]

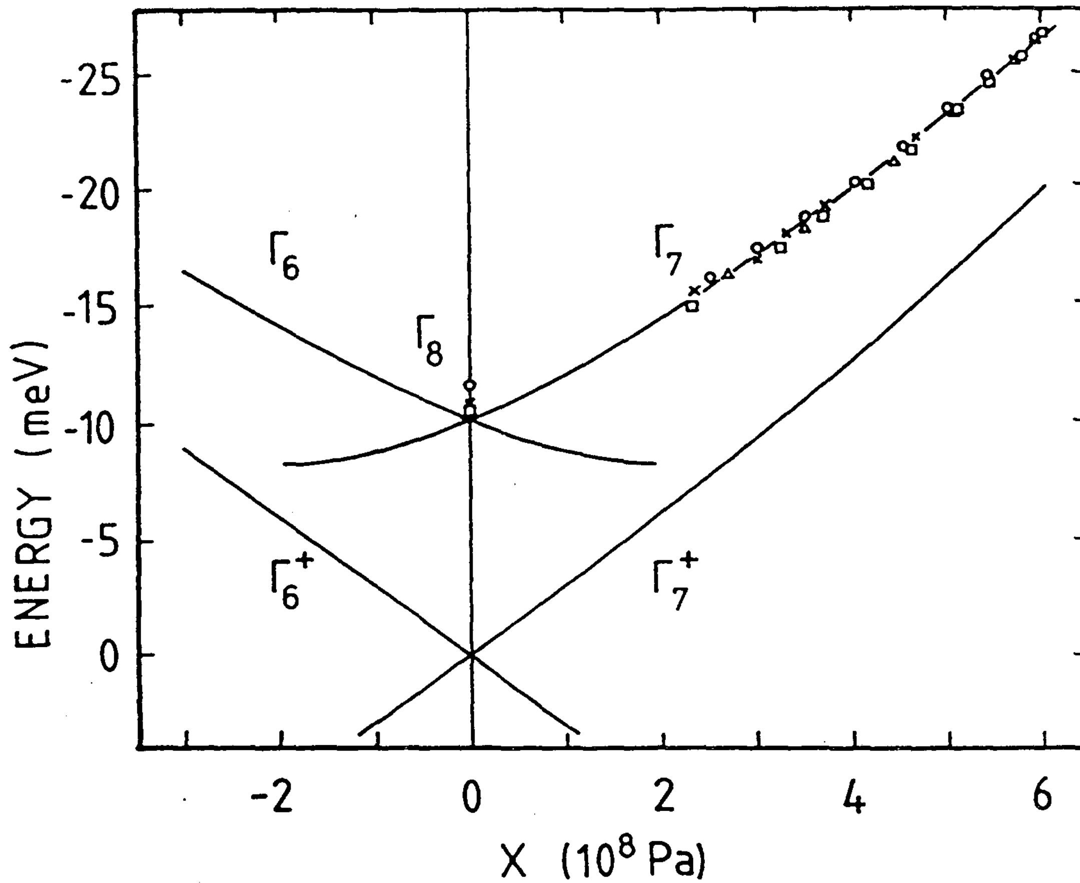

Figure 2.3. Energies of the valence band edges (marked Γ_6^+ and Γ_7^+) and of the acceptor ground-state components (marked Γ_6 and Γ_7) obtained by variational calculation (solid line) compared with acceptor ground-state binding energies for Al (triangles and x's), In (circles) and B (squares) as a function of uniaxial stress X, resulting from a force applied along the [001] orientation. $X>0$ and $X<0$ signify compressive and tensile stress, respectively.[28]

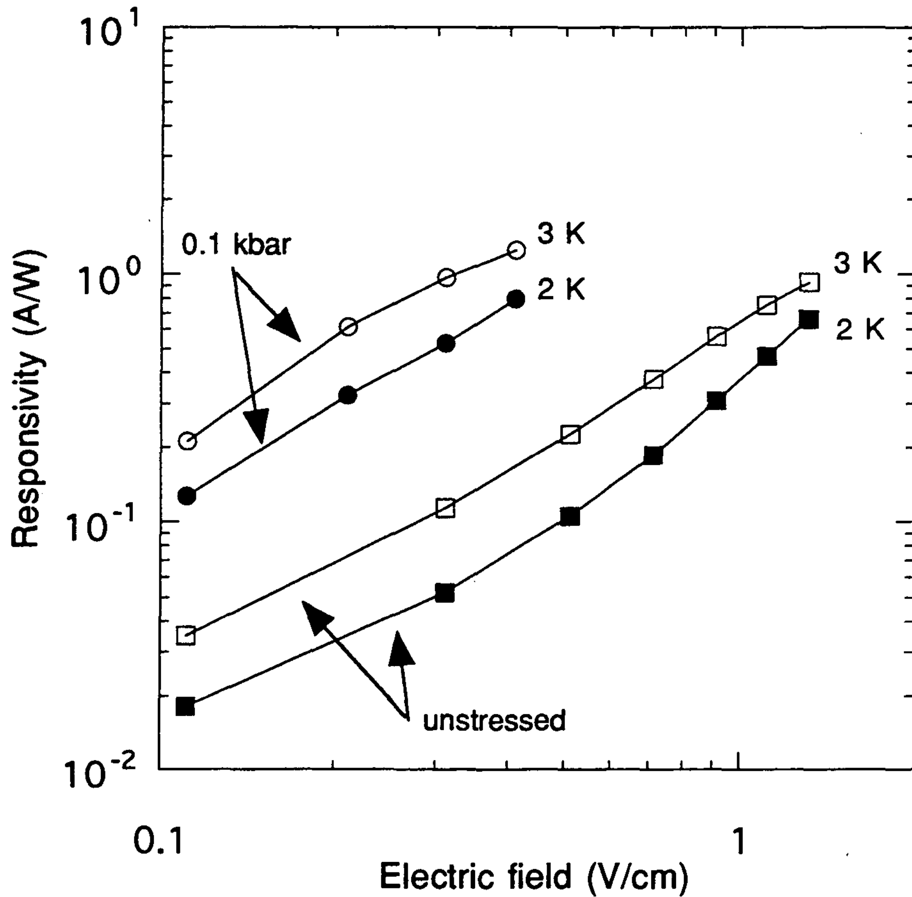

Figure 2.4. Responsivity of a 1 mm^3 Ge:Ga photoconductive detector as a function of applied field and temperature for zero-stress and uniaxially stressed conditions. Measurement conditions: 98.9 μm bandpass filter arrangement (0.91 μm bandwidth, 19% transmission), rms photon signal=1.4×10^{-13} W, background-limited NEP=3.0×10^{-17} W/$Hz^{1/2}$ (measurement courtesy of J. W. Beeman).

sensitive to the application of uniaxial stress (Eq. 1.4). More specifically, the effect of uniaxial stress on the physical mechanism(s) controlling the lifetime must be understood.

2.1 Capture cross sections in unstressed p-Ge

The hole lifetime is a key factor determining detector performance and depends on the physical mechanism by which the holes are captured. The non-radiative capture of mobile charge carriers by Coulomb–attractive centers has received considerable attention as it plays a significant role in the trapping and recombination processes which occur in semiconductors at low temperatures.[33-36] The probability with which a center captures a charge carrier is measured by a quantity known as the capture cross section, σ, which is given by (assuming capture is an isotropic process)

$$\sigma = \left(\frac{4r_T}{3l_E}\right)\pi r_T^2 \tag{2.1}$$

where r_T is the maximum distance from the impurity center for which the carrier is captured and l_E is the average distance a carrier travels in order to lose enough energy to be captured. The term in parentheses is the probability that a carrier will suffer an energy losing collision within a sphere of radius r_T centered at the impurity. The quantity $4r_T/3$ is the average distance within a sphere of radius r_T.

The most widely accepted mechanism for low temperature, non-radiative capture has been the phonon-mediated cascade of carriers through the bound excited states of these centers. This model was first proposed by Lax[32] and later refined by Abakumov *et al.*[35,36] In this picture a carrier is captured by losing energy via the emission of acoustic phonons. The bound excited states of the hydrogenic impurity serve as a ladder of energy states into which the

carrier can relax upon phonon emission. The critical radius r_T is defined in this case by the condition

$$\frac{Zq^2}{4\pi\varepsilon_0\varepsilon_r r_T} = k_B T \tag{2.2}$$

where k_B is Boltzmann's constant, ε_0 is the permittivity of vacuum, T is temperature, and Z is the charge of the center (equal to 1 for an ionized monovalent impurity such as Ga in Ge). The carrier is trapped when it has insufficient thermal energy to overcome the Coulomb attraction due to the charged impurity. When acoustic phonon emission is the energy losing process,

$$l_E = l_{ac}\left(\frac{k_B T}{2m^* s^2}\right) \tag{2.3}$$

where s is the speed of sound in the semiconductor and l_{ac} is the mean free path between acoustic phonon scattering events. Equation 2.3 applies when the carrier thermal energy is much greater than the minimum energy for a carrier to emit one phonon (i.e., $k_B T >> ms^2$). For germanium, $s = 5.4\times10^5$ cm/s and $ms^2 = 0.063$ meV (or 0.73 K).

By combining Eq. 2.1-2.3, one can formulate σ within the framework of the cascade capture (cc) model:

$$\sigma_{cc} = \left(\frac{4\pi}{3 l_{ac}}\right)\left(\frac{2m^* s^2}{k_B T}\right)\left(\frac{q^2}{\varepsilon_0\varepsilon_r k_B T}\right)^3 . \tag{2.4}$$

Because l_{ac} is inversely proportional to T, the cross section for cascade capture depends on temperature as T^{-3}. The functional dependence of σ_{cc} on T has great historical significance as the validity of capture models has traditionally been evaluated via the comparison of the predicted temperature and impurity charge-state (Z) dependencies of the capture cross sections with the experimentally determined ones (Fig. 2.5).

A different mechanism for the capture of holes by acceptors in germanium has been proposed recently, one in which holes are captured

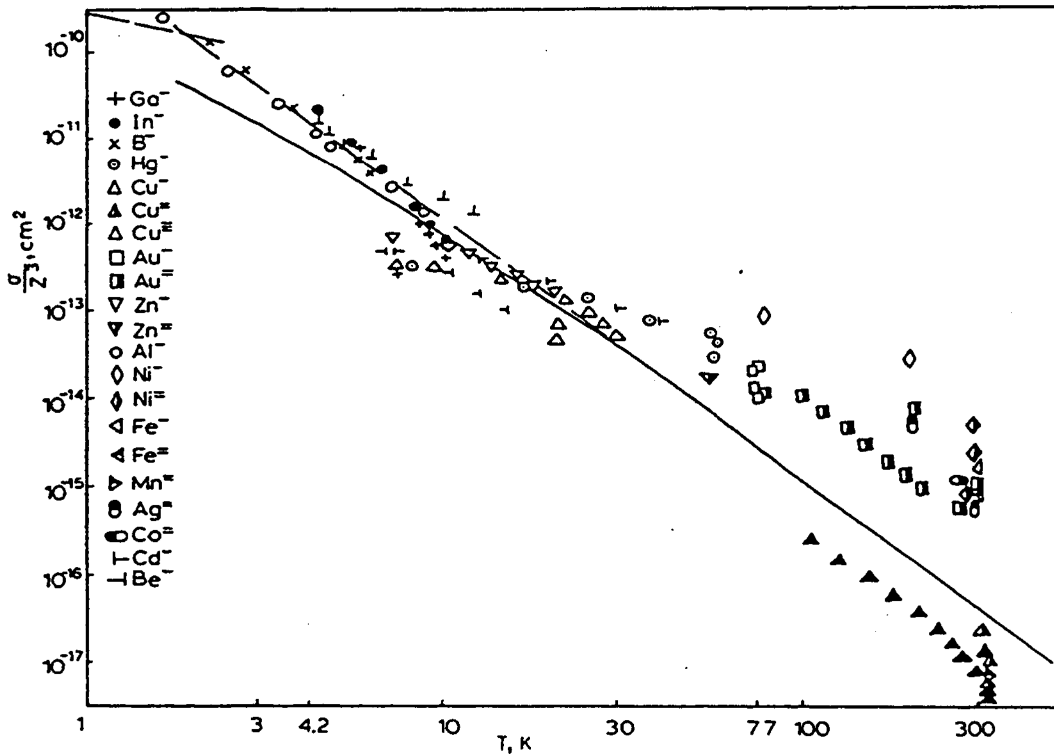

Figure 2.5. Capture cross section for free holes by ionized centers in germanium. The lines indicate the values expected from cascade theory.[35]

directly into the acceptor ground state.[37-40] Darken and co-workers have observed capture cross-sections exhibiting a T^{-1} dependence (Fig. 2.6). They observed a dependence between the valence band effective density of states (N_V), the hole lifetime τ, the free hole concentration p (that is, the concentration of ionized acceptors when p is much greater than the concentration of compensating donors), and temperature given by[39]

$$\frac{N_V}{p\tau} \approx \frac{k_B T}{h} \tag{2.5}$$

where h is Planck's constant. From this empirical relation they derived an expression of the cross section for this direct capture (dc) process by acceptors:[40]

$$\sigma_{dc} = \left(\frac{m_0}{m^*}\right)\left(\frac{6.4\times10^{-12}}{T}\right)\ \text{cm}^2\ . \tag{2.6}$$

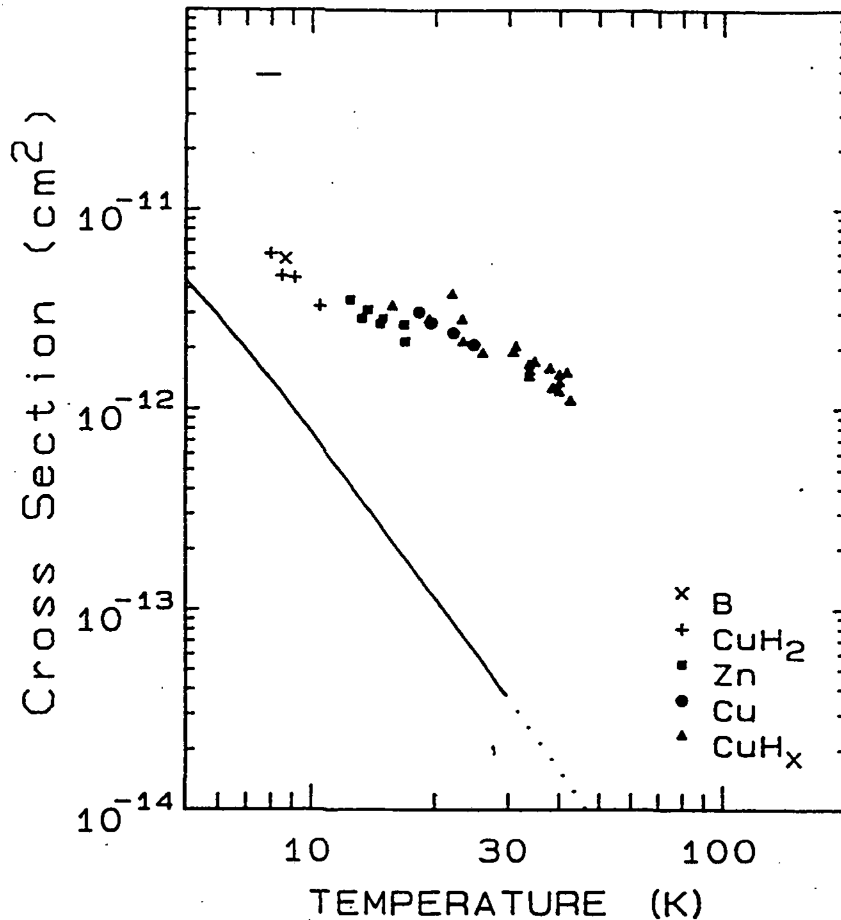

Figure 2.6. Hole capture cross sections for several singly ionized acceptors in germanium versus temperature, compared to cascade theory (solid line).[38]

2.2 Capture cross sections in stressed p-Ge: m* dependence

2.2.1 Introduction

Whereas both the cascade and direct capture models predict an increase in the capture cross section with decreasing temperature T, they exhibit very different functional dependencies on the effective mass, m*. Therefore, low temperature photo–Hall effect measurements have been performed on

germanium crystals doped with gallium acceptors and placed under uniaxial stress. By this method it has been possible to study the effective–mass dependence of the hole lifetime (and necessarily the capture cross section) and to clearly distinguish between direct capture and cascade capture in this material.

From the Eq. 2.4 and the relation between mobility μ and mean free path ($\mu_{ac}=ql_{ac}/m^* v_{th}$), the capture cross section that is based on cascade capture (σ_{cc}) has a dependence on temperature and effective mass given by

$$\sigma_{cc} \propto T^{-4} (\mu_{ac} v_{th})^{-1} \tag{2.7}$$

where the average thermal velocity v_{th} is proportional to $T^{1/2} m^{*-1/2}$ and the acoustic-phonon-scattering component of the hole mobility μ_{ac} is proportional to $T^{-3/2} m^{*-5/2}$ at zero stress.[19] On the other hand, the direct capture model yields a cross section

$$\sigma_{dc} \propto T^{-1} (m^*)^{-1} . \tag{2.8}$$

The simple relation given in Eq. 2.8 shows the temperature and effective mass dependencies irrespective of the energy loss mechanism.

Whether direct or cascade capture is the dominant mechanism has significant consequences for the hole lifetime τ. In p-type Ge at sufficiently low temperature, practically all holes are frozen out on acceptors, and the ionized acceptor concentration, i.e., the density of hole capture centers, is equal to the concentration of compensating donors N_D. In this case the hole lifetime is given by[17,41]

$$\tau = \frac{1}{\beta N_D \sigma v_{th}} \tag{2.9}$$

where β is the valence band degeneracy (equal to 4 for unstressed and 2 for uniaxially stressed Ge). Because the thermal velocity is inversely proportional to $m^{*1/2}$, the lifetime depends on the effective mass as

$$\tau_{cc} \propto \beta^{-1} \mu_{ac} \tag{2.10}$$

and

$$\tau_{dc} \propto \beta^{-1} m^{*3/2} \qquad (2.11)$$

for cascade capture and direct capture, respectively. The effective mass component of τ_{cc} is expressed in terms of μ_{ac} alone as the m* dependence is fully contained in μ_{ac} (which is proportional $m^{*-5/2}$). Therefore, the lifetime *increases* according to the cascade picture yet *decreases* for direct capture if the effective mass decreases.

2.2.2 Experimental approach and results

In order to study the effect of uniaxial stress on the hole lifetime, photo-Hall effect measurements have been performed on p-type Ge samples. Although only an indirect method of determining the hole lifetime, photo-Hall effect yields additional information regarding the hole mobility when measured in conjunction with the electrical resistivity. Direct observation of the lifetime by photoconductivity decay experiments has been restricted by the limited access to adequate pulsed, far-infrared radiation sources such as free-electron lasers necessary for the photoionization of exclusively shallow acceptor levels.

The Ge samples were produced from two 1 mm-thick wafers, of crystals #773 and #783, having gallium concentrations of $(1.4\pm0.1)\times10^{14}$ cm^{-3} and $(1.1\pm0.1)\times10^{14}$ cm^{-3}, respectively. The wafers were cut from two, Czochralski-grown, Ga-doped Ge bulk crystals (#773 and #783). Both sides of the wafers were lapped in a 4μm-SiC/water slurry and etched in a 3:1 HNO_3:HF mixture for 90 seconds. Two boron implants (25 keV/1×10^{14} cm^{-2} and 50 keV/2×10^{14} cm^{-2}) and subsequent metallization (20 nm of Pd and 400 nm of Au in this sequence) were performed for later use in the formation of electrical contacts. Thermal annealing at 300 °C for 1 hour under Ar flow followed the metallization. The wafers were cut to produce a 1x1x5 mm^3 final geometry for each sample.

All resulting surfaces were <100> oriented. For each sample the electrical contacts necessary for the Hall effect measurements were masked on two opposing 1x5 mm^2 contacted surfaces, and all excess metallization and implanted layers were removed via KBr solution (1 minute) and 3:1 HNO_3:HF (30 seconds) etches, respectively.

Uniaxial stress up to 4.2 kbar was applied parallel to the long axis of the bar-shaped samples by a leaf-spring stress apparatus which was mounted in a LakeShore CT-310 continuous flow cryostat. The sample space consisted of a closed cavity containing both the sample and a photon emitter (emissivity = 0.9), the latter needed for photo-Hall measurements. Hall coefficients were obtained for a Hall-bar sample geometry with a Keithley 110 Hall effect measuring system and a magnetic induction of 0.3 Tesla. The temperature was monitored with a calibrated Allen-Bradley, 1/8 watt, 1 kΩ, carbon composite resistor. Further experimental details can be found in Appendix A.

Hole concentrations obtained from the Hall effect measurements for sample #783 are shown in Fig. 2.7. The filled circles and squares correspond to data taken when the sample was illuminated. The solid line was calculated using the equation[42]

$$\frac{p\,(p+N_D)}{N_A - N_D - p} = \frac{N_V}{\beta} \exp\left(-\frac{E_A}{k_B T}\right) \qquad (2.12)$$

where p is the hole concentration, N_A and N_D are the acceptor (Ga) and donor concentrations, respectively, the band degeneracy is equal to 4, k_B is the Boltzmann constant, N_V is the effective density of states, and E_A is the gallium acceptor binding energy. Therefore, a best fit to the zero stress data yields N_A and N_D. The dashed line was obtained by using the impurity concentrations (N_A and N_D) determined from the zero-stress measurement and adjusting both N_V and E_A so as to provide the best fit to the data (using Eq. 2.12). E_A was confirmed by photoconductivity spectroscopy measurements (Fig. 2.8). In

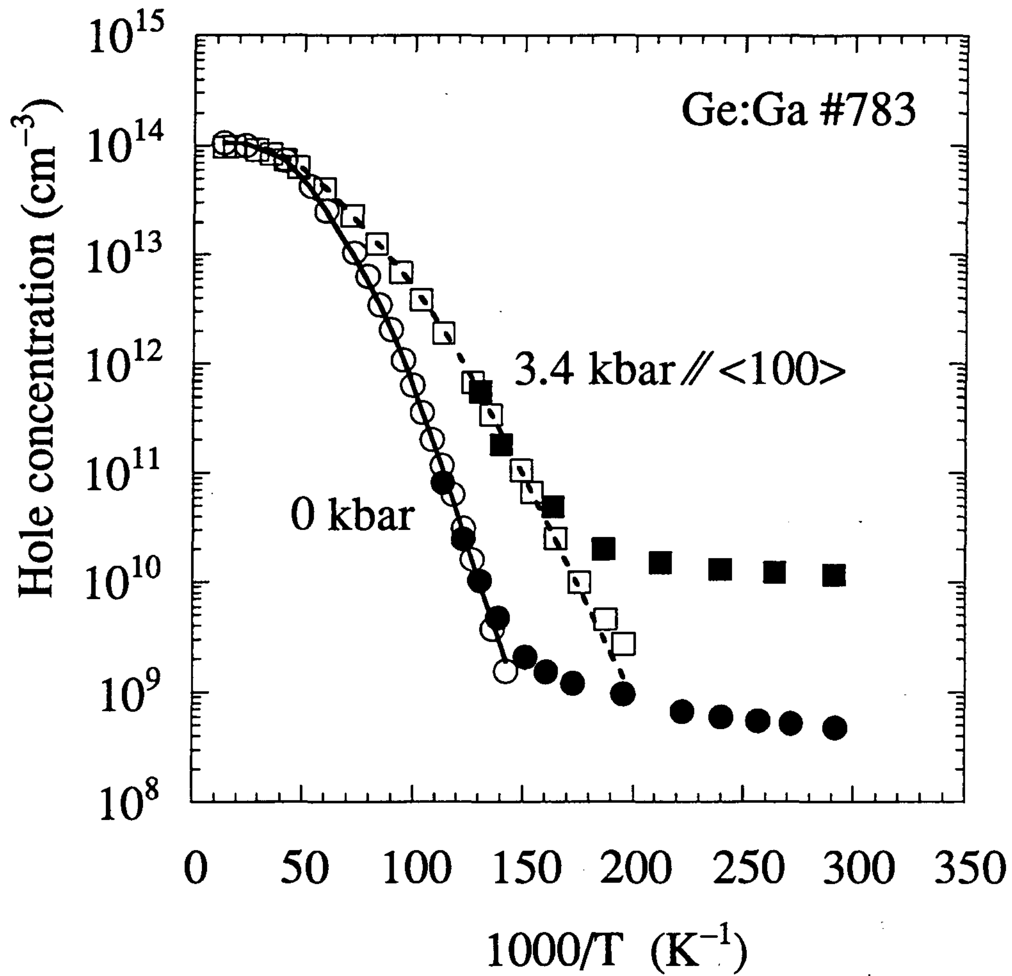

Figure 2.7. Hole concentration as a function of inverse temperature obtained from Hall effect (clear symbols) and photo-Hall effect (filled symbols) measurements. The open circles were fit using the following parameters: $N_A=1.1\times10^{14}$ cm^{-3}, $N_D=3.5\times10^{12}$ cm^{-3}, $E_A=11.1$ meV, $N_V=1.2\times10^{15}T^{3/2}$ cm^{-3}, and $\beta=4$. The data taken at a uniaxial stress of 3.4 kbar//<100> (clear squares) were fit using $E_A=7.5$ meV, $\beta=2$ and $N_V=1.44\times10^{14}T^{3/2}$ cm^{-3} (i.e., $m^*=0.089m_0$) while maintaining the same values for the impurity concentrations N_A and N_D.

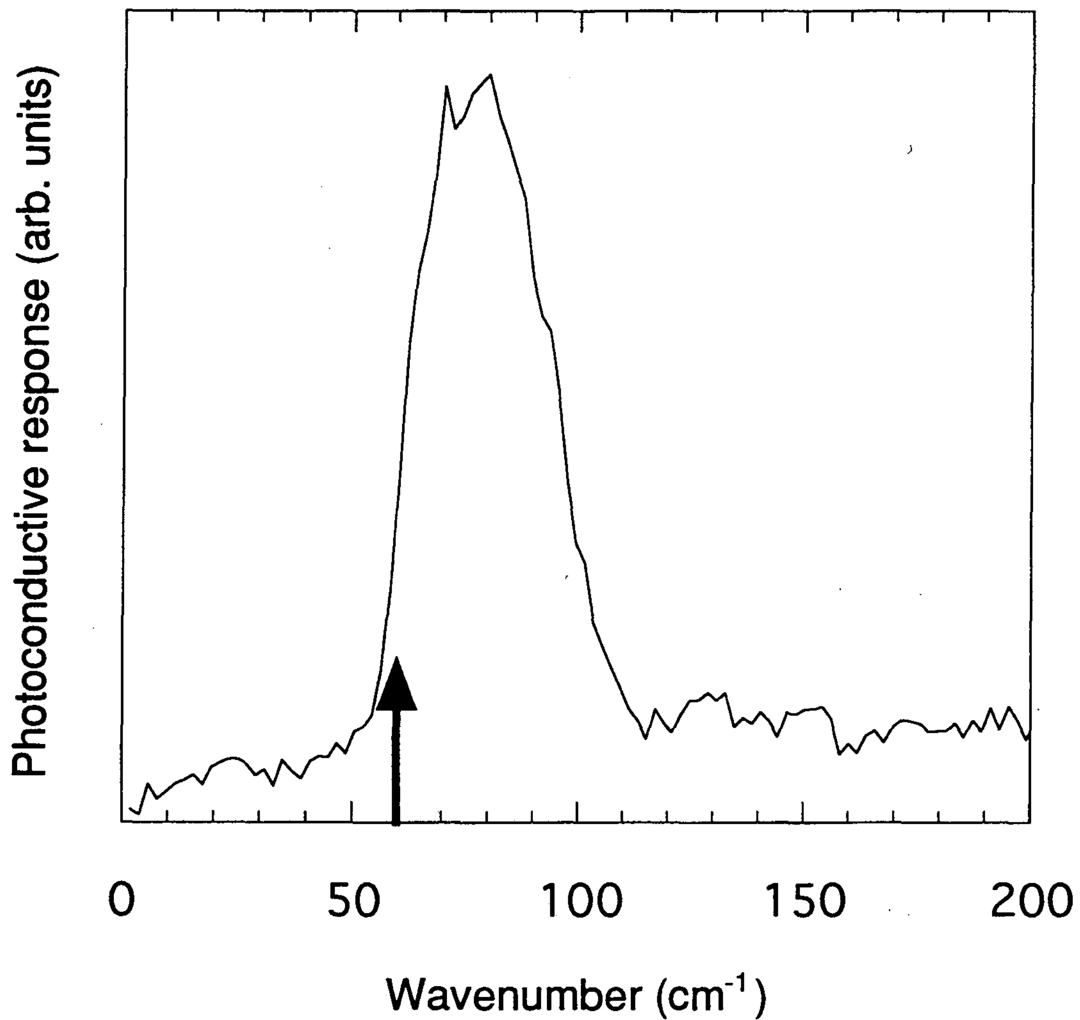

Figure 2.8. Spectral response of the stressed sample also shown in Figure 2.7. The activation energy determined from the Hall measurements (7.5 meV) is indicated by the arrow. The drop of the photoconductivity response near 100 cm^{-1} is due to a low-pass, mesh filter (courtesy of P. Aide) used in the measurement. Experimental details can be found in Appendix B.

addition, uniaxial stress reduces the valence band degeneracy β from 4 to 2. The change in the effective density of states then reflects a change in the effective mass.

From the photo-Hall measurements (filled symbols in Fig. 2.7) the hole lifetime τ_{ph} has been estimated. In the region where the hole concentration is determined by the rate of photogeneration, $\tau_{ph} = p_{opt}/g_{opt}$ where g_{opt} is the optical generation rate and p_{opt} is the concentration of photogenerated holes. The calculated generation rates are 3×10^{16} $cm^{-3}s^{-1}$ and 8×10^{16} $cm^{-3}s^{-1}$ for the photo-Hall measurements shown in Fig. 2.7 in the zero-stress (filled circles) and stressed (filled squares) conditions, respectively.

The dependence of the lifetime on stress at 3.7 K for samples #773 and #783 is shown in Figure 2.9. The zero-stress values of the hole lifetime agree within a factor of two with previous results for Ge doped with shallow acceptors. For the largest applied stress of 4.2 kbar, the lifetime has increased by one order of magnitude compared to the zero-stress value. Such increase has been observed throughout the temperature range over which photo-Hall measurements were made (Fig. 2.7). It is clear from Figure 2.9 that the direct capture model does not describe the effect of stress on the hole lifetime that has been observed as the lifetime *has increased* by the application of stress even though the direct capture model would predict a decrease in τ.

From the stress-induced change in N_V, the density of states effective mass has been determined as a function of stress (Fig. 2.10). Therefore, the hole lifetime can be plotted as a function of m^* as indicated in Fig. 2.11. The ratio between $\beta\tau$ and the zero-stress value of $\beta\tau$ has been plotted in order to show the functional dependence of τ on the effective mass alone. In addition, the stress dependence of the mobility μ (Fig. 2.12) has been studied in the context of acoustic phonon (ac), ionized impurity (ii) and neutral impurity (ni)

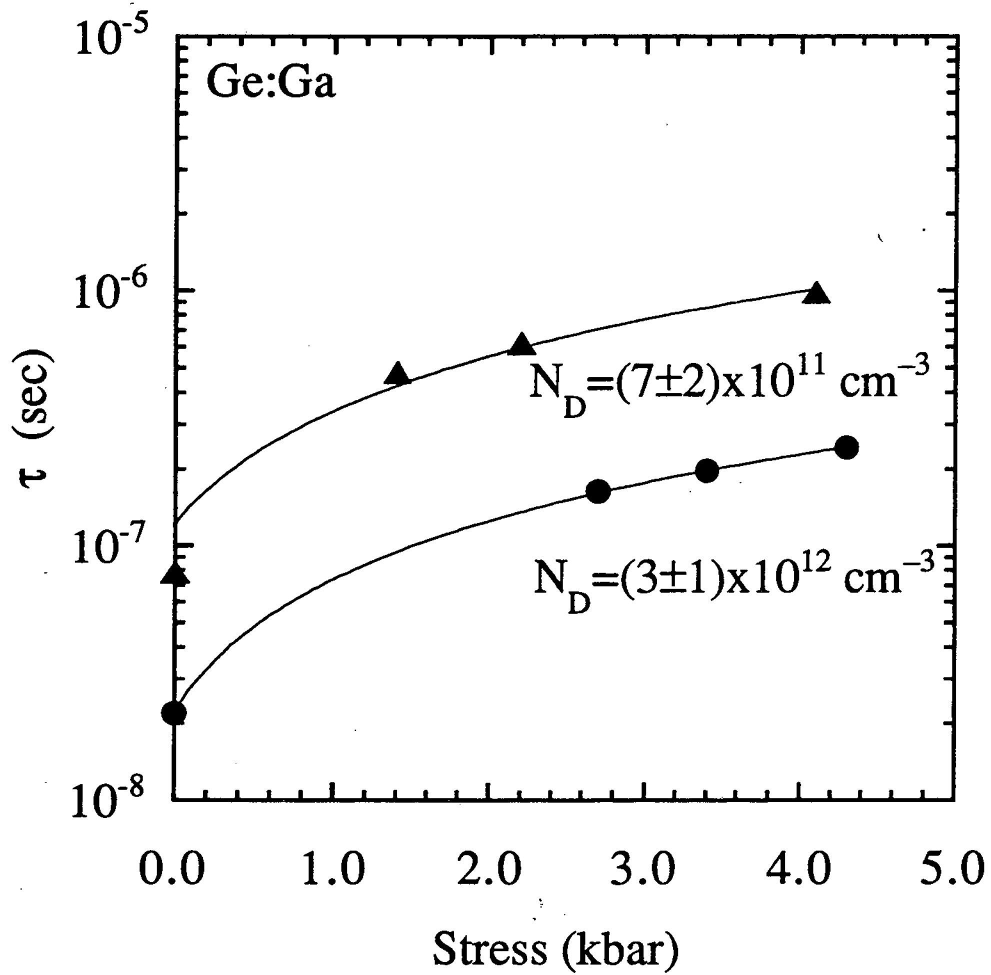

Figure 2.9. Hole lifetime as a function of applied uniaxial stress. The triangles and circles denote samples #773 and #783, respectively.

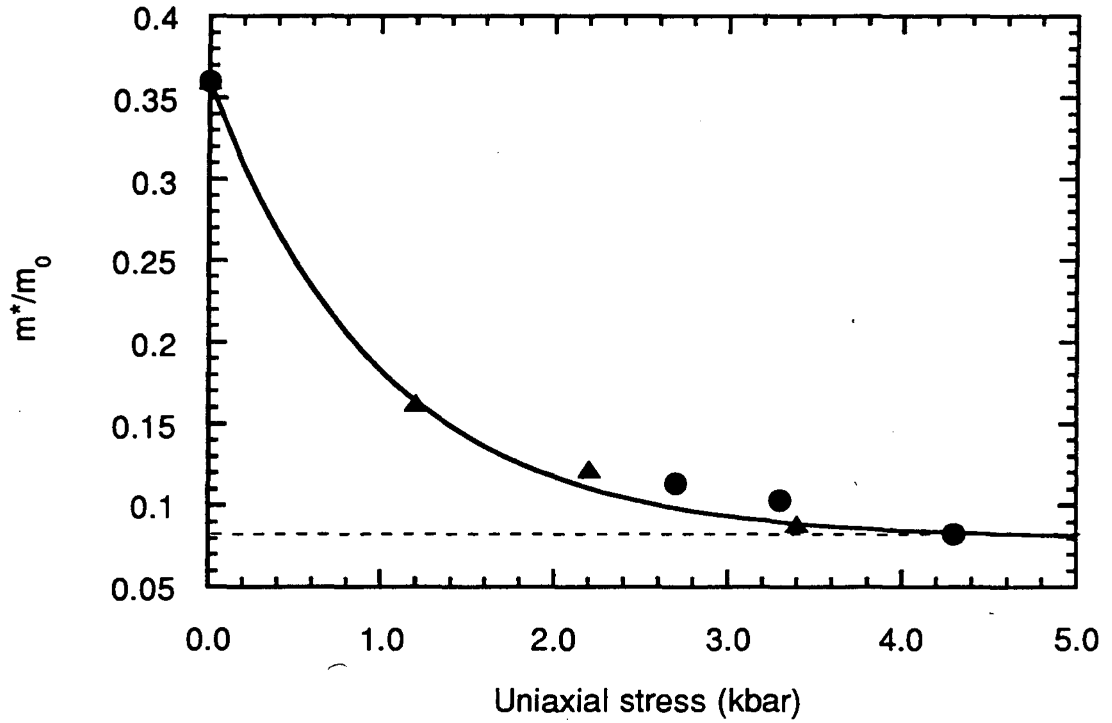

Figure 2.10. Stress dependence of the density-of-states effective mass. The magnitude of m* has been determined by changes in the effective density of states, N_V, due to stress as seen in Fig. 2.7.

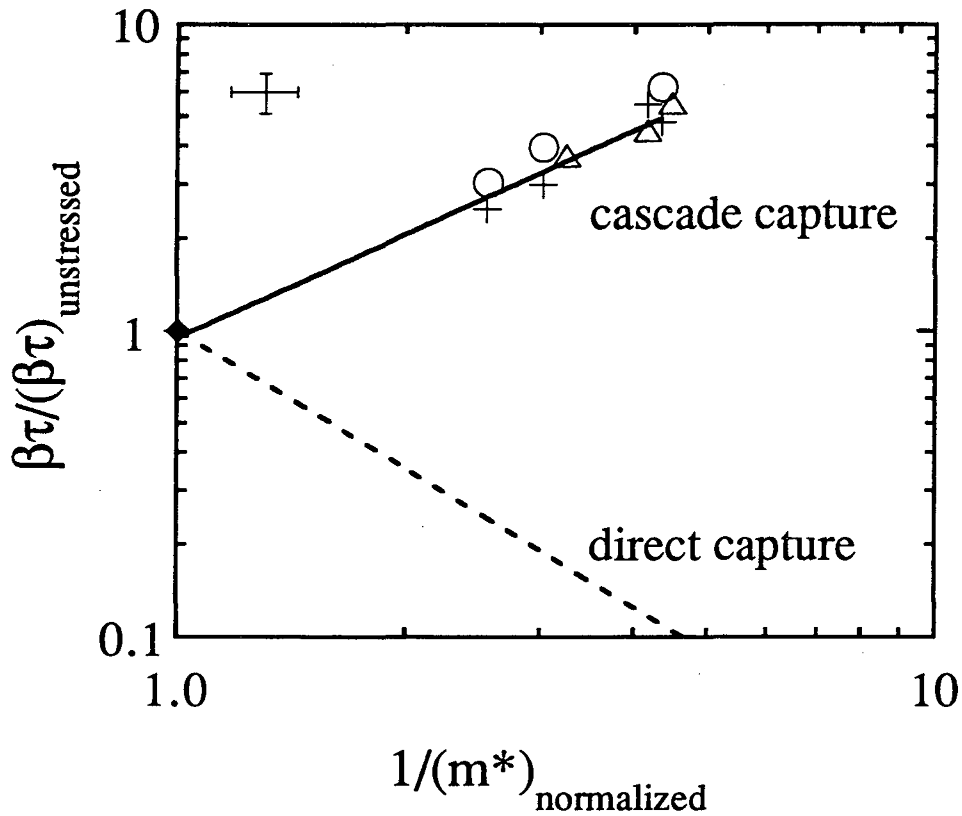

Figure 2.11. Product of the hole lifetime and band degeneracy as a function of the inverse normalized effective mass [$(m^*)_{normalized}=m^*/(m^*)_{unstressed}$]. The circles denote sample #773 while the triangles are from sample #783. The solid line has been obtained by fitting the scaled μ_{ac}'s (crosses) and reflects the change in the lifetime that is expected from cascade capture theory (Eq. 2.10).

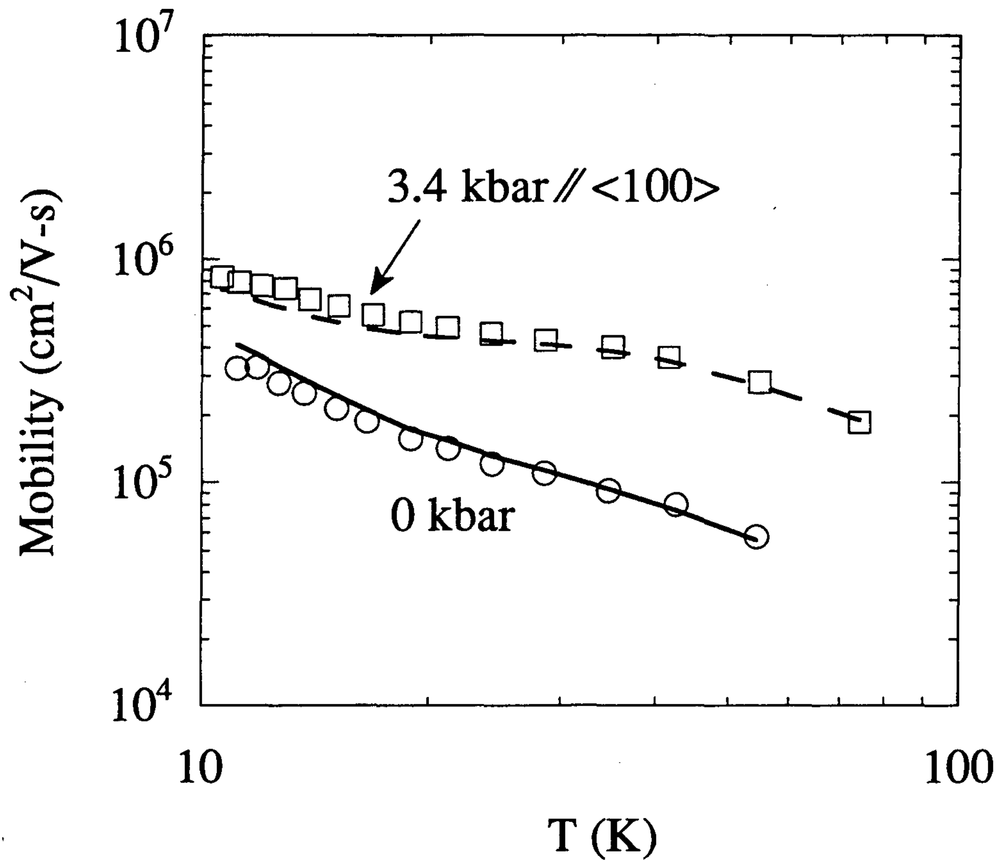

Figure 2.12. Mobility as a function of temperature obtained from Hall effect measurements with the corresponding concentrations shown in Figure 2.7. The circles are in good agreement with the mobility expected for p-type Ge (solid line). Increasing μ_{ac} by a factor of 5.5 and scaling μ_{ii} and μ_{ni} with the proper effective mass (m^*=0.089m_0 and m_H=0.14m_0 at 3.4 kbar) produce a good fit to the data for stressed Ge:Ga at the higher temperatures where scattering by acoustic phonons dominates– compare the squares with the dashed line.

scattering (Eq. 1.2). From these results, the increase of μ_{ac} as a function of stress (and effective mass) has been estimated. These values are plotted in Fig. 2.11 (crosses) by the use of Eq. 2.11. The solid line in Fig. 2.11 is fit to this data and provides an excellent fit to the lifetimes determined from the photo-Hall measurements (circles and triangles) as well. Thus, it is found from the *independently obtained* experimental lifetimes and mobilities that

$$\tau_{ph} \propto \beta^{-1}(\mu_{ac})_{exp} \quad (2.13)$$

The agreement between Eq. 2.11 and Eq. 2.14 provides a very compelling argument supporting the dominance of phonon-mediated cascade capture of holes by gallium acceptors in Ge.

2.3 A second look at the experimental capture cross sections

The photo-Hall measurements on stressed Ge strongly support the cascade capture model which has been has been used to explain experimental data pre-dating 1972.[35,36] However, the data obtained more recently on acceptors which include CuH_2^-, Zn^- and Cu^- in germanium clearly cannot be explained within the well-accepted formulation of cascade capture.[37-40] It is therefore not surprising that a different mechanism has been proposed even if its formulation may not be exactly right. Reconciling the entirety of the data is critical in furthering the understanding of the capture process.

Figure 2.13 is a compilation of the data for monovalent impurities including CuH_2^-. The dashed line represents the value of σ_{cc} predicted by the cascade capture model. The general agreement is very good. Figure 2.14 is a compilation of data for singly-ionized multivalent acceptors and the copper triple acceptor, which exhibit hydrogenic bound-excited state when binding two and three holes, respectively. Although the lower lying data (filled symbols) have been used to support cascade capture (Fig. 2.5), clearly their temperature

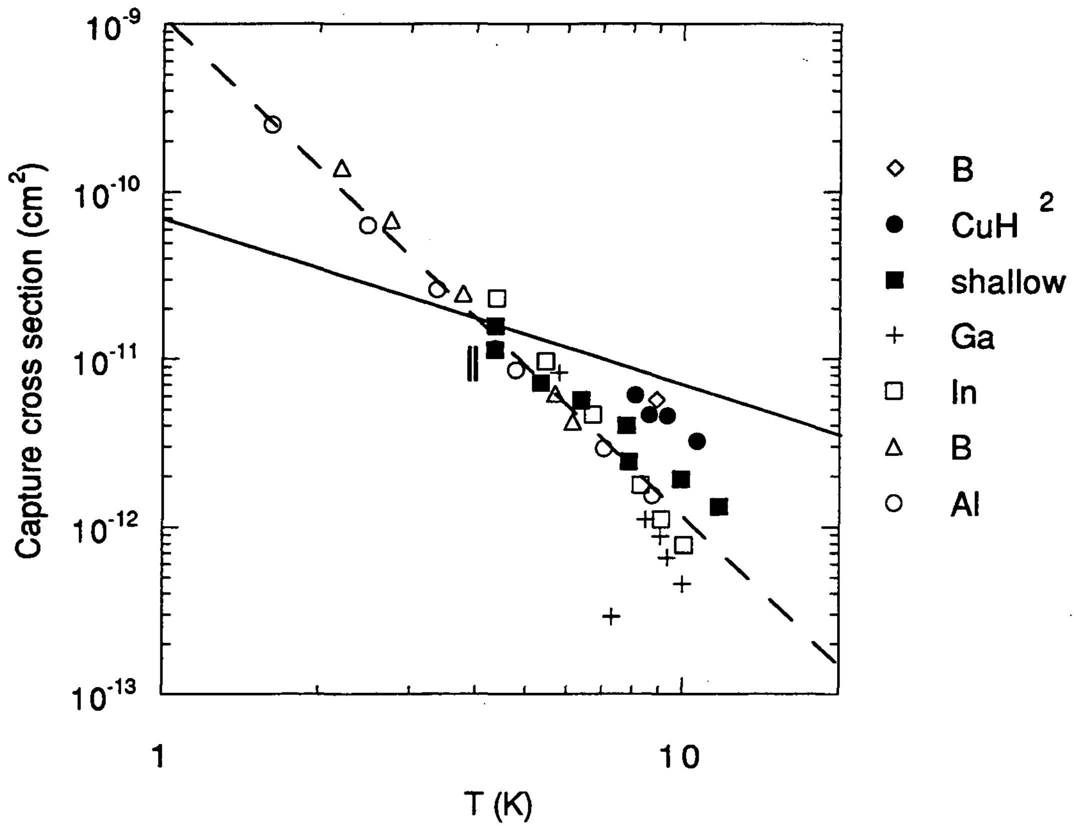

Figure 2.13. Capture cross section of singly ionized, monovalent acceptors. The solid and dashed lines show the expected values for the direct and cascade capture models, respecitively. The vertical parallel lines indicate the capture cross sections obtained from the lifetime data in Figure 2.9 (after Abakumov *et al.*[35] and Darken *et al.*[38,39] and references therein).

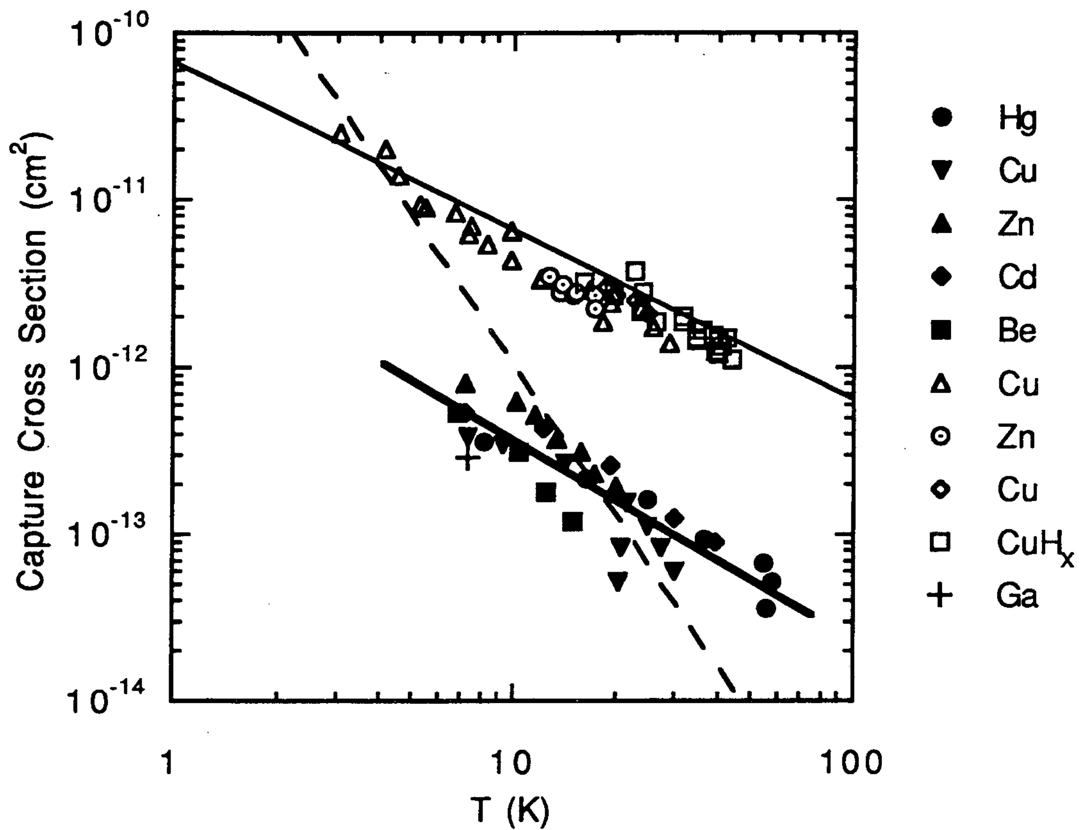

Figure 2.14. Capture cross section of singly-ionized multivalent acceptors plus Ga. The thin solid and dashed lines show the expected values for direct and cascade capture models, respectively (after Abakumov *et al.*[35] and Darken *et al.*[38,39] and references therein). The data represented by the filled symbols show a dependence on temperature given by the thick solid line (σ proportional to $T^{-1.2}$).

dependence is similar to the upper grouping (clear symbols) which has been used in support of the direct capture model. In Figure 2.14 the capture cross section for Ga is presented, datum gathered by the same group that obtained most of the lower lying data.[43-45] If one scales the lower data (clear symbols) by the factor with which the Ga cross section must be scaled in order for it to agree with the cascade model (and indeed be in agreement with the other data for single acceptors), then both sets of data are in clear agreement. *Cascade capture seems to apply to monovalent shallow impurities but not to double acceptors and the copper triple acceptor.* Perhaps the role of core states (i.e., the central cell) is important in the capture process. Photo-Hall measurements of multivalent acceptors are therefore of great interest.

2.4 A final comment Ge:Ga stressed detectors

The effect of uniaxial stress on the responsivity of Ge:Ga stressed detectors can be explained. The application of stresses as low as 1 kbar is enough to produce an increase in both the mobility and the lifetime. Because the responsivity is proportional to the $\mu\tau$ product, the responsivity increases with stress by a factor comparable to the stress-induced increase of $\mu\tau$. For a stress of 1 kbar, the mobility has been shown to increase by a factor of 2 and the lifetime by a factor of 3-4 (Fig. 2.9) to yield an expected factor of 6-8 increase of the responsivity from its zero-stress value in good agreement with the data shown in Figure 2.4.

3. Uniaxially stressed germanium doped with divalent acceptors

Double acceptors in germanium include beryllium, zinc, cadmium and mercury. Unlike single acceptors whose binding energies are very similar to each other and close in magnitude to the theoretically predicted value (from effective mass theory), in their neutral state double acceptors bind holes with a wide range of energies depending on the chemical nature of the acceptor. Beryllium is very much effective-mass-like and in its neutral state binds holes with an energy of 25 meV while the core states of mercury distort the Coulomb potential (i.e., central cell distortion) resulting in a first ionization potential of 90 meV. Because it is composed of the product of two single-particle states, the ground state of these acceptors is a multiplet ($\Gamma_1+\Gamma_3+\Gamma_5$).[46,47] Hole-hole interaction may split the otherwise degenerate multiplet, and in the case of Be in Ge, it has been shown that the ground state is split by an energy $\Delta E \approx 0.1$ meV (implying weak hole-hole interaction) into two levels, Γ_1 and $\Gamma_3+\Gamma_5$, as shown in Figure 3.1. Strong hole-hole interaction has been observed for Zn double acceptors.

When applied in a [100] direction, uniaxial stress reduces the symmetry of the acceptor from T_d to D_{2d}. The ground state splits into three components when the stress-induced splitting is much greater than that which is due to hole-hole interaction as is the case for Be in Ge.[48] The two bound holes occupy the level that minimizes the total energy of the acceptor, and a reduction of the binding energy is observed (Fig. 3.2) similarly to single acceptors [Fig. 2.2(c)].

3.1 Characteristics of Be-doped Ge: Be^+ centers

Beryllium can bind a third hole to become positively charged (Be^+).[14] The fourfold degeneracy at the valence-band edge of Ge allows for the

Figure 3.1. Energy-level diagram of the group-III and group-II substitutional acceptors in Ge (GS denotes ground state, VB denotes valence band). The figure shows ground-to-excited-state transitions.[48]

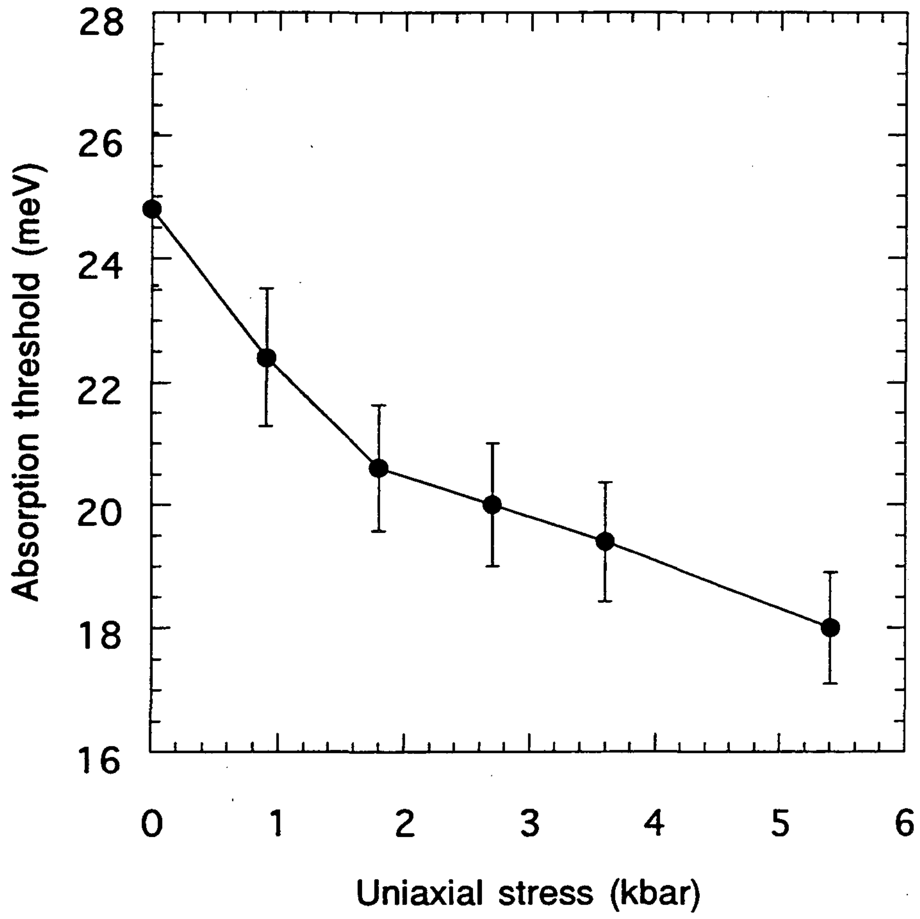

Figure 3.2. Stress dependence of the Be absorption threshold in Ge:Be.

accommodation of up to four holes in the *1s* lowest one-particle level, which would be equivalent to having electrons with a pseudospin of 3/2. Other acceptors can become overcharged as well. Shallow single acceptors can bind a second hole with an energy in the order of 1 meV.[49] The copper triple acceptor can bind a fourth hole (Cu^+) with an energy of approximately 1 meV.[50] Variational calculations have given support to the experimental observation that the third hole in Be is bound with an energy of approximately 5 meV![51,52] This is significant as this energy is of sufficient magnitude for the existence of an optically detectable concentration of these centers at liquid helium temperatures.

An excitation source (e.g., light) is required for the observation of overcharged centers. Normally holes will freeze-out onto ionized acceptors in a temperature range where the thermal energy is too great for neutral centers to bind an extra hole (given the small magnitude of the binding energy associated with the overcharged center). However, at low temperatures where practically all holes have frozen out, the ionization of neutral centers by low level illumination produces an excess population of holes in the valence band which can be trapped by the abundance of neutral centers (under the typical condition of less than 1% compensation for Ge:Be) to produce overcharged ones. The effect of trapping by neutral Be can be removed by the application of uniaxial stress. This will occur at a pressure whereby the splitting of the *1s* ground state is comparable to the energy with which the extra hole is bound (between 0.5 kbar and 1 kbar). The occurrence of Be^+ in Ge is not merely a interesting problem in semiconductor physics; it is a phenomenon that has significant implications on the transient behavior of Ge:Be detectors.[51,53,54]

3.2 Characteristics of Ge:Be detectors

Germanium doped with beryllium is well suited for the detection of photons in the 50-30 μm range.[23] The detection of higher energy photons is limited by absorption in the bulk from optically active multiphonon modes (Figure 3.3).[55] Because of the smaller Bohr radius of Be, germanium crystals can be doped up to one order of magnitude higher with Be atoms than with Ga without degrading detector performance therefore increasing the material's optical density.[11] The Be concentration is typically 10^{15} cm^{-3}.

Ge:Be detectors show adequate responsivity at 4.2 K. However, their performance can be limited by noise arising from high dark currents if (a) the Be concentration is greater than $3x10^{15}$ cm^{-3} or (b) the background concentration of shallow acceptors is greater than that of donors. The dark current refers to the current passing through the detector in the absence of a photon signal. Both (a) and (b) can be avoided by growing the bulk Ge crystals under proper conditions. Otherwise dark currents can be reduced by lowering the detector operating temperature. The unfortunate additional effect of reducing the operating temperature is to lower the detector responsivity to a level where other noise sources lead to an inadequate signal-to-noise ratio. Figure 3.4 shows the decrease in responsivity as a function of temperature for various applied electric fields. Already at 3 K the signal has deminished by almost a factor of 3.

It has been found that the application of small amounts of stress (< 1 kbar) will result in an increase of the detector responsivity (Fig. 3.4). In addition, the signal has become relatively temperature insensitive compared to the zero-stress signal. That is, the $\mu\tau$ product exhibits a functional dependence on T that varies with stress. This is attributed largely to the stress dependence of the hole

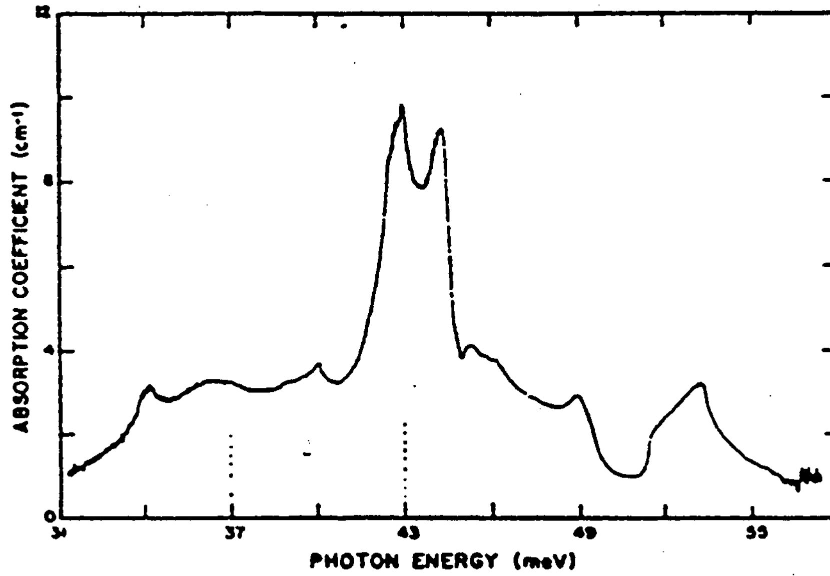

Figure 3.3. Part of the lattice absorption spectrum of intrinsic germanium at liquid Helium temperature.[56]

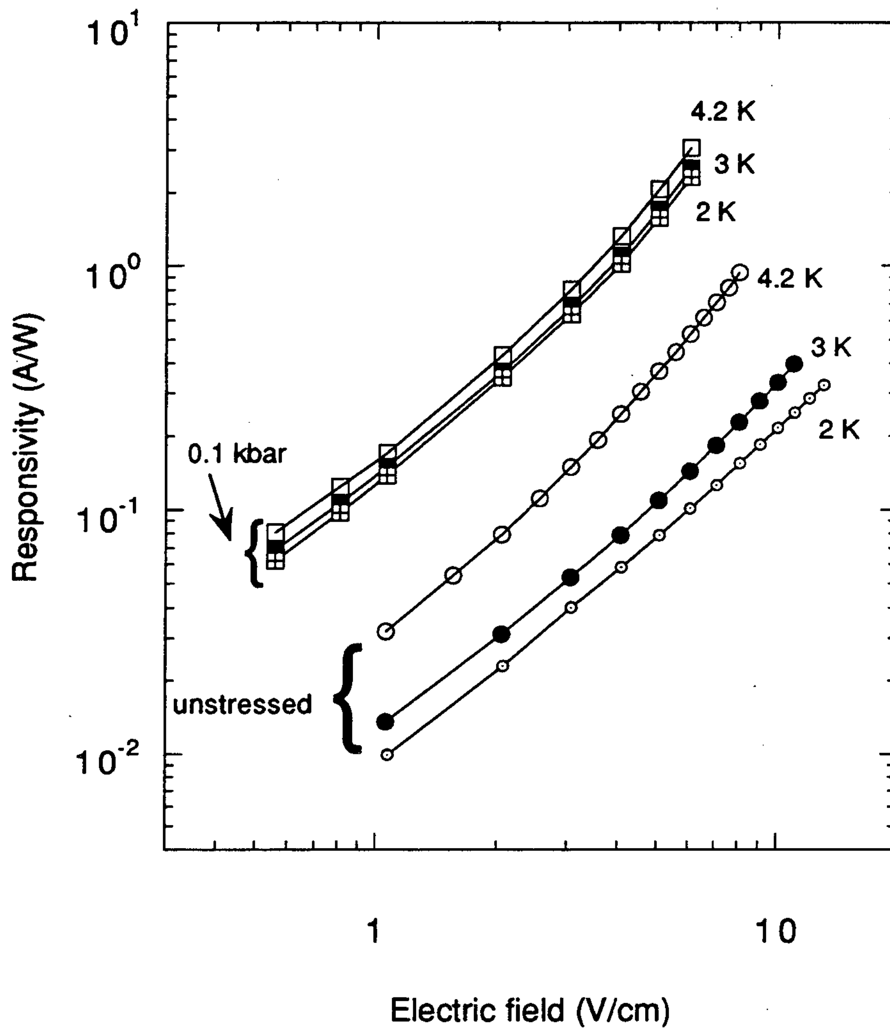

Figure 3.4. Responsivity as a function of temperature and electric field of a Ge:Be detector. Measurement conditions: 42.8 μm bandpass filter arrangement (0.79 μm bandwidth, 13% transmission), rms photon signal=3.1×10^{-12} W, background-limited NEP=1.6×10^{-16} W/$Hz^{1/2}$ (measurement courtesy of J. W. Beeman).

lifetime as the mobility at these low temperatures is dominated by a single scattering mechanism, neutral impurity scattering.

3.3 Hall and Photo-Hall measurements of Ge:Be

Beryllium doped germanium samples were obtained from a Czochralski-grown, Be-doped crystal (#728).[23,57] They were processed as described for Ge:Ga crystals (Section 2.2) with the additional steps of soaking in a 10% KCN in water solution and annealing at 700°C for 1 hour prior to processing for electrical contacts. The annealing removes Be-H acceptor complexes, which form shallow levels in Ge crystals grown in a hydrogen atmosphere.[58-60] The KCN-solution soak prevents copper from diffusing into the wafer during the annealing period.[61] Results were obtained for several states of compressive stress.

Figures 3.5 and 3.6 are plots of the hole concentration as a function of inverse temperature for two samples. The beryllium and minority (donor) impurity concentrations are approximately 1.2×10^{15} cm^{-3} and 2.4×10^{12} cm^{-3}, respectively. As was observed in the Ge:Ga system, the application of uniaxial stress reduces the activation energy for the emission of a hole from a neutral Be atom. Below 10 K the measured hole concentration is largely due to photoionization of neutral Be. From this data one sees that in the low temperature limit the hole concentration increases by more than one order of magnitude with stress suggesting a significant increase in the hole lifetime.

Unlike the photo-Hall data measured on Ge:Ga crystals, the data of the Be-doped samples indicate that the temperature dependence of the lifetime varies markedly with pressure. The lifetime shows the greatest temperature dependence at zero stress. The application of a small amount of pressure changes the temperature dependence of the concentration (i.e., lifetime) of

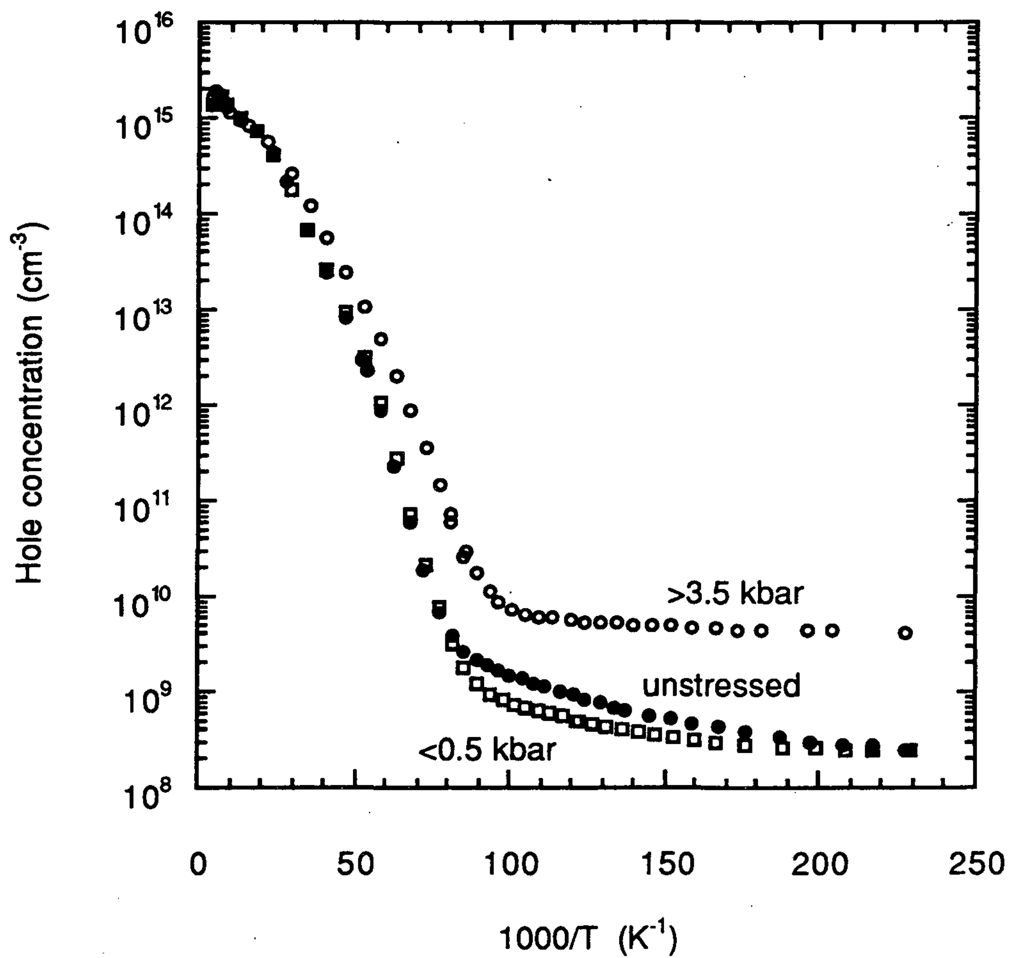

Figure 3.5. Hole concentration as a function of temperature for a Be-doped sample measured for three different pressures. Below 10 K (1000/T=100) the hole concentration is mainly determined by the photoexcitation of holes from the Be acceptors. $T_{emitter}$=77 K.

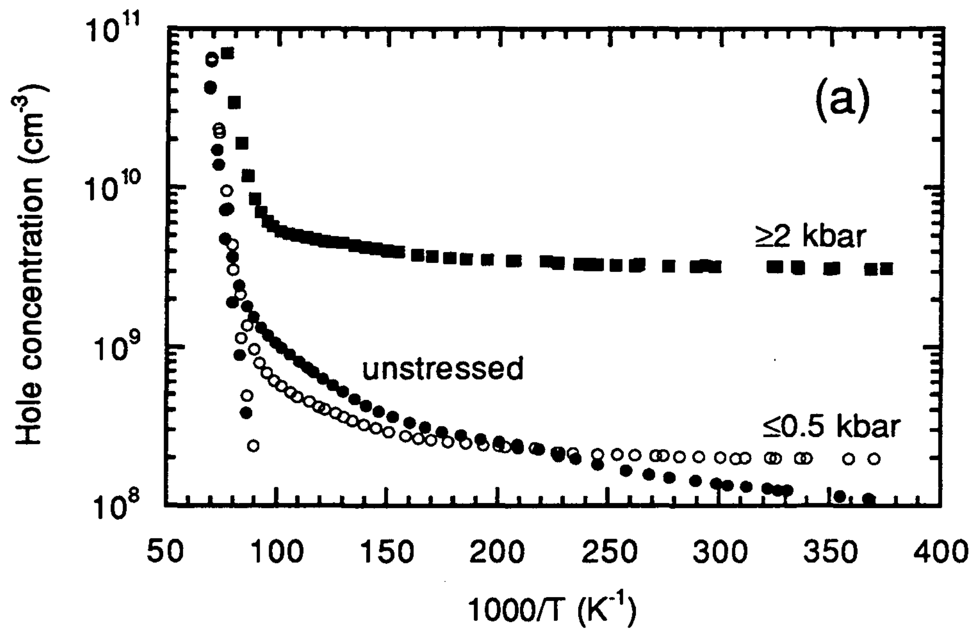

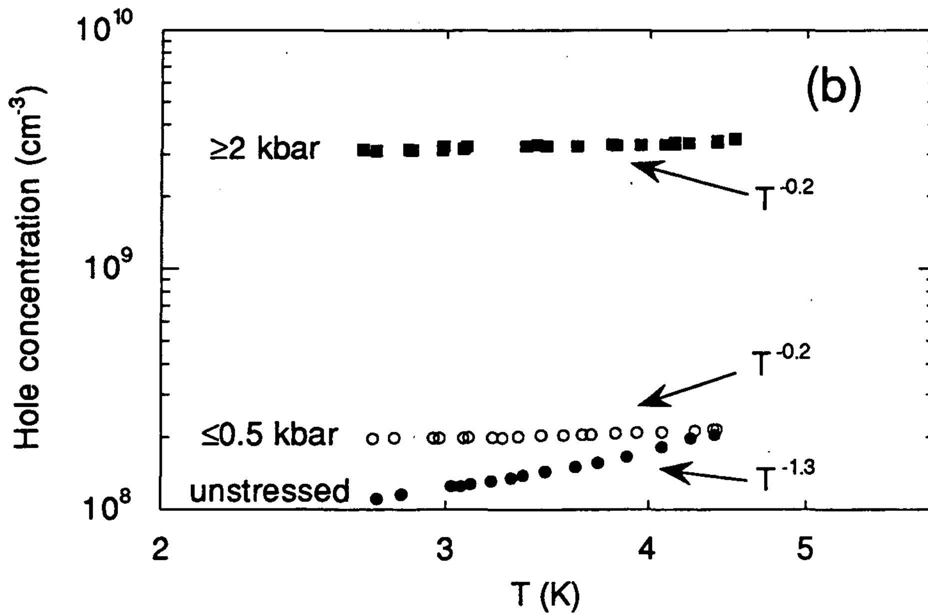

Figure 3.6. Hole concentration of Ge:Be as a function of (a) inverse temperature and (b) temperature for three states of stress. Below 6 K the concentrations measured under slightly and highly stressed conditions exhibit a similar temperature dependence; however, the additional pressure induces a significant increase in the magnitude of the hole concentration suggesting a likewise increase of the hole lifetime. $T_{emitter}$=77 K.

photoexcited holes. At a larger pressure the concentration has changed mostly in magnitude and not significantly in temperature dependence.

This previously unobserved behavior is not surprising given the pressure sensitivity in the transient response of Be-doped Ge crystals.[53,54] It has been shown that the formation of overcharged Be center produces a slow-transient response of the photocurrent to a step-function increase in the photon signal incident on Ge:Be crystals. However, the application of approximately 0.7 kbar uniaxial compression eliminates the slow-transients as the Be^{+} centers no longer form. This hole trapping phenomenon can be used to explain the photo-Hall data.

The capture of holes by neutral impurities in semiconductor was first treated by Lax in 1960.[33] Evidence for the existence of overcharged impurities were first reported by Gershenzon more than ten years later.[49] Since this time the literature concerning the role of neutral impurities in controlling the carrier lifetime has been limited in part because the binding energies associated with overcharged centers are typically rather small (< 2 meV) thus achieving relevance in the capture process only near or below liquid helium temperatures. Lax predicted a capture cross section that was inversely proportional to T and therefore a lifetime proportional to the square root of T (from Eq. 2.9). The experimentally reported lifetimes for carrier capture by a neutral impurity have had a range of temperature dependencies from $T^{1.5}$ to $T^{3.6}$.[49,62-64]

3.4 Analysis of the photo-Hall data

In order to obtain actual values of the hole lifetimes from the photo-Hall data, the optical generation rates, g_{opt}'s, must be calculated. However, the method used for the Ge:Ga data cannot be applied to Ge:Be. This is the case because, among other factors, a) there is limited information regarding the

energy dependence of the absorption coefficient of Be in Ge and b) Be-doped germanium lies in a spectral range where absorption by the bulk germanium is very strong due to optically active multiphonon modes. The flux of photons incident on the samples can be calculated, but the fraction of incident photons that are absorbed cannot.

From the photon-flux dependence of the photo-Hall data and the observed relative differences of absorption spectra, one can estimate the difference in the optical generation rates between unstressed and highly stressed samples. From this and the calculated photon fluxes (Appendix A), the optical generation rates for highly stressed Ge:Be are between 10% and 30% greater than for unstressed Ge:Be. This is largely due to the extension of the spectral sensitivity of the Be absorption to lower photon energies by the application of uniaxial stress. At low stresses, g_{opt} is assumed to have the same value as for zero stress.

Because $\tau = p_{opt} g_{opt}$, the lifetime is assumed to have the same T dependence as the concentration of photoexcited holes. The zero-stress photo-Hall concentrations of this work (e.g., Figure 3.6) show approximately a $T^{2.5}$ to $T^{1.3}$ dependence. Above 6 K, the lifetime has a stronger temperature dependence as a result of additional trapping by residual, ionized shallow impurities, an effect that is well documented for both Si and Ge.[40,59] The zero-stress temperature dependence of the hole lifetime below 6 K is attributed to the capture of holes by both singly ionized and neutral centers:

$$\frac{1}{\tau} = \frac{1}{\tau_{ionized}} + \frac{1}{\tau_{neutral}} \approx \beta v_{th}\left(N_D\, \sigma_{ionized} + N_A\, \sigma_{neutral}\right) \quad (3.1)$$

Because the concentration of neutral Be, N_A, is over 400 times larger than N_D (the concentration of ionized Be via compensation), the capture cross section for neutral centers $\sigma_{neutral}$ can be smaller than that for ionized centers ($\sigma_{ionized}$)

and still have a considerable impact on the hole lifetime. By the application of uniaxial stress, the effect of the second term in Eq. 3.1 is removed, and the lifetime is controlled by hole capture into negatively ionized Be (Figure 3.6).

Additional evidence supporting the importance of capture by neutral Be is derived from the data taken on Ge:Ga. Neutral Ga binds an extra hole with an energy ≤ 2 meV. Additionally, a typical concentration of Ga acceptors in the material tested is one order of magnitude less than that of Be-doped crystals. Therefore one would expect not to observe trapping by neutral centers in Ge:Ga. This is supported by the Ge:Ga photo-Hall measurements in which the T dependence in the limited range where photoionization dominates does not change with pressure (Fig. 2.7). Such insensitivity of the temperature dependence to small applied stresses is also evident in the responsivity data of Ge:Ga detectors (Fig. 2.4).

Because beryllium in germanium binds a third hole with a relatively large energy (about 5 meV), neutral Be plays a significant role in determining the hole lifetime at liquid helium temperatures and above. Ge doped with other double acceptors such as Zn, Cd and Hg should behave like Ge:Be because they possess relatively deep overcharged centers with binding energies equal to or greater than 4 meV.[50,65] Work in progress includes the study of mercury-doped Ge crystals; Hg has a first ionization potential of 90 meV and binds an extra hole with an energy of 10 meV! Therefore, photo-Hall measurements can be performed over a large temperature range.

3.5 Effective mass dependence of the capture cross section in Ge:Be

It is still possible to study the effect of stress on hole capture by Coulomb attractive centers. The stress dependence of the associated lifetime can be

analyzed in the range of low to high pressures rather than from zero stress; that is, the zero-stress values of the lifetime as a function of temperature will be approximated by those at a stress which is just sufficient to remove the effect of neutral impurity capture. In this case one can see that the temperature dependence for the capture cross section agrees well with that which has been previously observed for multivalent acceptors ($\sigma \propto T^{-1}$). However, the lifetime increases considerably with the application of uniaxial stress, contrary to the expected effect of stress on the direct capture model.

If the following assumptions are made, it is possible to get an effective mass dependence of the lifetime. First it is assumed that the optical generation rate is the same for both stressed and unstressed measurements. Secondly, the effective mass of the slightly stressed sample is approximately equal to that of unstressed germanium ($m^* \approx 0.3m_0$), and the highly stressed sample has an effective mass of $0.08m_0$, the value expected in the high stress limit. The observed increase in the concentration of photoexcited holes is about a factor of 15 (Fig. 3.5 and 3.6). Assuming that the capture cross section has a power law dependence on the effective mass and recalling that the hole thermal velocity is inversely proportional to the square root of m*, one can write

$$\frac{\tau_{\text{large stress}}}{\tau_{\text{small stress}}} = \frac{(\sigma v_{th})_{\text{small stress}}}{(\sigma v_{th})_{\text{large stress}}} = \left(\frac{0.3}{0.08}\right)^f \left(\frac{0.3}{0.08}\right)^{-1/2} \approx 15 \qquad (3.2)$$

where f is a constant such that σ is proportional to $(m^*)^f$. The above expression yields f=2.6. As mentioned previously the optical generation rate may be as much as 30% greater for the measurements on stressed Ge:Be compared to the zero-stress value of g_{opt}. This introduces an error less than 5% to the magnitude of f. The above results has been obtained under the assumption that the fourfold degeneracy of the valence band is lifted for all magnitudes of

stress (i.e., β=2). Thus, the cross section for the capture of holes by singly ionized double acceptors is proportional to $m^{*2.6\pm0.3}T^{-0.7}$.

3.6 A final comment Ge:Be stressed detectors

Given the above results it is possible to qualitatively explain the effect of stress on the performance of Ge:Be detectors. With zero stress the responsivity decreases with temperature due to the significant T dependence of the lifetime as capture by neutral Be controls τ. The application of small amounts of stress eliminates hole capture at neutral sites whereby capture at ionized Be centers becomes the dominant process in determining τ. This results in an increase in the hole lifetime and thus an increase in the responsivity. The magnitude by which the responsivity increases is also determined by the observed increase of the hole mobility by the application of stress. The reduced sensitivity of the responsivity to a decrease of the temperature occurs because the cross section for capture by Be^- shows a weaker temperature dependence than that for capture by neutral Be.

The weak dependence of the resposivity in stressed Ge:Be detectors has potential technological significance. It allows for these detectors to be integrated into systems that require cooling below 4.2 K (for example, far infrared telescopes having stressed Ge:Ga detectors) without suffering in performance. The performance of highly stressed Ge:Be crystals for the detection of radiation in the 50 μm-65 μm range remains to be evaluated.

4. Uniaxially stressed germanium doped with the copper triple acceptor

4.1 Copper in germanium

As a substitutional impurity copper is a triple acceptor in germanium, and in its neutral state it binds three holes with a first ionization potential of 43.2 meV. Because of the fourfold degeneracy of the valence band, the three holes populate the lowest *1s* one-particle level which as previously mentioned is analogous to having electrons of hypothetical spin 3/2 and a $(1s)^3$ ground-state configuration. Copper in germanium is unique among all impurities that introduce more than two levels in the bandgap of a semiconductor in that it exhibits in its neutral state hydrogenic, bound excited states like those of shallow acceptors.[56] Copper in silicon is also thought to be a triple acceptor in its substitutional form; however, its low solubility as a single substitutional impurity has made electrical and spectral investigations inconclusive up to now.[66,67]

Ge:Cu is a very well studied system that has yielded an abundance of information regarding the interaction of impurities to form complexes[68-70] and the diffusion of impurities in semiconductors.[61,71,72] It has been shown that substitutional copper can interact with hydrogen to form complexes that result in acceptor energy levels in the Ge bandgap.[68,69,73] Complexing between copper and shallow donors has recently been shown to produce a variety of acceptor levels as well.[70] In both cases, these levels are shallower than the hole binding energy by neutral copper (43.2 meV). Passivation of copper can be achieved by the formation of CuH_3 if hydrogen is incorporated in the germanium during crystal growth.[24] This process has been critical in the development of high purity germanium radiation detectors whereby residual ionized impurities (such

as unpassivated Cu) can trap radiation-induced mobile charge which would otherwise be collected thus degrading detector performance.[74] The effect of hydrogen passivation in semiconductors is now a well established field of great technological importance due to the wide electronic applications of semiconductor thin films synthesized by methods involving hydrogen and hydrogen-containing compounds.[75]

Copper is a fast diffusing impurity in germanium and therefore provides a serious challenge for applications requiring high purity thermal processing (or the controlled addition of impurities). At 700°C the diffusion coefficient of Cu is over seven orders of magnitude greater than that associated with shallow monovalent acceptors! It diffuses via the "dissociative mechanism" first proposed by Frank and Turnbull:[72,76]

$$Cu_s \leftrightarrows Cu_i + \text{Vacancy}$$

where Cu_s and Cu_i refer to copper in substitutional and interstitial positions, respectively. The interstitial species is extremely mobile compared to its substitutional counterpart. A substitutional copper atom moves through a crystal by switching into an interstitial position (via the above mechanism), traveling as an interstitial species, and then reassuming a substitutional position by recombining with a vacancy. Interstitial copper generally exhibits a lower solubility than substitutional copper and is a deep donor.[61]

Copper has a limited solubility which is given by[71]

$$\text{Solubility}=2.4\text{x}10^{24}\exp(-1.9\ \text{eV}/k_BT)\ \text{cm}^{-3} \qquad (4.1)$$

for temperatures up to 650°C, the Ge-Cu eutectic temperature. Above 650°C the enthalpy of solution decreases from 1.9 eV to 1.7 eV, and copper achieves a maximum solubility of $2.5\text{x}10^{16}$ cm^{-3} at 850°C, decreasing above this temperature. Because of its high diffusivity and low solubility, it is possible to

introduce Cu into germanium crystals at controlled concentrations by simple annealing treatments.

4.2 Germanium IR detectors containing copper

Although viewed as a contaminant in applications such as high-purity germanium radiation detectors, copper has been used in infrared photoconductive detector applications as itself an IR absorbing species and as an impurity used for engineering the performance of Ge:Ga detectors. Like with the Be double acceptor, germanium can be doped with copper in the 10^{15} cm^{-3} range without adversely affecting detector performance. Due to their broadband spectral response (350-2000 cm^{-1}) and low noise characteristics, Ge:Cu crystals are well suited for the detection of midinfrared photons.

Copper has also been used in the development of high-responsivity Ge:Ga detectors.[22] It has been found that the optimum concentration for Ga-doped germanium detectors is about 10^{14} cm^{-3} with a compensation of 1% (i.e., donor concentration of 10^{12} cm^{-3}). These can be operated with applied electric fields up to 3-4 V/cm beyond which device breakdown occurs mainly due to impact ionization of neutral centers by the field accelerated free holes. Because the low temperature hole lifetime and mobility, hence the detector responsivity, can be enhanced by the suppression of compensating donors, Ga-doped crystals with a compensation 0.05% have previously been studied for detector applications. A lower density of acceptors that are ionized by compensating donors raises the free hole lifetime and increases the mobility due to the reduction of the density of ionized scattering centers. However, such benefits to the responsivity by having a lower compensation are offset by the reduction of the maximum operating electric field (about 1 V/cm).

The operating bias of detectors with low compensation can be extended to higher values by the introduction of copper. Because of its high diffusivity at relatively low temperatures, copper can be diffused into germanium crystals without affecting other dopant profiles. In p-type material doped with shallow acceptors such as Ga, the substitutional copper remains neutral as the donors still partially compensate the shallow acceptors. In this case the copper enhances neutral impurity scattering therefore reducing the hole mobility, yet the lifetime remains high since no additional ionized acceptors have been introduced. The lower mobility extends the range of operating biases as the free-hole drift velocity necessary for impact ionization is reached at a higher electric field (Eq. 1.1). The results of this study are summarized in Figure 4.1.

Studies have previously been performed to investigate the effect of copper diffusion on the performance of stressed Ge:Ga detectors.[77,78] Similarly to lightly compensated crystals, stressed Ge:Ga detectors exhibit low breakdown fields (about 0.3 V/cm for a standard stressed detector) as a result of the higher lifetime and mobility. In addition, the acceptor level in stressed detectors is shallower leading to field-assisted ionization at lower applied biases. The study yielded the very interesting results depicted in Figure 4.2. In addition to having a low and unstable responsivity, the copper-containing crystal has a dark current that remains high in the 4.2-1.3 K temperature range unlike the dark current corresponding to the same crystal but without copper diffusion. The decrease of the dark current observed for the undiffused sample is caused by the freeze-out of free holes onto the ionized Ga atoms. This process occurs in the copper indiffused material as well, but an additional process must occur which results in the temperature-insensitive dark current. Because of the electrostatic repulsion between copper and gallium acceptors, it is expected that such high dark current may be related to copper alone (and not

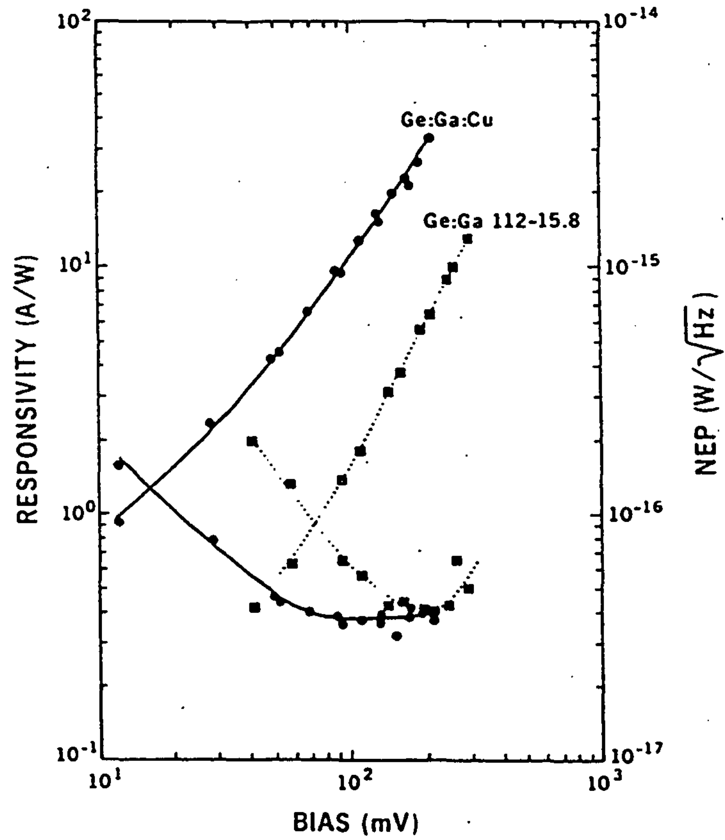

Figure 4.1. Responsivity (labeled curves) and NEP as a function of bias for a Cu-diffused Ge: Ga detector (1x1x3 mm^3, N_{Ga}=2x10^{14} cm^{-3}, N_{Cu}=10^{14} cm^{-3} and N_D≈2x10^{10} cm^{-3}) and a standard Ge:Ga detector (1x1x3 mm^3, N_{Ga}=2x10^{14} cm^{-3}, N_D≈1x10^{12} cm^{-3}) using narrow-band filters at 93 μm at T=3 K.[22]

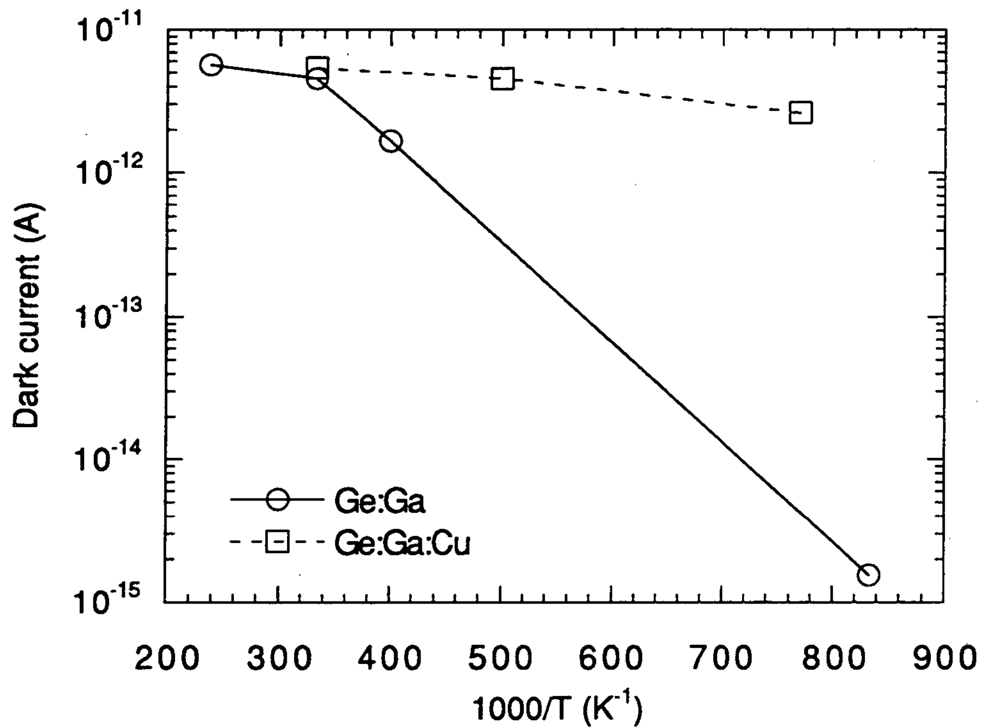

Figure 4.2. Dark current measured as a function of inverse temperature for two uniaxially stressed samples that were obtained from the same bulk Ge crystal (#751) having a Ga concentration of 5×10^{13} cm^{-3}. The applied bias for the data shown was 0.1 V/cm. For both samples the pressure was greater than 3 kbar. For the sample represented by the squares, copper was indiffused to produce approximately 10^{15} cm^{-3} additional acceptors (measurements courtesy of J. W. Beeman).

a Cu-Ga complex) and that such effects will be observed in uniaxially stressed crystals in which copper is the majority impurity.

4.3 Spectroscopy of uniaxially stressed copper doped germanium

Detailed piezospectroscopic measurements have been performed to study the electronic nature of substitutional copper, and it has been found that the excited-state structure of neutral copper in Ge is remarkably similar to that of group III acceptors.[56] This is in part because the ground state is made up of three *1s*-like single-particle (Γ_8) states whose direct product yields the same *1s*-like state (Γ_8), which also describes the ground state of group III acceptors (Fig. 2.3). The application of uniaxial stress in a [100] direction likewise reduces the symmetry of the acceptor lowest one-particle level from T_d to D_{2d} producing two, doubly degenerate energy levels (Γ_6 and Γ_7).[78] For single acceptors the bound hole is accommodated in the split level (designated Γ_7 in Fig. 2.3) that minimizes the total energy of this state. However, for triple acceptors two holes occupy the Γ_7 state while the third hole necessarily resides in the higher energy split level (designated Γ_6 in Fig.2.3) when stress is applied. Although careful copper-related piezospectroscopy studies have been reported, neither theoretical nor experimental information exists regarding the effect of *large* uniaxial stresses (such as those used for stressed Ge detectors) on Cu-doped Ge.

In order to study the effect of large, uniaxial stresses on the electronic nature of the copper triple acceptor, photoconductivity (PC) response measurements have been performed on a copper-diffused, n-type Ge wafer from a Czochralski-grown Ge crystal (#463). A 200 nm-thick Cu layer was Ar sputtered on either surface of the wafer which was then sealed under vacuum in a quartz ampule, annealed at 700 °C for 24 hours, and finally quenched in

ethylene glycol. Both sides were then lapped in a 4µm-SiC/water slurry and etched in a 3:1 $HN0_3$:HF mixture for 90 seconds. Two boron implants (25 keV/1x10^{14} cm^{-2} and 50 keV/2x10^{14} cm^{-2}) and subsequent metallization (20 nm of Pd and 400 nm of Au in this sequence) were performed for later use in the formation of electrical contacts. Thermal annealing at 300 °C for 1 hour under Ar flow followed the metallization.

The wafer was cut to produce a 1x1x6 mm^3 final geometry for each sample. All resulting surfaces were <100> oriented. Uniaxial stress was applied parallel to the long axis of the bar-shaped samples. For each sample the two electrical contacts necessary for the PC measurements were masked on one of the 1x6 mm^2 surfaces, and all excess metallization and implanted layers were removed with KBr solution (1 minute) and 3:1 HNO_3:HF (30 seconds) etches, respectively.

In addition samples from the same wafer were prepared for Hall effect measurements. The results are shown in Figure 4.3, and they indicate that he thermal treatment introduced 3x10^{15} cm^{-3} substitutional copper atoms into the Ge crystal. The expected concentration determined from Equation 4.1 is 3.9x10^{15} cm^{-3}. The compensation is given by the concentration of donors already in the crystal, estimated to be (2-6)x10^{11} cm^{-3}.

The photoconductivity response of the copper-diffused samples were measured as a function of photon energy with a far infrared Fourier transform spectrometer. A combination of warm and cold black polyethylene foils was used to block high energy photons with $\omega > 500$ cm^{-1}. A piston-lever apparatus was used for the application of uniaxial compression. The spectra were taken at a temperature above 8 K in which case there is essentially no photoconductivity response from residual group III impurities which would

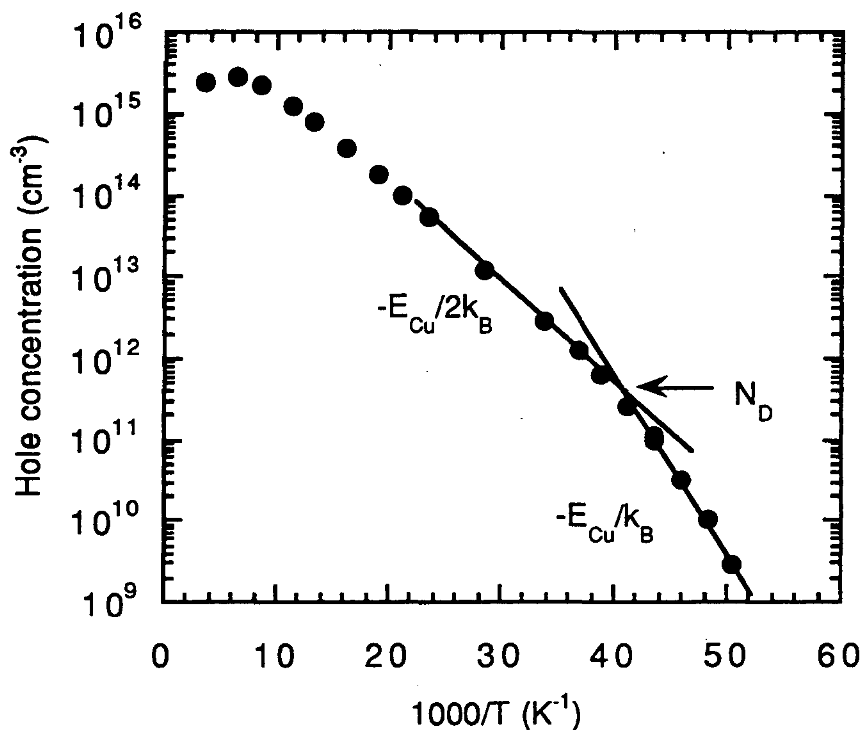

Figure 4.3. Hole concentration as function of inverse temperature of a copper-doped germanium sample obtained from Hall effect measurements. The copper was diffused at 700°C for 24 hours.

otherwise have become neutral by capturing holes that have been photoexcited from copper centers. Further experimental details are found in Appendix B.

Figure 4.4 shows a series of five photoconductivity spectra as a function of stress between 0 and 8 kbar. The threshold of the PC response in the zero-stress spectrum occurs at a photon energy of 350 cm^{-1}, as expected from previously reported data on the first ionization potential of copper. The large

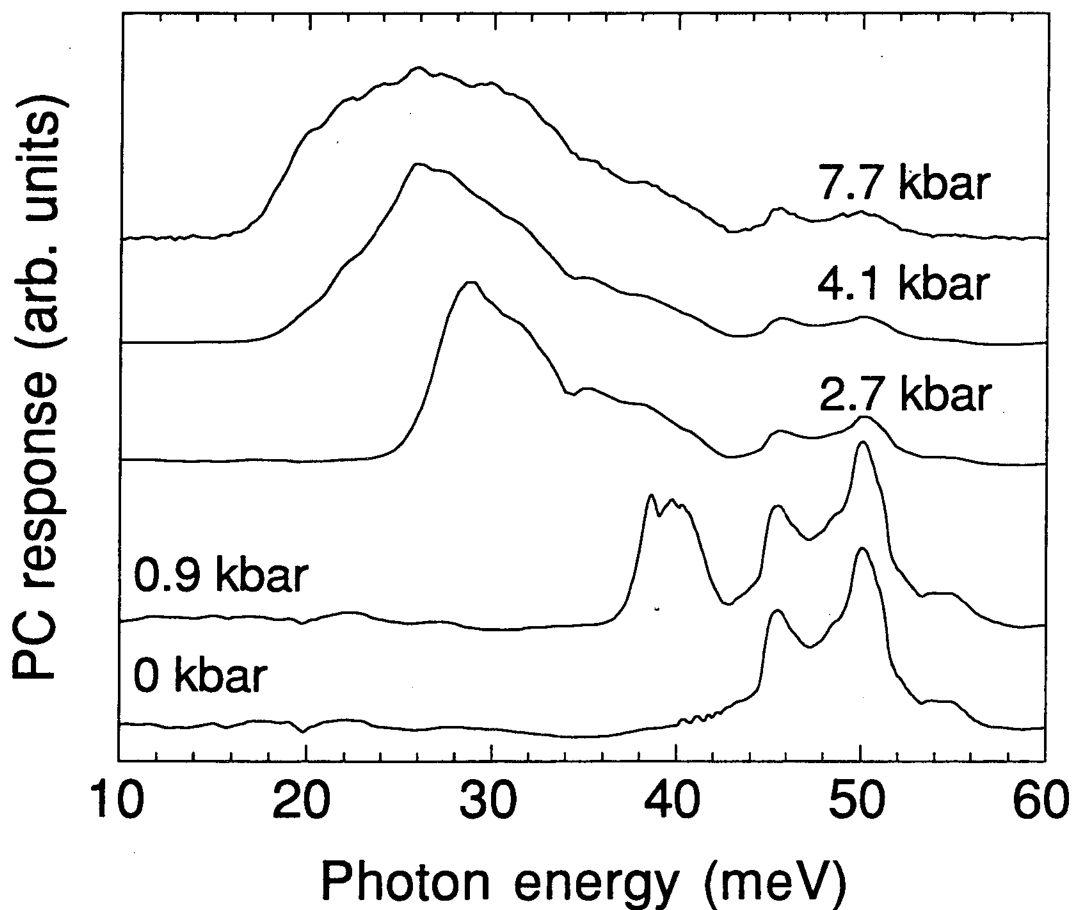

Figure 4.4. Photoconductivity (PC) response spectra as a function of stress. The shift of the PC threshold is caused by the reduction of the first ionization potential of copper with increasing stress.

dips appearing, for example, in the 350-400 cm^{-1} region are caused by absorption arising from optically active multiphonon modes (Fig. 3.3).[55,56] This coupling reduces the number of photons available for absorption by the copper centers thus decreasing the PC response. As the applied stress increases, the threshold of the PC response shifts to lower energies becoming constant at stresses above 4 kbar. The binding energy is reduced from 43.2 meV (349 cm^{-1}) to about 17 meV (137 cm^{-1}).

The energy shift of the first ionization potential is approximately 26 meV for Cu acceptors compared to 6-8 meV observed for group III and Be in Ge. The decrease of the binding energy is limited to approximately this value because the separation between the lower lying, split $1s(\Gamma_7)$ level (in which the holes reside) and the split Γ_7^+ valence band (to which the holes are excited) changes only slightly in the high stress limit (transition A in Fig. 4.5).

Copper differs from single and double acceptors by the fact that it binds *three* holes. When stress is applied and the one-particle states split, two holes are accommodated in the $1s(\Gamma_7)$ level and the third in the higher energy $1s(\Gamma_6)$ level. An increase in the stress significantly reduces the energy with which the third hole is bound since the split $1s(\Gamma_6)$ level-- which it populates-- increases in energy with respect to its zero-stress value (transition B in Fig. 4.5). Therefore, the separation between this level and the split valence band has a strong dependence on the applied stress.

At sufficiently high stresses the excited one-particle levels associated with the lower Γ_7^+ valence band should cross the $1s(\Gamma_6)$ level of the third hole. The lowest lying and thus the first excited level that crosses is the $2s(\Gamma_7)$. When the $2s(\Gamma_7)$ level is lower in energy than the upward-moving $1s(\Gamma_6)$ level, the ground state of copper reconfigures from its usual $[1s(\Gamma_7)]^2[1s(\Gamma_6)]^1$ configuration to the more stable one $[1s(\Gamma_7)]^2[2s(\Gamma_7)]^1$. The binding energy of

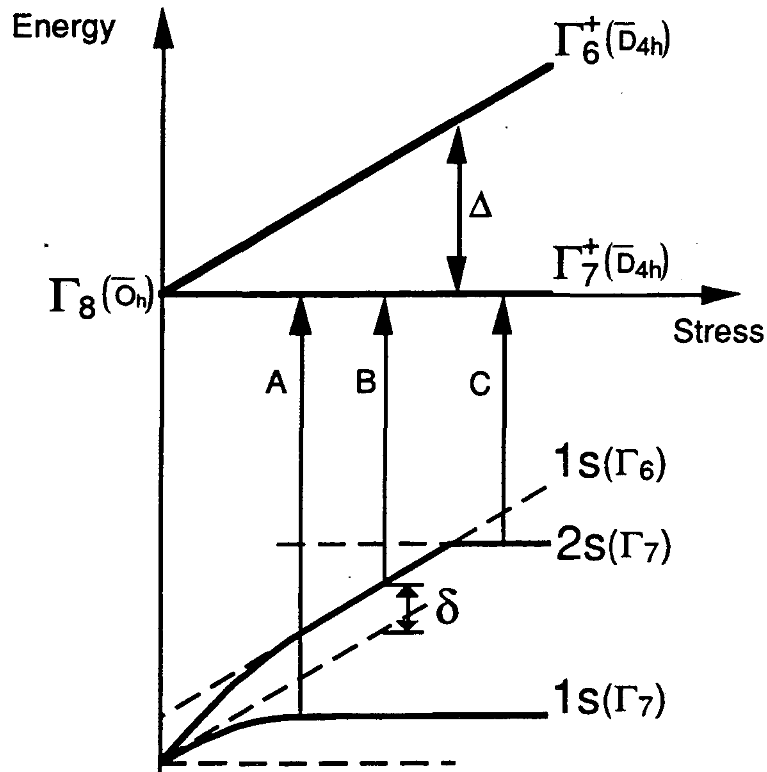

Figure 4.5. Schematic of the splitting of the valence band and the copper ground state as a function of a [100] uniaxial stress. The electronic band states change from O_h to D_{4h} symmetry while the impurity states go from T_d to D_{2d} symmetry. Transition A corresponds to that of a hole for a neutral single. Transitions B and C are those of a hole for a neutral triple acceptor such as copper.

the third *2s* hole becomes roughly constant as in the case of the bound excited Γ_7 states of shallow levels (transition C in Fig. 4.5). A conceptually similar crossing of states has been observed in the photoluminescence spectra of bound multiexciton complexes containing three holes in uniaxially stressed silicon.[79,80]

That the hole binding energy of neutral copper decreases significantly with stress had not been reported. However, evidence of this pressure-induced effect already existed for ten years. Figure 4.6 depicts two absorption spectra of copper-doped Ge measured by Salib *et al.*[56] The spectra were measured for two pressures, 0.572 kbar and 1.140 kbar. At the lower pressure an increase in the absorption coefficient occurs at a photon energy of about 40 meV (by the peak labeled C_2). The increased absorption persists at higher photon energies as if the holes were being photoexcited to a continuum of states (such as the valence band) with an absorption threshold at about 40 meV. The spectrum measured at 1.140 kbar shows a similar feature with the important difference that the threshold occurs at about 37 meV suggesting that the increase in the applied stress has shifted the onset of absorption to lower photon energies. This is very consistent with the model presented above, the absorption threshold being equivalent to transition B in Figure 4.5.

A transformation of the ground-state configuration, as described above, occurs if there is a cross-over in the minimum total energy of the system. Therefore, the pressure-dependent total energies and first ionization potentials of both configurations have been estimated by a variational calculation. A calculation of the $(1s)^3$ total energy has been performed following the method of Wu and Falicov[15] and a value of (- 8.62 + Δ) a.u. was obtained, where Δ is the splitting of the valence band as a function of pressure and the atomic unit (a.u.) for Ge is $4\pi^2 m^* e^4/\varepsilon^2 h^2$ = 22.4 meV. The $(1s)^2(2s)^1$ state was obtained from the observed lithium spectrum, by adding (in a.u.) the ionization potentials of Li^0, Li^+, and Li^{++}.[81] It yields an equivalent total energy of (- 0.20 - 2.79 - 4.50) a.u. = (- 7.49) a.u.

For either neutral ground-state configuration the removal of one hole from the neutral copper center produces a $(1s)^2$(free hole) final state, which has

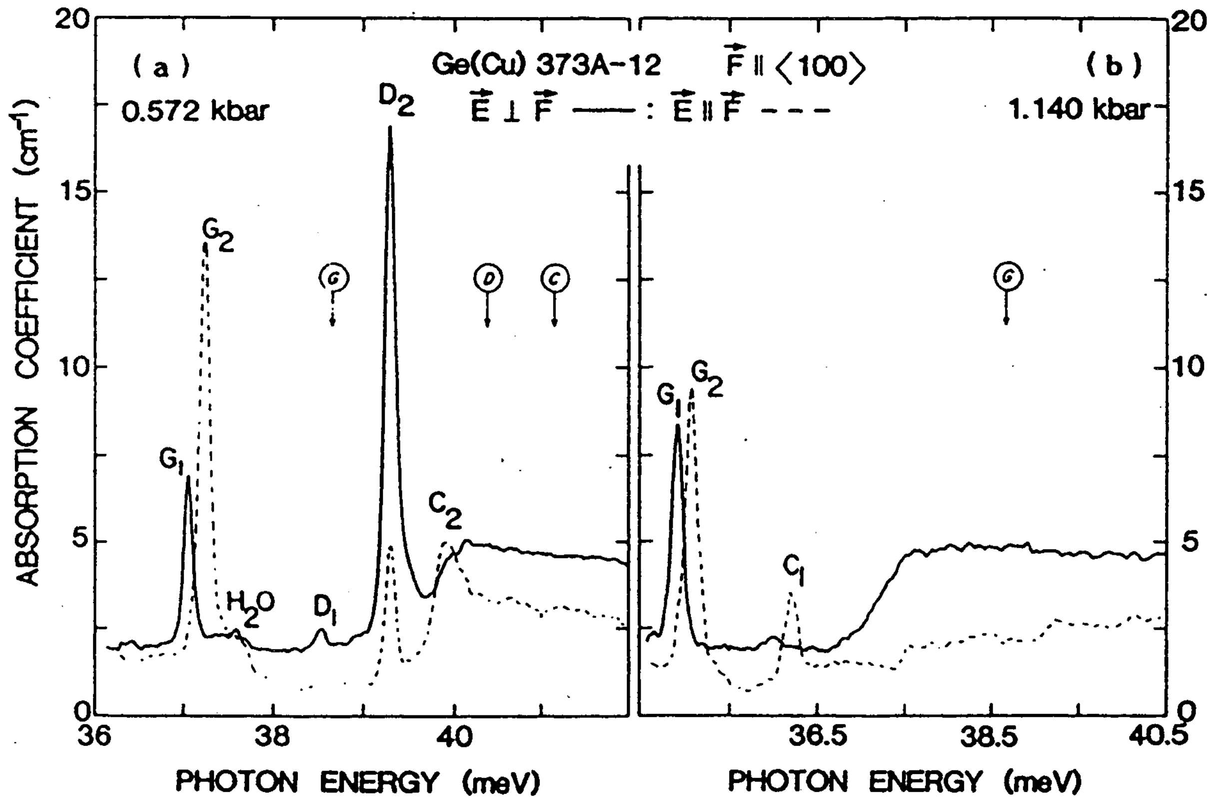

Figure 4.6. Effect of a compressive uniaxial stress **F** on the spectrum of neutral copper in germanium with **F**||<100> for a stress of (a) 0.572 and (b) 1.140 kbar cooled with liquid helium. **E** is the electric field of the radiation. Copper was diffused at 730°C; $N_{Cu}=4.7\times10^{15}$ cm^{-3}. The encircled letters with their associated arrows designate the zero-stress absorption lines.[56]

an energy of (- 2.79 - 4.50) a.u. = (- 7.29) a.u. Thus, one arrives at the first ionization potentials (IP's): IP[$(1s)^3$] = (1.33 – Δ) a.u. and IP[$(1s)^2(2s)^1$] = 0.20 a.u. Because the final state is the same in both cases, the cross-over from the $(1s)^3$ to the $(1s)^2(2s)^1$ ground state occurs at the pressure for which the ionization potentials are equal.

The experimentally observed, zero-stress value of IP[$(1s)^3$] is 43.2 meV compared to the calculated value 29.8 meV. The difference between these two is the central cell correction, 13.4 meV = 0.60 a.u. The central cell correction of the $(1s)^2(2s)^1$ configuration, estimated from the variational values of the wavefunctions at the Cu site, increases IP[$(1s)^2(2s)^1$] by 12.9 meV = 0.58 a.u. Therefore, the $(1s)^2(2s)^1$ configuration becomes the stable one for $\Delta > 1.15$ a.u. = 25.8 meV, and the central-cell adjusted values of the ionization potentials are

$$\mathrm{IP}[(1s)^3] = (43.2 - \Delta)\ \mathrm{meV}$$

valid for $\Delta < 25.8$ meV, and

$$\mathrm{IP}[(1s)^2(2s)^1] = 17.4\ \mathrm{meV}$$

valid for $\Delta > 25.8$ meV. The reader is referred to Appendix C for a more detailed description of the calculation.

Figure 4.7 is a plot of the measured binding energy of the outer hole as a function of stress. The binding energy was measured from spectra such as those in Fig. 4.4 and was evaluated at the photon energy at which the onset of the PC threshold occurs. The valence band splitting (Δ) was determined from the equation

$$\Delta = 2\ b\ (S_{11} - S_{12})\ T \quad ,$$

where T is the applied stress, b is a deformation potential, and S_{11} and S_{12} are elastic constants. For germanium b has a value 2.4 eV while S_{11} and S_{12} are equal to 9.6×10^{-4} kbar^{-1} and -2.6×10^{-4} kbar^{-1}, respectively.[82,83] Therefore,

$$\Delta = (6\ \mathrm{meV/kbar})\ (\text{applied stress in kbar}).$$

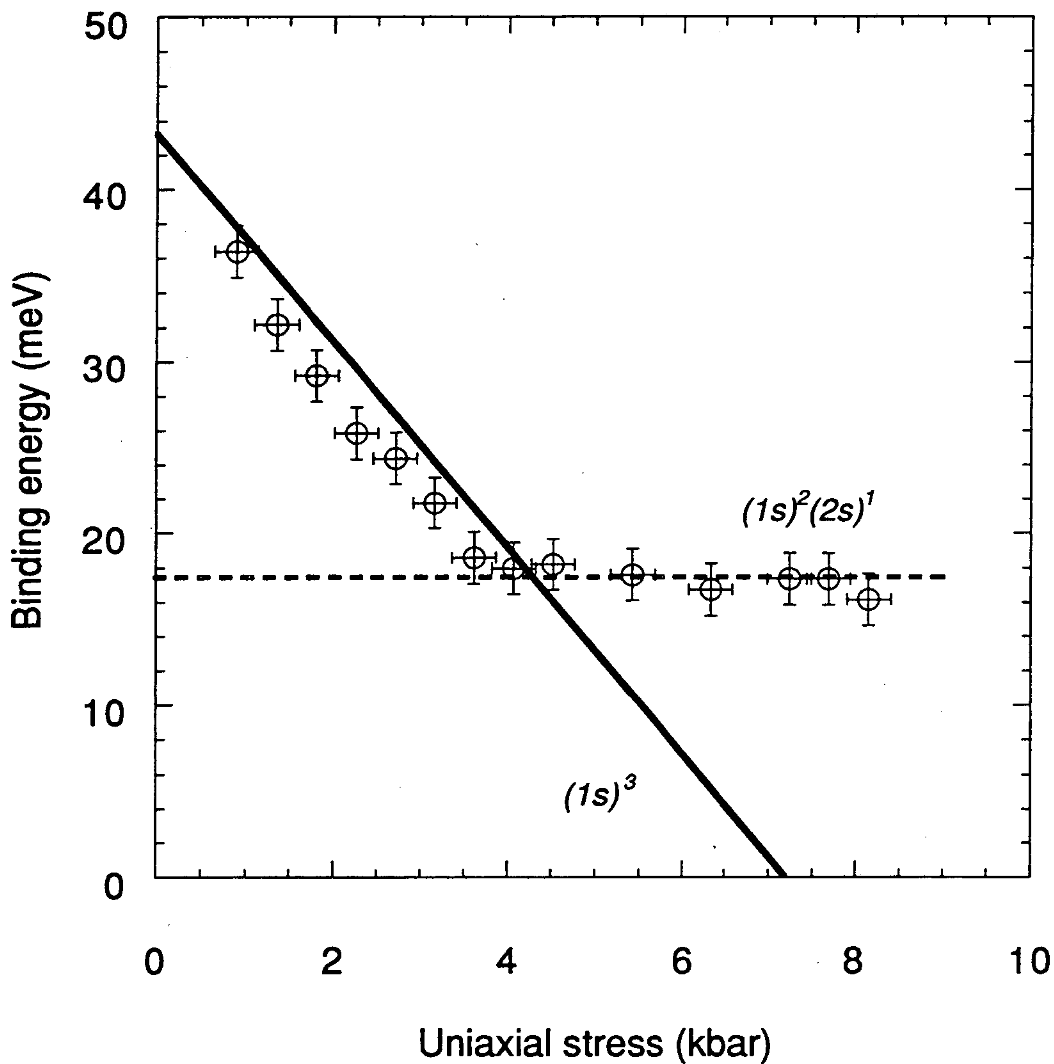

Figure 4.7. Measured and calculated binding energies as a function of stress. The experimental points were determined from the PC response spectra. Above a pressure of 4 kbar, the experimental binding energies cease to depend on stress. This is in strong agreement with the stress dependence of the calculated ionization potentials (straight lines); above 4.3 kbar the ground state of the neutral copper acceptors changes from a $(1s)^3$ to a $(1s)^2(2s)^1$ configuration, the latter having a stress-insensitive first ionization potential.

The lines represent the binding energies (i.e., the IP's) obtained from the variational calculations.

Deviation between the experimental results and the *(1s)*^{3}-calculated line results from the approximation made in the calculations that the splitting of the *1s* energy level equals the splitting of the valence band. Although appropriate for large stresses, this approximation is not valid at low stresses (below 1 kbar) for which the observed ground-state splitting is 3 meV/kbar. Therefore, the calculated IP's are slightly larger than the actual values by an amount δ (as indicated in Fig. 4.5) and IP[*(1s)*^{3}] = $43.2-\delta-\Delta$. Nevertheless, the data presented in Fig. 4.7 agree very well with the calculated values in two important features: 1) the stress at which the configurational transformation should occur and 2) the magnitude of the IP subsequent to the transformation.

Variational calculations indicate that two distinct sets of bound excited states (one set for each configuration) should be observable (Appendix C). Up to now PC measurements have not revealed such states. That the excited-state intensities of neutral copper in Ge vanish even at low stress is well documented.[56] However, this behavior is unlike that of shallow acceptors whose spectra show a set of bound excited states even at stresses as high as 6 kbar. The origin of the vanishing of the bound excited states in spectra of uniaxially stressed Ge:Cu is not known. It seems that inhomogeneity in the applied stress is not sufficient to explain the disappearance of these lines.

The pressured dependence of the photoconductivity behavior of Cu-doped germanium is indeed very dramatic. However, this alone does not explain the high dark current observed in uniaxially stressed, copper-diffused, Ge:Ga single crystals (Figure 4.2). Because of its weak temperature dependence and the relatively large hole binding energy of substitutional copper compared to that of shallow acceptors even at large stresses, the dark

current is not expected to be mainly due to free holes that remain thermally excited in the valence band from the copper centers. Rather it probably occurs by some other impurity-related conduction mechanism in which the extended nature of the copper wavefunctions plays a significant role.

4.4 Electronic conduction in doped semiconductors

The conductivity, σ, of a moderately to heavily doped semiconductor is described by[17]

$$\sigma=q\mu n+\sigma_2+\sigma_3 \qquad (4.2)$$

where the first term is the contribution from free carriers (electron/holes) and σ_2 and σ_3 are of the form $\sigma_i=\sigma_{0i}\exp(-\varepsilon_i/k_BT)$. The second and third terms result from conduction via impurity states, or impurity conduction, and are usually observed in crystals with high dopant concentrations and at temperatures low enough that most carriers populate the impurity states (and not the valence or conduction band). Although both σ_2 and σ_3 depend on the majority dopant concentration, only one term (traditionally designated σ_3) depends on the density of compensating minority impurities as well.

Figure 4.8 shows the resistivity of a series of Ge:Sb crystals as a function of inverse temperature.[84] The antimony concentration varies from 5.3×10^{14} cm^{-3} to 9.5×10^{17} cm^{-3}. At the lowest concentration the resistivity exhibits a strong temperature dependence that is associated with electrons in the conduction band. The freeze out of these electrons onto the Sb donors results in the resistivity increase as fewer electrons are available for conduction within the conduction band. This process is represented in Eq. 4.2 by the first term where the carrier concentration n is proportional to $\exp(-E_{Sb}/2k_BT)$ in the "half-slope" region and $\exp(-E_{Sb}/k_BT)$ in the "full-slope" region, E_{Sb} being the ionization energy of the Sb donors.[42]

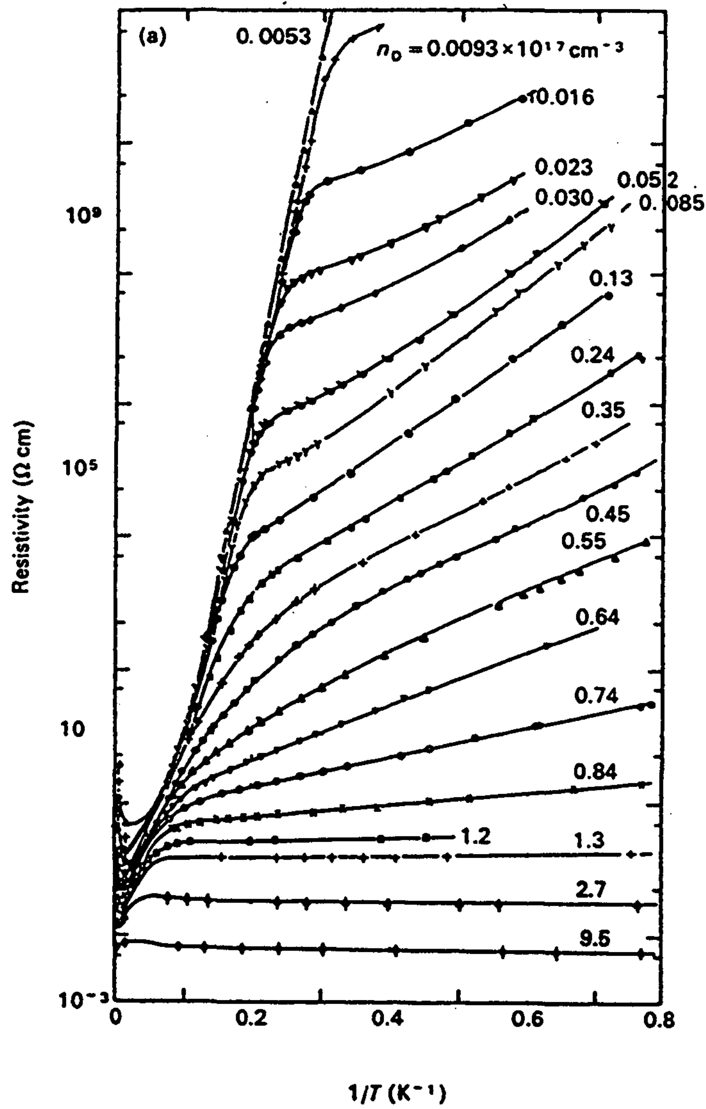

Figure 4.8. Temperature dependence of the resistivity of antimony-doped germanium for various concentration regimes (after Fritzsche *et al.*).[84,85]

With an increase in the antimony concentration an additional conduction process occurs at lower temperatures and appears in Figure 4.8 as a weakening of the temperature dependence of the resistivity. At a sufficiently low temperature, the thermal energy is not enough to ionized the Sb-bound electrons yet is sufficient to allow a bound electron to hop from an occupied Sb donor (Sb^0) to an empty Sb donor (Sb^+). At the lowest concentration the Sb atoms are sufficiently separated that this hopping process cannot occur. However, an increase in the Sb concentration results in the overlap of the donor wavefunctions due to the large Bohr radii of shallow dopants making this phonon-assisted hopping process possible. Hopping conduction gives rise to σ_3 in Equation 4.2 where $\varepsilon_3 < E_{Sb}$. This conduction mechanism requires the presence of compensating minority impurities. In the example of Ge:Sb, the presence of acceptors produces a concentration of ionized donors through the compensation process irrespective of the temperature thus providing Sb sites into which electrons can hop. This process is schematically shown in Figure 4.9. Hopping conduction has been extensively studied for many years, and its understanding is of fundamental and technological interest for the development of bolometric detectors for astrophysics and condensed matter research.[86-88]

At yet higher concentrations (>3.5×10^{16} cm^{-3} in Figure 4.8) the third conduction process, "ε_2 conduction," becomes significant. This mechanism is characterized by an activation energy that decreases strongly with increasing concentration. At a critical concentration, n_c, ε_2 vanishes and the resistivity becomes essentially temperature independent similarly to a metal. For Ge:Sb this transition in the resistivity behavior from non-metal-like to metal-like, also known as the metal-insulator (MI) transition,[85,89] occurs at a critical concentration n_c of approximately 1.2×10^{17} cm^{-3} as shown in Figure 4.8. Unlike

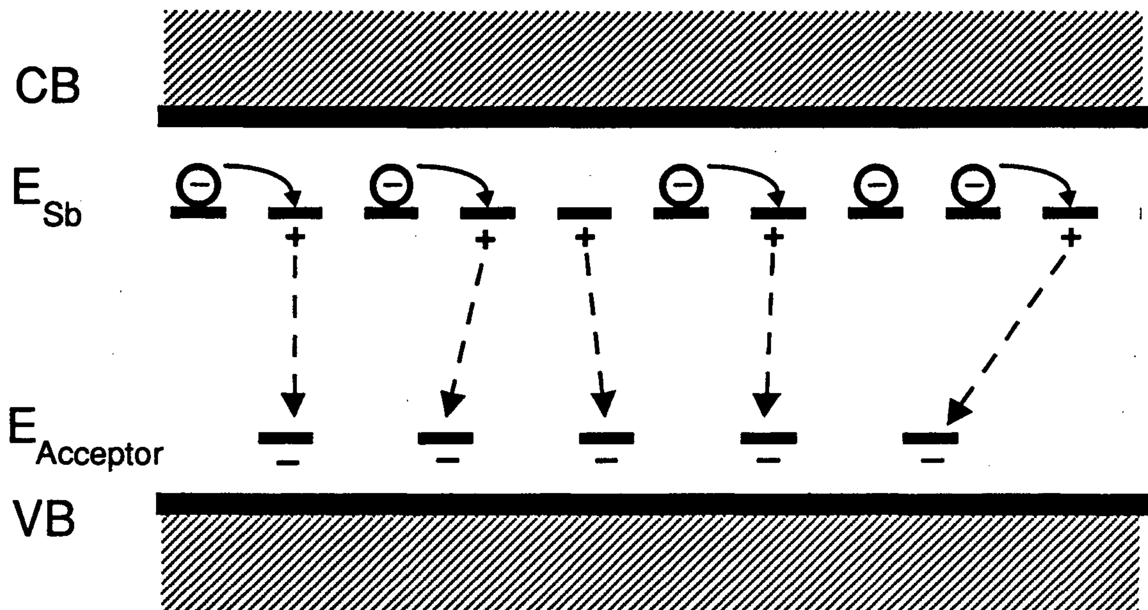

Figure 4.9. Schematic energy level diagram of n-type germanium doped with antimony. The antimony level is partially compensated by acceptors (dashed arrows) allowing for conduction of bound electrons by the hopping conduction mechanism (continuous arrows). CB and VB indicate the conduction and valence bands, respectively.

hopping conduction, ε_2 conduction depends only on the majority and not the minority impurity concentration, and its origin will be discussed in greater detail later.

4.5 Electronic conduction in uniaxially stressed Cu-doped Ge

From Figure 4.2 and the dopant profile of the related crystal, one can already speculate that ε_2 conduction is the most likely source of the high dark current observed in uniaxially stressed, Cu-indiffused Ge:Ga crystals. First, the dark current is proportional to σ, and it shows only a weak temperature dependence as in the case of moderately-to-heavily doped Ge:Sb. Secondly

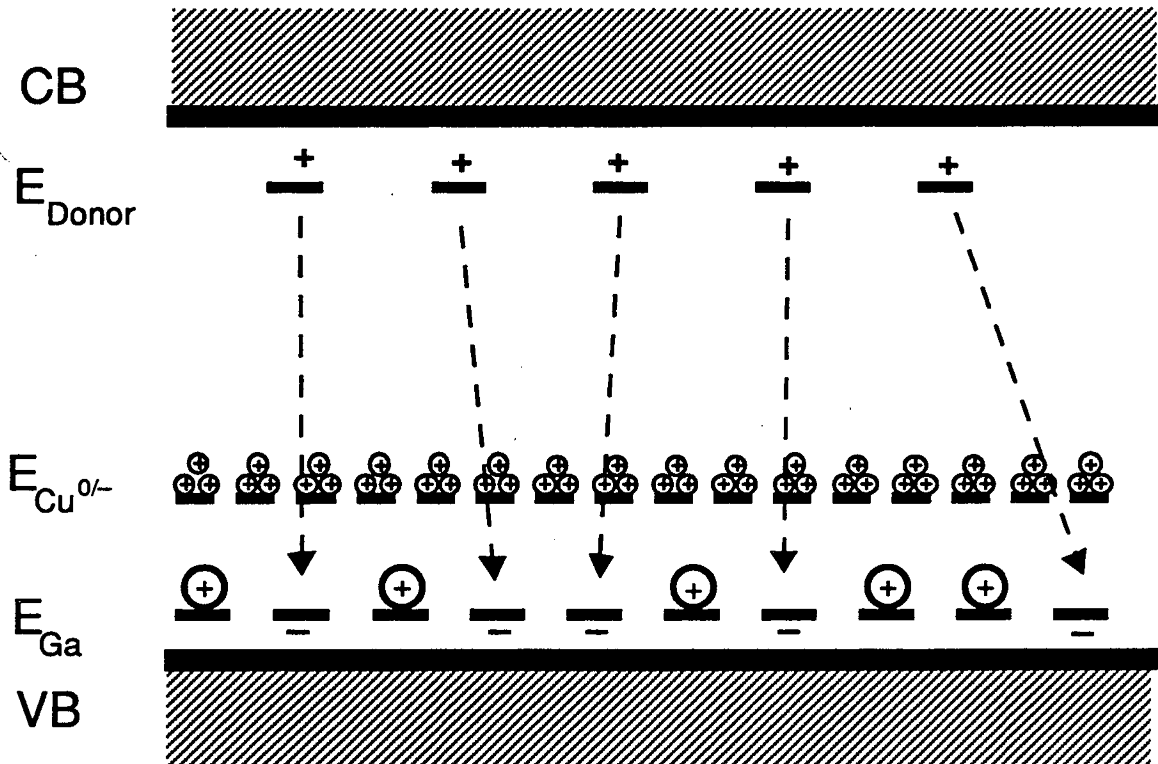

Figure 4.10. Schematic energy level diagram of copper-diffused Ge:Ga. The gallium acceptors are partially compensated by donors while the copper acceptors remain neutral.

and more importantly, the crystal for which the dark current is shown in Fig. 4.2 has a multilevel dopant profile in which the Ga acceptors are partially compensated while the substitutional Cu atoms remain neutral at liquid helium temperatures (Figure 4.10). Therefore, the low temperature conduction observed in Figure 4.2 is related to *uncompensated* copper acceptors!

4.5.1 Experimental approach and results

Experiments designed to investigate the nature of impurity conduction in uniaxially stressed Ge:Cu are currently in progress. These include two- and

four-point resistivity and Hall effect measurements. Table 4.1 lists the three crystals that have been tested and the characterization technique thus far used to study uniaxially stressed samples. The third column refers to the net shallow dopant concentration of the crystal prior to copper diffusion. That is, crystals #1 and #2 were n-type (hence the "-" sign) prior to copper diffusion while #3 was p-type. Therefore, the copper acceptors are partially compensated in crystals #1 and #2 and uncompensated in #3.

Crystal #	N_{Cu} (cm^{-3})	$(N_A-N_D)_{shallow}$ (cm^{-3})	Characterization
1	$3x10^{15}$	$-4x10^{11}$	4 pt. resistivity, Hall effect
2	$6x10^{13}$	$-4x10^{11}$	2 pt. resistivity
3	$3x10^{15}$	$4x10^{10}$	2 pt. resistivity

Table 4.1

Figure 4.11 shows the resistivity (2 pt. measurement) versus pressure for crystals #2 and #3. The data have been evaluated by the method described in Appendix C, using a transimpedance amplifier for the higher pressure measurements and a integrating amplifier for stresses that yield a sample resistance greater than 10^{10} Ohm. Pressure was applied to 1x1x1 mm^3 samples with a standard stressed-detector mount.[90] With this technique measurements could be performed in low background conditions, but the applied stress could not be precisely determined as indicated by the error bars.

The resistivity has been measured as a function of temperature (Fig. 4.12) for a sample of dimensions 2.5x3x10 mm^3 obtained from crystal #2 with uniaxial stress applied parallel to the long axis of the crystal. The

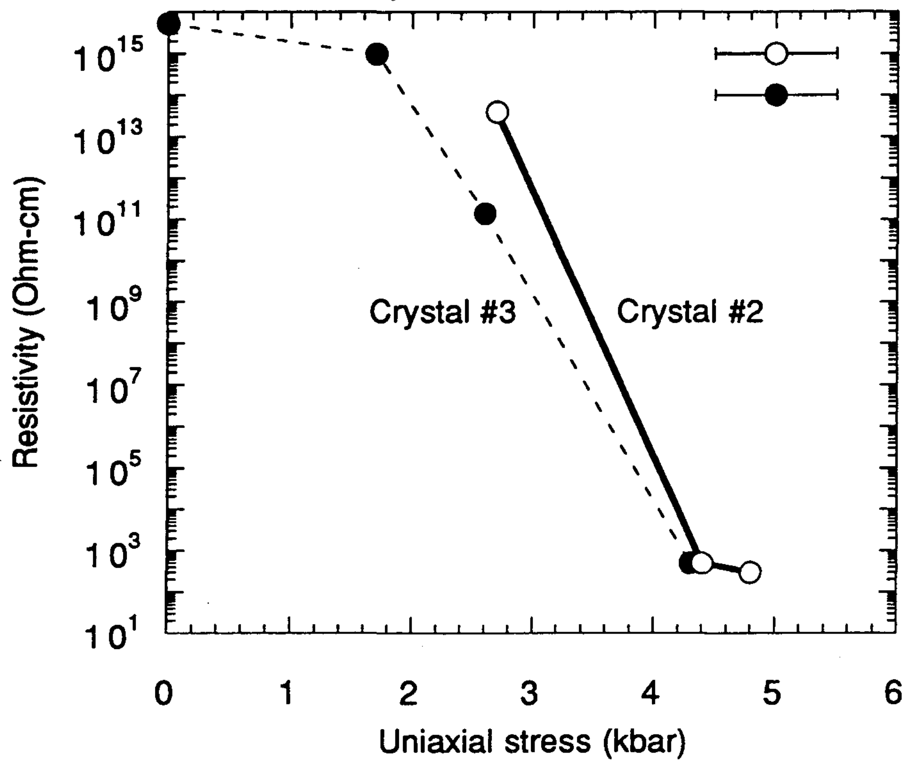

Figure 4.11 Two-point resistivity as a function of uniaxial stress for crystals #2 and #3.

measurements allowed for the precise determination of the stress but could be made only for sample resistances in the range 10^1-10^8 Ohm. A constant voltage of 150 mV was applied across the sample, and a Keithley 617 electrometer was used to measure the current through the sample. The weakly pressure-dependent resistivity is due to holes that have been photoexcited into the valence band by stray radiation as elucidated by Figure 4.12 (b).

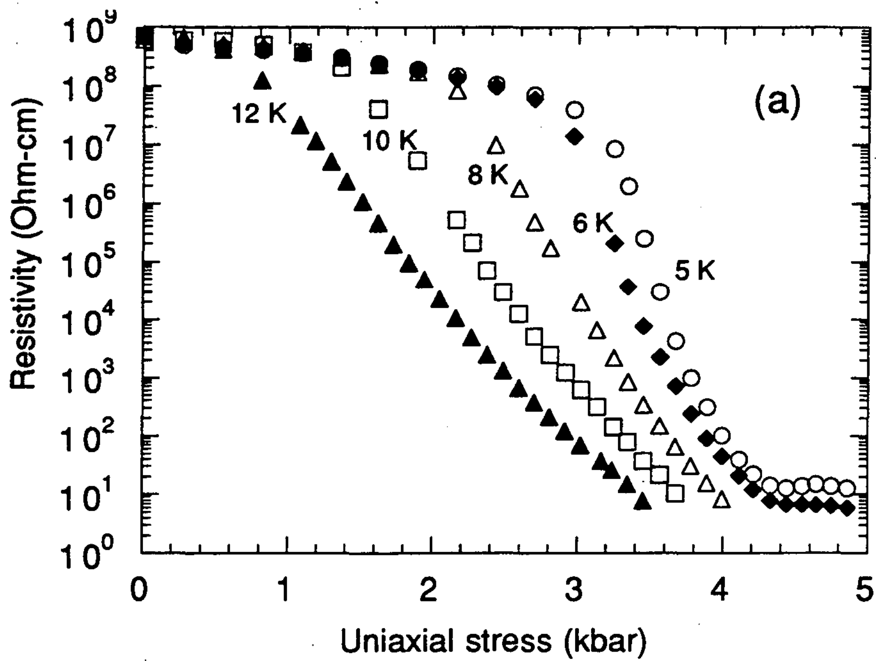

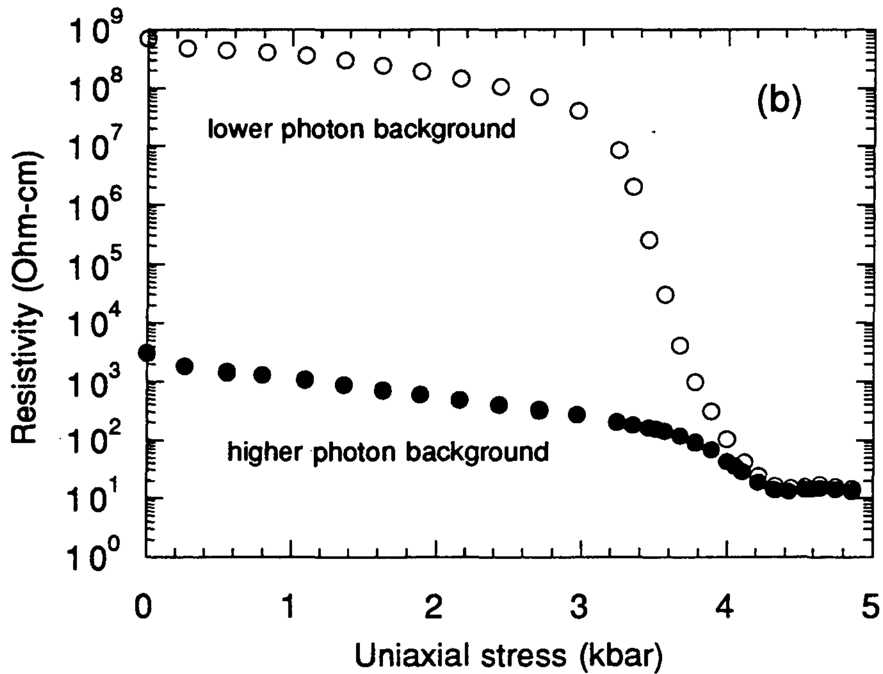

Figure 4.12. Two-point resistivity as a function of uniaxial stress measured (a) at different temperatures and (b) at 5 K for two different photon backgrounds.

Although not as reliable a method as the four-point technique, the two-point resistivity measurements still provide significant general information. First, Figure 4.11 shows that the application of uniaxial pressure results in a reduction of the sample resistivity of many orders of magnitude. Second, the stress-induced increase of the resistivity is most pronounced in the range of 2 to 4 kbar. From Figure 4.12 (a) one sees that raising the temperature broadens the strong decrease in resistivity toward lower stress suggesting that holes can be thermally excited into this conducting state and that pressure controls the magnitude of the activation barrier. In the low temperature limit a threshold for conduction may occur at a pressure above which the crystal is highly conducting and below which it is highly resistive similarly to an MI transition.

The data in Figure 4.12 suggest that a "critical" stress lies near 4 kbar. This is in the pressure range for which IR spectroscopy (Section 4.3) has revealed a change in the ground-state configuration of the copper triple acceptor. Such a change in the acceptor one-particle wavefunction can help explain the dramatic change in the impurity conduction process that would result in the behavior shown in Figures 4.11 and 4.12. Below the ground-state transition, the $(1s)^3$-like acceptor wavefunctions do not overlap enough to cause substantial impurity conduction. A stress-induced change to a $(1s)^2(2s)^1$-like ground-state is accompanied by a significant increase in the Bohr radius. The *2s*-like acceptor wavefunctions overlap due to their extended nature leading to ε_2 conduction (Figure 4.13).

4.5.2 Hopping conduction in Ge:Cu

Impurity conduction occurs in semiconductors doped at a high enough concentration that wavefunction-overlap facilitates the motion of carriers through the impurity states without them having to enter the valence or

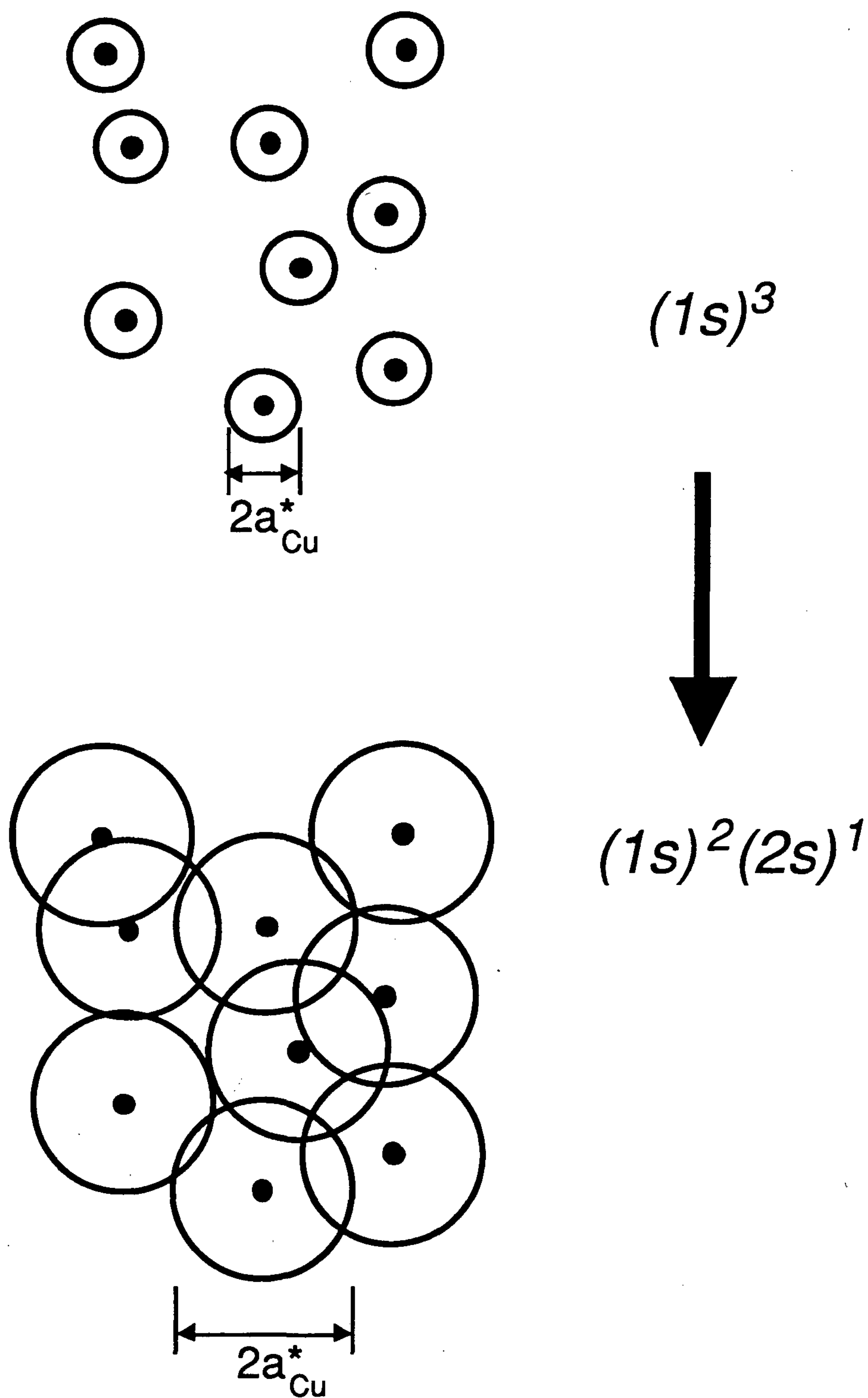

Figure 4.13. Schematic representation of Bohr radii for the two ground-states of neutral copper acceptors. The stress-induced ground-state transformation results in an increase of the Bohr radius associated with the 2s-like wavefunctions.

conduction band. Figure 4.8 shows that already at an antimony concentration of 9.3×10^{14} cm^{-3} hopping conduction in Ge:Sb is observed. The metal-insulator (MI) transition associated with ε_2 conduction occurs at an antimony concentration that is over three orders of magnitude greater. The Bohr radius of Sb in Ge is about 46 Å, which is within a factor of three of 126 Å, the approximate distance between Sb atoms at the MI transition, d_{MI}, where $d_{MI} \approx (3/4\pi N_{Sb})^{1/3}$.

Neutral copper binds holes with an energy that is more than four times greater than the electron binding energy of Sb (E_{Sb}=10.2 meV). The Bohr radius associated with copper, a_{Cu}, is equal to $(E_{Ry}/E_{Cu})^{1/2}a^*$, where E_{Ry} is the Rydberg energy for Ge (equal to 11.2 meV), E_{Cu} is the hole binding energy of neutral copper acceptors (equal to 43.2 meV), and a^* is the effective Bohr radius of a hydrogenic shallow acceptor in Ge (equal to 40 Å). The square root term is the central cell correction to the effective Bohr radius.[91] Using these values, one can estimate the magnitude of a_{Cu} to be 20 Å, half the size of a^*! Because of the low solubility (~10^{17} cm^{-3}) and the small Bohr radius of copper acceptors, a metal-insulator transition has not been observed in Ge for which copper is the majority dopant.

Evidence that copper acceptors have so small a Bohr radius was observed in a study by Rollin and Russell where they investigated impurity conduction in copper-doped germanium.[92] They observed that the density of substitutional copper is ten times higher than the shallow acceptor concentration required to produce the same resistivity in Ge. From their analysis of the resistivities in the hopping conduction region for a series of Ge:Cu samples, they estimated a_{Cu} to be half the size of a^*. However, observation of hopping conduction over an extended temperature range was not achieved in samples with copper concentrations less than 7×10^{15} cm^{-3}. At

this concentration the onset of hopping conduction occurred at a sample resistivity in the 10^9 Ohm-cm range. An onset of hopping at this sample resistivity corresponds to an acceptor concentration of 8×10^{14} cm^{-3} in Ge:Ga.[86]

4.5.3 ε_2 conduction in doped semiconductors

A neutral donor can capture an extra electron becoming negatively charged (D^- state). The extra electron is only weakly bound and resides in a large orbit about the donor impurity. Because shallow levels have spatially extended wavefunctions associated with both the *1s*-like and overcharged states, dopant concentrations can easily be reached whereby the neighboring dopant levels interact with each other and broaden into impurity bands as in a tight-binding approach. The resulting quasi-particle density of states is schematically shown in Figure 4.14. With increasing concentration the two impurity-related bands begin to overlap, and finally they merge with the conduction band at a sufficiently high concentration.

Mott first proposed that the activation energy associated with ε_2 conduction was related to the energy required to move an electron from one neutral center to another, this energy essentially corresponding to the energy gap between the D (lower Hubbard) and D^- (upper Hubbard) bands.[89,93-95] The energy ε_2 is determined by the electron-electron interaction energy, or 'Hubbard U,' between the two electrons of the overcharged donor:

$$U=\iint |\Psi(\mathbf{r}_1)|^2|\Psi(\mathbf{r}_2)|^2(q^2/4\pi\varepsilon_0\varepsilon_r \mathbf{r}_{12})d\mathbf{r}_1 d\mathbf{r}_2$$

where $\Psi(\mathbf{r}_1)$ and $\Psi(\mathbf{r}_2)$ are the 1s-like envelope wavefunctions for the two electrons of opposite spin and $\mathbf{r}_{12}$ is the inter-electron distance. In this picture, the metal-insulator transition, or Mott transition, occurs when the Hubbard U equals the average bandwidth, B, of the upper and lower Hubbard bands (i.e.

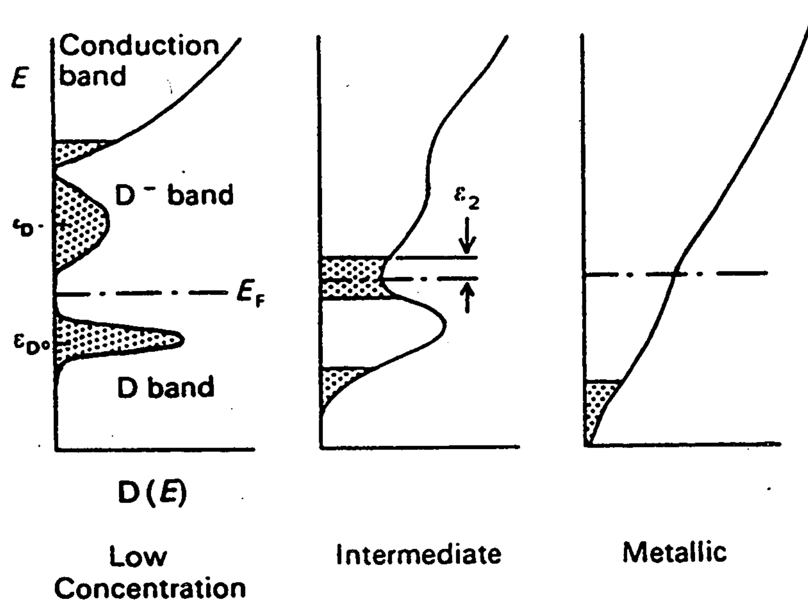

Figure 4.14. Schematic density of states for various donor concentrations. Shaded regions represent localized states. When there is one electron per donor on average (the half-filled case), the D band is just full with E_F in between the two bands.[85]

when the two bands merge). For impurities distributed in a periodic arrangement (of spacing *a*), $B \approx 2zI$ where z is the coordination number (equal to 6 for a simple cubic lattice). *I* is the overlap integral between electrons of neighboring donor centers:

$$I = \int |\Psi(|\mathbf{r}-\mathbf{a}|) H \Psi(|\mathbf{r}|) d\mathbf{r}$$

where H is the Hamiltonian. It has been shown that for wavefunctions of the form $A\exp(-\mathbf{r}/a^*)$, the overlap integral yields $I \approx 5E_{Ry}\exp(-a/a^*)$ while $U \approx (5/8)E_{Ry}$. Equating B with U and setting the inter-donor distance *a* equal to $n_c^{-1/3}$, one

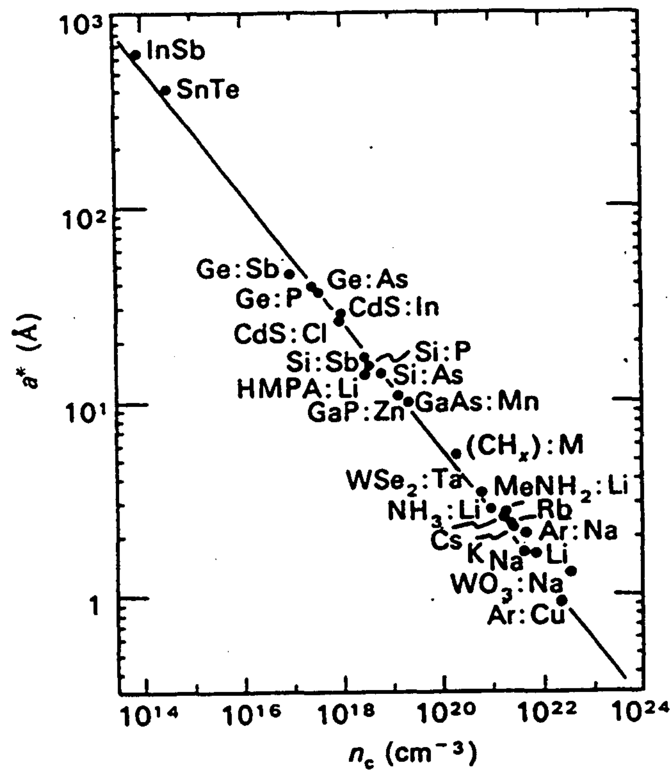

Figure 4.15. Effective Bohr radius, a*, plotted against the critical concentration of donors, n_c, for various systems. The straight line represents $n_c^{1/3}a^*=0.26$ (after Edwards *et al.*[96] and Mott *et al.*[97]).[85]

arrives at the relation for dopants distributed in a simple cubic arrangement: $n_c^{1/3}a^*=0.23$.

Figure 4.15 is a plot of a* versus critical concentration for a wide range of semiconductors. Remarkably the entirety of the data is well modeled by the relation $n_c^{1/3}a^*=0.26$. This is in good agreement with Mott's model for the MI transition in semiconductors. However, it is now more widely accepted that ε_2 conduction arises from a) the electron-electron interaction within an impurity center as described above and b) Anderson localization of the electrons.[98]

Anderson showed that the electron wavefunctions of a system of random potentials can become localized. Mott proposed that heavily doped semiconductors are an example of Anderson localization because the random distribution of donors leads to variations in the donor potential as each donor has a different local environment due to the randomness. Localization occurs if the variation of the donor potentials, V_0, is greater than twice the band width B (Figure 4.16), $V_0 \geq 2B$.[89,95]

Figure 4.14 can be reinterpreted within the framework of Anderson localization. At the low concentration all states are Anderson localized due to the small extent of B. As the concentration of donors increases, the bandwidth becomes large enough that the condition $V_0 \geq 2B$ is not met except at the band tails. Therefore, the electron wavefunctions become extended except at the band tails [Figure 4.16 (b)]. The energy at which the wavefunctions change from localized to extended is called the mobility edge since localized electrons have zero mobility. In the case of an uncompensated system and zero temperature, the Fermi energy lies between the merging tails of the lower and upper Hubbard bands where the electrons are localized. The activation energy ε_2 then corresponds to the difference between the upper Hubbard-band mobility edge (E_c) and the Fermi energy (E_F) as indicated in Figure 4.14. Above E_c the extended electron wavefunctions result in a finite mobility, and electronic conduction takes place. Finally, at the critical concentration n_c all states become extended (E_c-E_F=0) and the system behaves metallic. The condition for this (Anderson) transition to a metallic state is that $V_0 \approx 2B$. V_0 is of the order of E_{Ry}, and $n_c^{1/3}a^* \approx 0.2$. Therefore, although both the Mott and Anderson transitions differ in their physical origin, they yield similar conditions for their occurrence.

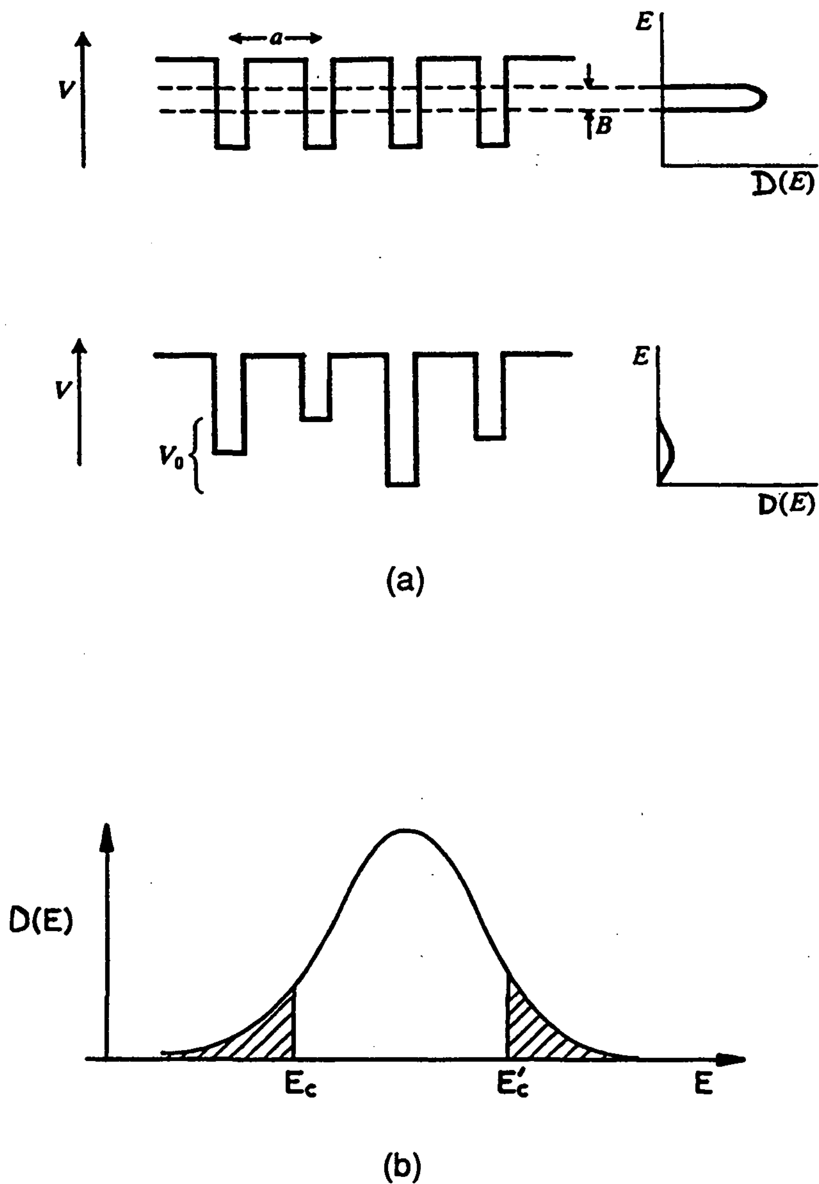

Figure 4.16. (a) Schematic of constant versus random potential energy wells. The density of states D(E) is also shown.[95] (b) Density of states for band of random potentials. The shaded regions indicate localized states.[91]

4.5.4 ε_2 conduction in uniaxially stressed Cu-doped Ge

The application of uniaxial stress can be used to induce a metal-insulator transition in p-type semiconductors having an impurity concentration below n_c.[99] The stressed-induced reduction in the hole effective mass not only decreases the acceptor ionization energy but also increases the acceptor Bohr radius. Thus, the interaction of acceptor wavefunctions required for an MI transition takes place at a lower dopant concentration. For germanium doped with shallow acceptors, the Bohr radius increases from its zero-stress value of 40 Å to 80 Å in the high-stress limit. Using the "universal" relation $n_c^{1/3}a^*=0.26$, one obtains a critical concentration for stressed Ge:Ga of 3.4×10^{16} cm^{-3} compared to its zero-stress value of 2.7×10^{17} cm^{-3}.

The application of uniaxial stress also increases the Bohr radius of the copper triple acceptor in germanium. For a $(1s)^3$-like ground-state, the copper Bohr radius at the transition pressure, where the ionization energy is about 17 meV, is approximately equal to $(6/17)^{1/2}80$ Å or 48 Å. This Bohr radius is slightly larger than the zero-stress a* of shallow levels and yields a critical concentration $n_c=1.6\times10^{17}$ cm^{-3}. For the $(1s)^2(2s)^1$, lithium-like configuration, the Bohr radius is not known. However, it can be estimated by scaling a* with the ratio of the Bohr radius of the hydrogen atom (0.53 Å) with that of the lithium atom (1.59 Å). This results in a radius of (1.59/0.53)80 Å or 240 Å for which $n_c=1.27\times10^{15}$ cm^{-3}! This large Bohr radius does not take into account any central cell effect. The binding energy derived from effective mass theory (Appendix C) is 4.5 meV. The estimated central cell correction is then $(4.5/17)^{1/2}$ which gives a Bohr radius of 123 Å and n_c equal to 9.3×10^{15} cm^{-3}.

This analysis is very approximate but points to the possibility that a metal-insulator transition can take place in uniaxially stressed Ge:Cu crystals having a concentration in the 10^{15} cm^{-3} range. A shortcoming of the above analysis is

that *1s*-type wavefunctions were used in the evaluation of the Hubbard U and overlap energy *I* integrals. The use of *2s*-type wavefunctions adds an additional level of complexity to the theoretical development of this problem as has been shown by Slater.[100] Nevertheless, the wide applicability of the relation $n_c^{1/3}a^*=0.26$ makes its use a good initial approach to this new problem.

4.5.5 Hall effect measurements of uniaxially stressed Ge:Cu

One method of probing whether or not metallic behavior is possible in uniaxially stressed Ge with low concentrations of substitutional copper is by making Hall effect measurements. These have been performed in the manner described in Appendix A and already used successfully in the study of uniaxially stressed Ge:Ga crystals (Chapters 2). Therefore, it is expected that unique features appearing in the Ge:Cu system can be attributed to the nature of the copper acceptors.

Figure 4.17 is a plot of the hole concentration versus inverse temperature for a sample taken from crystal #1. The filled squares represent zero-stress measurements while the circles correspond to hole concentrations obtained for the sample under uniaxial stress of an undetermined magnitude. It is expected that the stress was greater than 3 kbar. The Hall effect reveals a striking feature. The hole concentration of the uniaxially stressed sample follows precisely an Arrhenius relation [hole concentration proportional to $\exp(-E_{Hall}/k_BT)$] with an activation energy of 3.1 meV. This value is considerably smaller than the photoionization energy previously determined for neutral copper centers in highly stressed Ge:Cu (Section 4.3) .

Figure 4.18 shows the spectral response of crystal #3 corresponding to the non-zero stress for which the Hall measurements are presented in Fig. 4.17. Clearly, the thermally activated process revealed in the Hall measurements

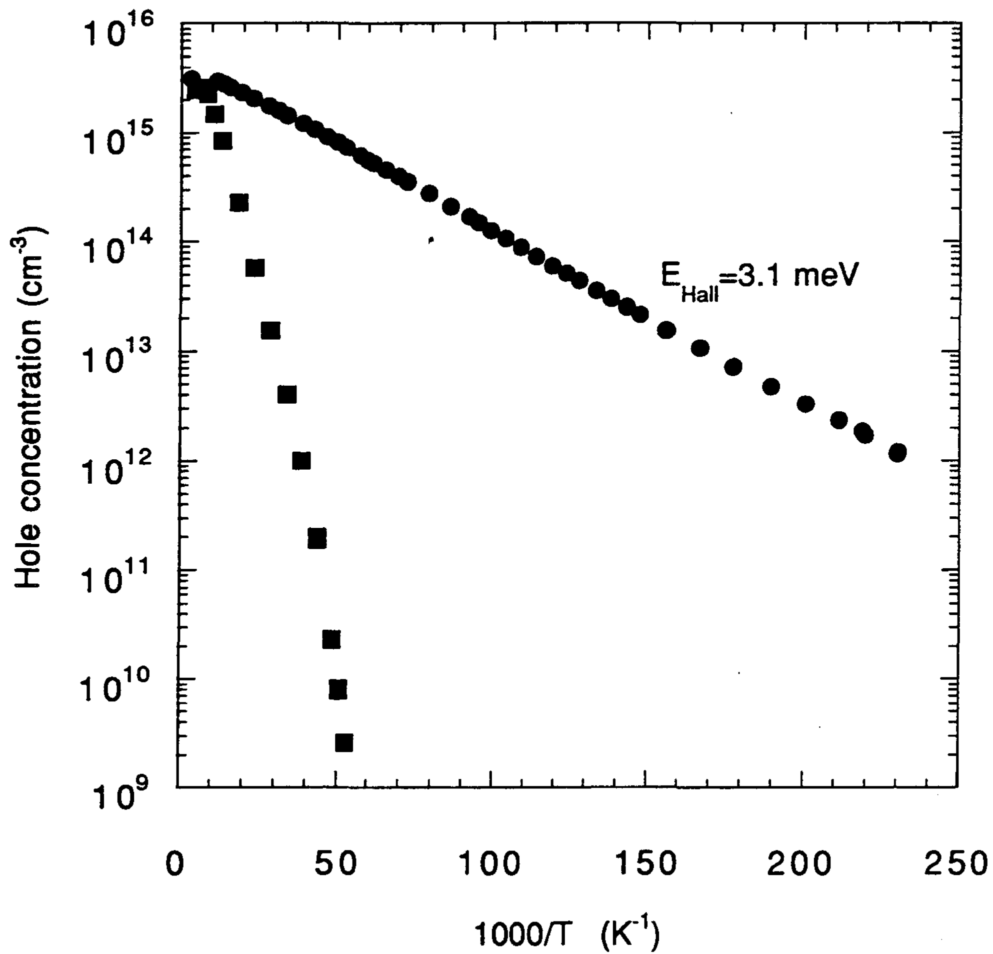

Figure 4.17. Hole concentration as a function of inverse temperature for crystal #1. The squares were taken for zero stress while the circles where obtained with the sample under uniaxial stress (>3 kbar).

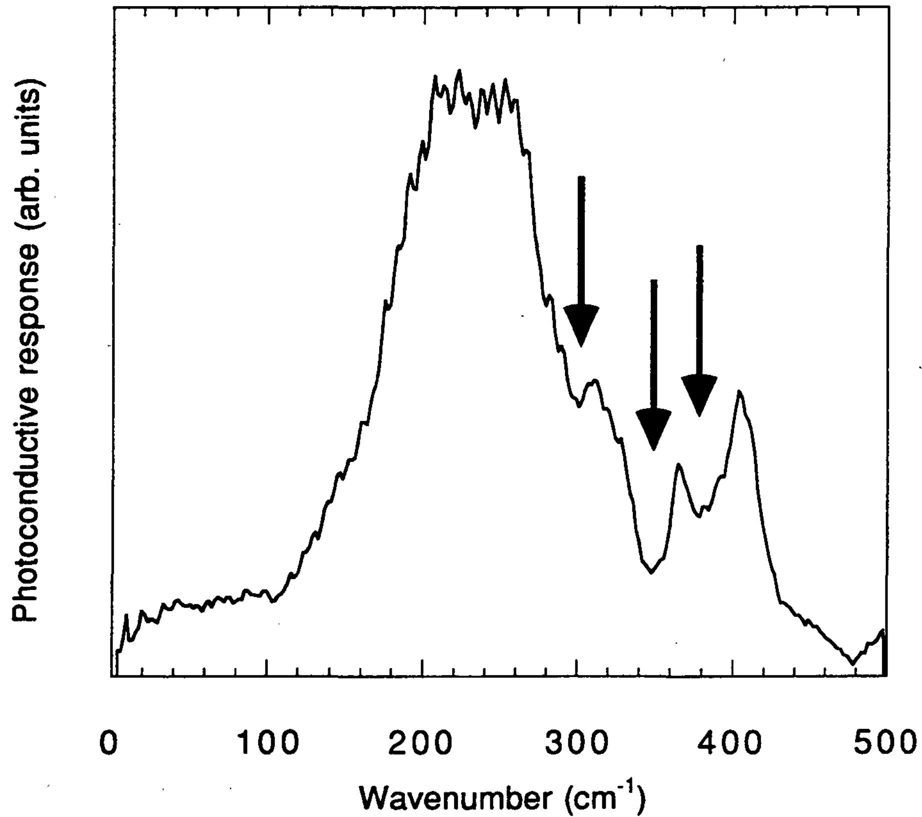

Figure 4.18. Photoconductivity response spectrum of crystal #1 measured at the same uniaxial stress for which the hole concentration is shown in Figure 4.17. The spectrum was measured for a sample temperature of 4.2 K using a 0.2 mm-thick black polyethylene filter also maintained at 4.2 K. The arrows indicate three of the optically active multiphonon modes that produce the dips in the photoconductivity response.

does not correspond to the ionization of neutral copper centers observed in the spectral measurements. Rather its is more likely related to a phonon-assisted transition between *s*-like impurity states, an optical transition forbidden from parity considerations.

If the copper concentration is above n_c and the applied stress is too small to produce the copper ground-state transformation, the $(1s)^2(2s)^1$ impurity band represents the merged lower and upper Hubbard bands associated with this electronic configuration, and the Fermi level lies on the $(1s)^3$ ground-state at low temperature. The activation energy observed in the Hall effect, E_{Hall}, is due to the thermal excitation of bound holes from the $(1s)^3$ localized ground-state to the $(1s)^2(2s)^1$ impurity band. It is equal to the sum of the energy required to excite a bound hole from the Fermi level to the lower Hubbard band, E_{LH}, and the energy required to excite another hole from the Fermi level to the upper Hubbard band, E_{UH}. Both E_{LH} and E_{UH} are equal to the energy difference between the $(1s)^3$ ground state and the $(1s)^2(2s)^1$ impurity band represented by E_1 in Figure 4.19(a). Therefore, E_{Hall}=$2E_1$.

At a pressure beyond the ground-state transition, the Hall activation energy vanishes (E_{LH}=E_{UH}=0) resulting in a temperature insensitive hole concentration. In the low temperature limit, the holes can be photoexcited from an energy within the impurity band corresponding to the Fermi energy to the valence band [Figure 4.19(b)]. The photoconductivity threshold should be stress-insensitive as has already been shown.

If the copper concentration is below n_c, the Hall activation energy can be interpreted as before, the sum of E_{LH} and E_{UH}. When the stress is large enough to transform the copper ground-state to a $(1s)^2(2s)^1$ configuration, E_{Hall} corresponds to the activation energy ε_2 previously shown in Figure 4.14 and depicted for the case of Cu-doped Ge in Figure 4.20 (E_{LH}=0 and E_{UH}=ε_2). The

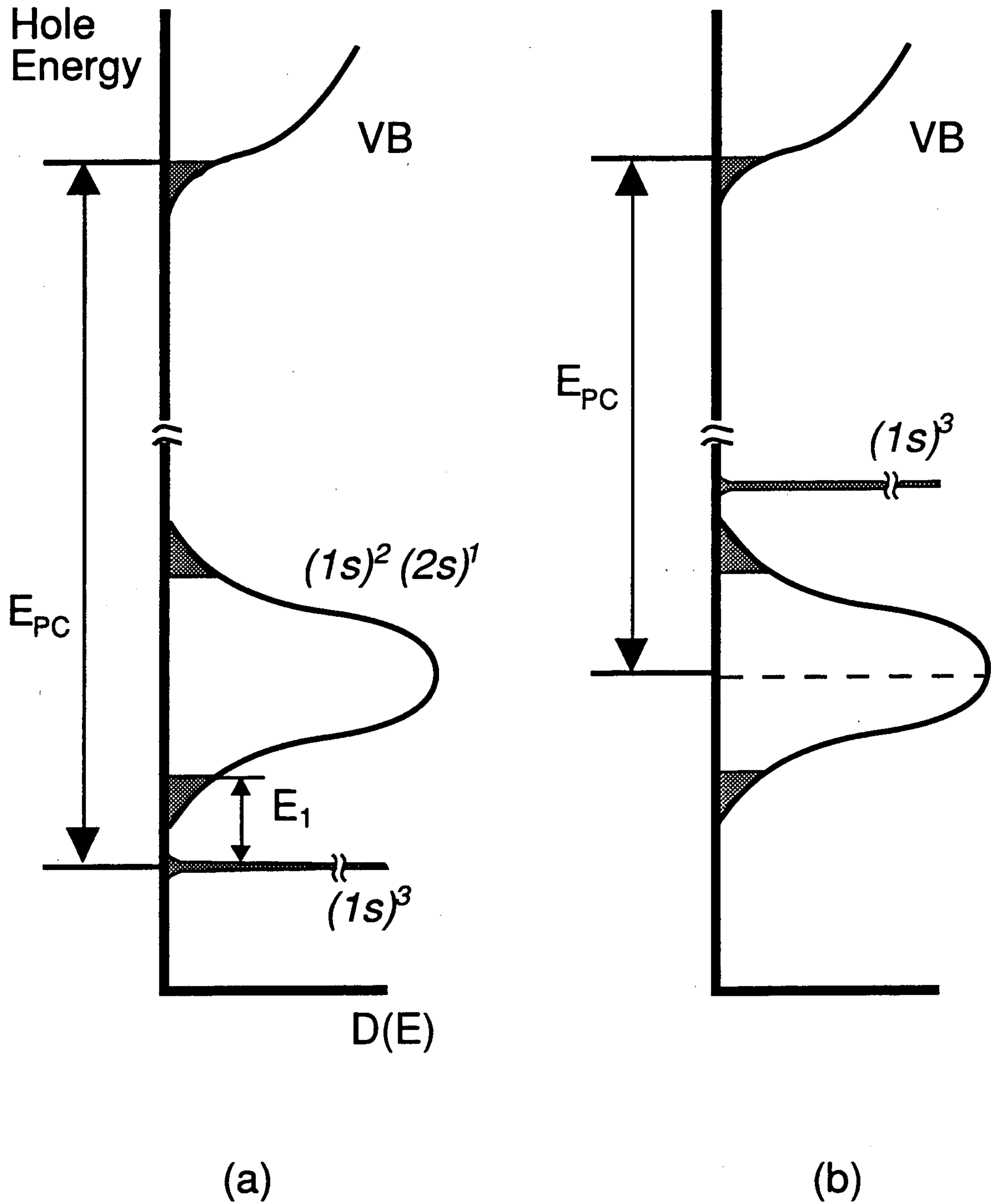

Figure 4.19. Schematic density of states of Ge:Cu stressed (a) below and (b) above the pressure required for the ground-state transition. The copper concentration is greater than n_c. The shaded regions denote localized states. The $(1s)^2(2s)^1$ impurity band is composed of the upper and lower Hubbard bands. The energy E_{PC} refers to the photoconductivity threshold expected in the low temperature limit.

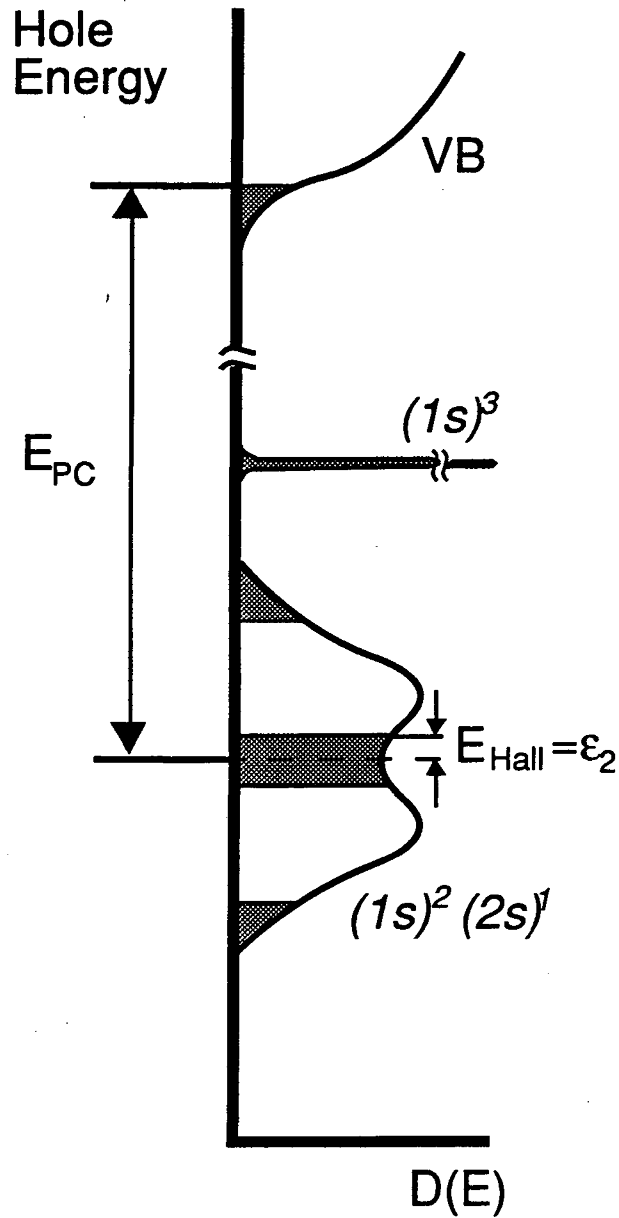

Figure 4.20. Schematic density of states of Ge:Cu stressed above the pressure required for the ground-state transition. The copper concentration is less than n_c, analogous to the intermediate concentration shown in Figure 4.14. The shaded regions denote localized states. The energy E_{PC} refers to the photoconductivity threshold expected in the low temperature limit.

hole concentration, hence the resistivity, exhibits a temperature dependence irrespective of the pressure, and the photoconductivity-response threshold remains stress-insensitive in the low-temperature limit. Clearly Hall measurements on more highly stressed samples are very important in determining the validity of this picture. However, these have not yet been achieved.

Further Hall measurements have also been performed at lower stresses. These are shown in Figure 4.21. The relative applied stress is denoted by S_i so that a data set labeled S_i has been taken at a lower stress than that labeled S_{i+1}, where i is an integer. With an increase in stress from S_1 to S_2, the temperature dependence of the hole concentration switches from obeying semiconductor statistics (i.e., holes freezing out onto copper acceptors), which is characterized by the "half-slope" and "full-slope" regions, to exhibiting the more simple Arrhenius behavior. The activation energy decreases with increasing pressure in agreement with the above model [Figure 4.19(a)].

The Hall mobility is very sensitive to the magnitude of the applied stress as shown in Figure 4.22. At a compressive stress S_1 the mobility has increased from its zero-stress value similarly to the pressure-induced enhancement of the mobility observed in germanium crystals doped with shallow acceptors. With a further increase in uniaxial stress, the mobility "peaks" at a magnitude above 10^7 cm^2/Vs possibly resulting from mixed conduction via the valence and impurity bands Although a proper interpretation of the Hall mobiltiy requires additional analysis, this result is remarkable given the fact that the highest mobility ever reported is about 10^7 cm^2/Vs for the highest quality quantum-well structures in the $GaAs/Al_xGa_{1-x}As$ system.[101,102] The Hall mobility could not be evaluated at the pressure S_2 and lower temperatures than what is shown due to the unreliable measurement of both the resistivity and the hole concentration.

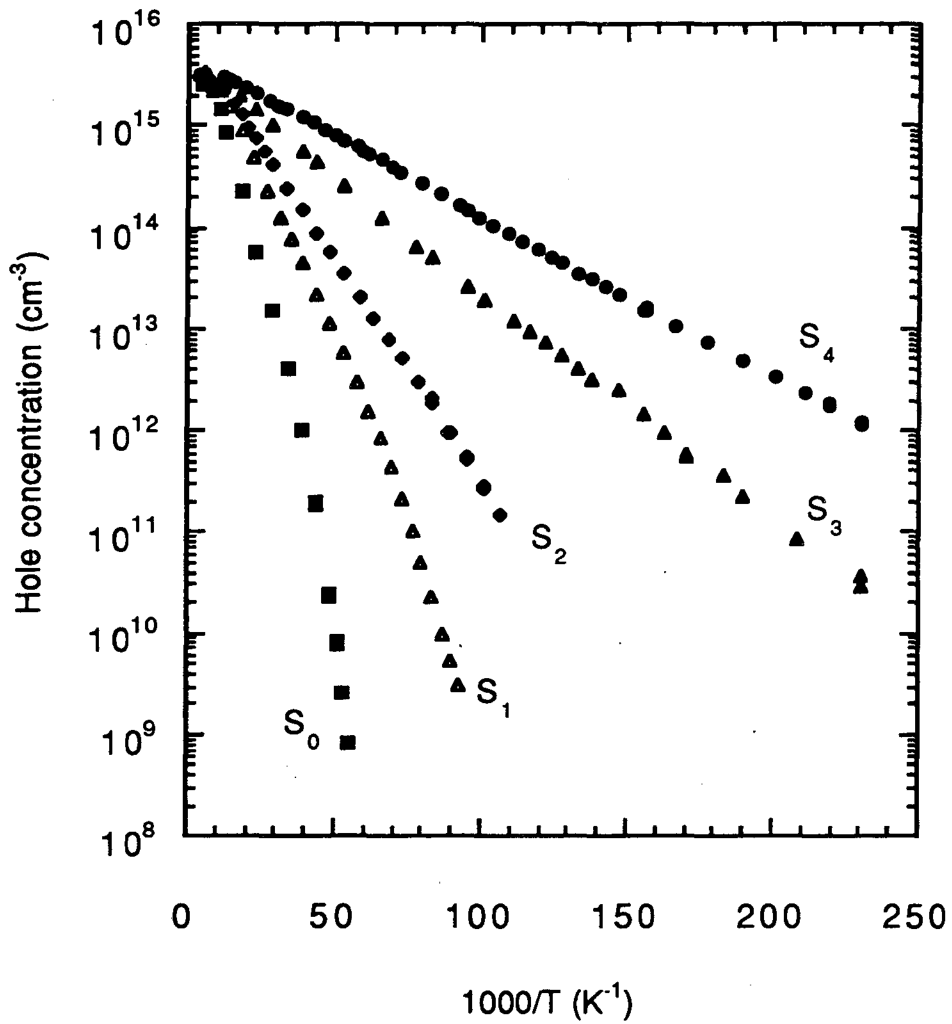

Figure 4.21. Hole concentration as a function of inverse temperature for crystal #1 measured for various applied stresses. The data labeled S_0 and S_4 have been shown in Figure 4.17. Data sets S_1, S_2, S_3 and S_4 were measure at sequentially higher stresses.

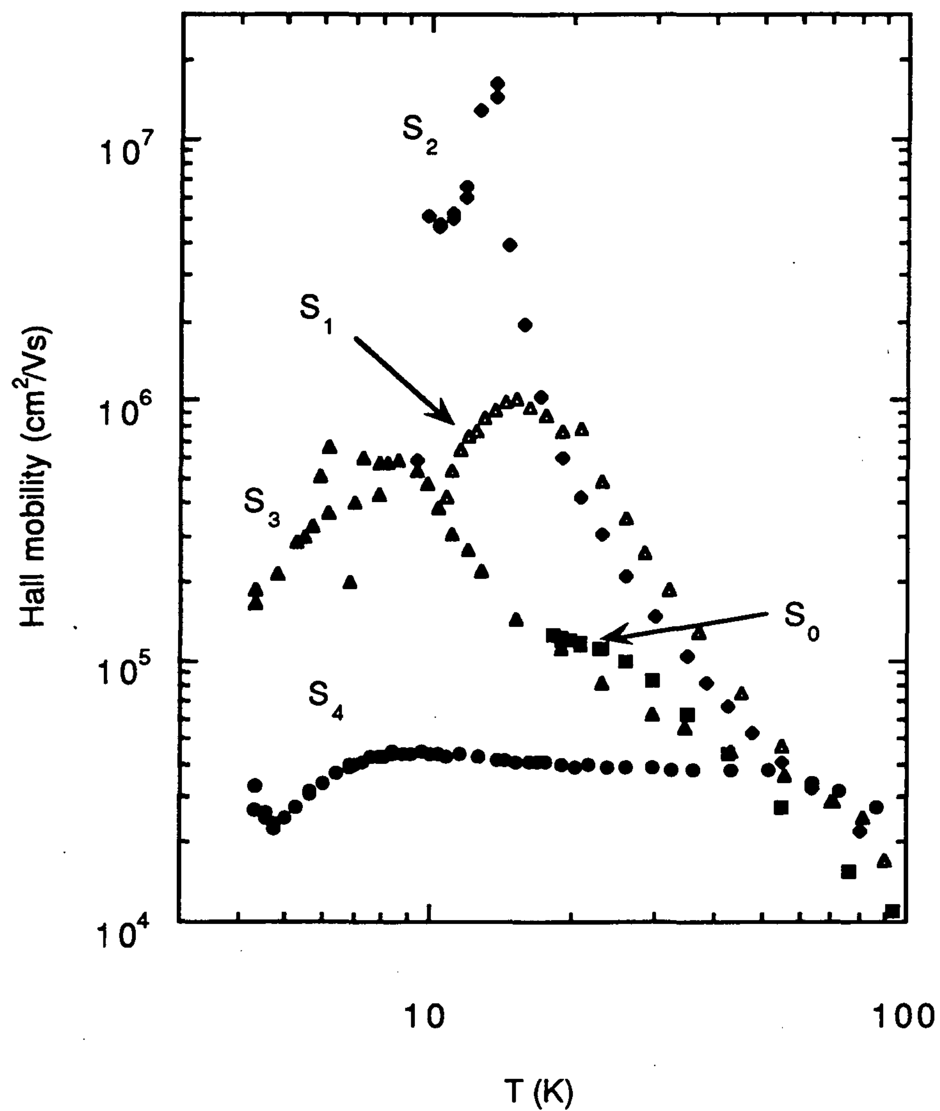

Figure 4.21. Hall mobility as a function of inverse temperature for crystal #1 measured for various applied stresses. The data labeled S_0 and S_4 have been shown in Figure 4.17. Data sets S_1, S_2, S_3 and S_4 were measured at sequentially higher stresses.

At a pressure S_3 the mobility has decreased and has a maximum value at a lower temperature than any of the lower stresses including zero stress. At the highest stress the mobility has decreased further and is weakly dependent on temperature suggesting that scattering by neutral impurities is the mechanism that determines the mobility in the impurity band. The high values of the Hall mobility even at the highest stress further indicate that E_{Hall} is associated with ε_2 conduction rather than hopping conduction. These results have preliminary character and are the subject of further studies.

4.5.6 Summary of electrical measurements

The electronic properties of copper-doped Ge can be dramatically changed by the application of uniaxial stress. One major effect is the pressure-induced transformation of the copper acceptor ground-state. The *2s*-like electron wavefunctions of the $(1s)^2(2s)^1$ high-pressure configuration become extended even at low copper concentrations making conduction via impurity states possible. The resulting "ε_2 conduction" produces the high dark currents that have been measured for uniaxially stressed, copper-diffused Ge:Ga crystals.

Some of the experimental observations are not yet well understood. First, crystals having a copper acceptor concentration as low as $6x10^{13}$ cm^{-3} exhibit large stress-induced changes in resistivity. Whether this is due to hopping or ε_2 conduction has not yet been determined. The fact that the resistivity is so low suggests that the conduction is of the latter type as shown schematically in Figure 4.20. Second, there exists a pressure condition (e.g., S_3) for which the Hall mobility achieves a "peak" magnitude at a given temperature. The discontinuous nature of this maximum suggests that this behavior may be related to an electronic phase transition. These results

suggest a rich array of electronic phenomena that requires further experimentation and theoretical development.

5. Conclusion

The effect of uniaxial stress on acceptor-related electronic processes in germanium single crystals doped with Ga, Be, and Cu have been studied by Hall and photo-Hall effect measurements in conjunction with infrared spectroscopy.

The stress dependence of the hole lifetime in gallium-doped germanium single crystals offers a critical test for competing models of the non-radiative capture of holes by acceptors. It has been shown that the hole lifetime increases by over one order of magnitude upon the application of uniaxial stress at liquid helium temperatures. The hole lifetime is proportional to the acoustic-phonon-scattering component of the hole mobility. These results are in very good agreement with the cascade capture theory for Coulomb-attractive centers, and they clearly show that the recently proposed model in which holes are directly captured into the acceptor ground state is not valid since it predicts a decrease in the hole lifetime upon the application of uniaxial stress. These results are consistent with the observed increase of the responsivity of Ge:Ga detectors when uniaxial stress is applied.

Photo-Hall measurements of Ge:Be crystals have shown a stress-induced change in the temperature dependence of the hole lifetime. This change is attributed to the role neutral Be centers play in the capture of holes. The application of uniaxial stress results in over a one order of magnitude increase in the lifetime. These results explain the observed temperature and stress dependence of the responsivity of Ge:Be detectors.

The temperature dependence of the cross section for the capture of holes by singly ionized Be is found to be in good agreement with existing data for multivalent acceptors. A recasting of the capture cross sections available for

many singly ionized, multivalent acceptors shows that the direct rather than cascade capture model better explains the temperature dependence of data. However, a model that explains *both* the temperature and stress dependence of the capture cross-section is not available.

The electronic properties of germanium doped with the copper triple acceptor dramatically change by the application of uniaxial stress. The threshold of the photoconductivity response shifts from its zero-stress value of 43.2 meV to lower energies achieving a nearly constant value of 17 meV above 4 kbar. A variational calculation has been performed and shows that this behavior is caused by a change in the copper ground-state configuration from a pseudo Li^0, $(1s)^3$-like to a normal Li^0, $(1s)^2(2s)^1$-like configuration having a stress-insensitive hole binding energy.

Accompanied with this ground-state transformation is a tremendous decrease in the electrical resistivity of many orders of magnitude. This effect is caused by the stress-induced onset of impurity band conduction. The *2s*-like electron wavefunctions of the $(1s)^2(2s)^1$ high-pressure configuration become extended even at low copper concentrations making conduction via impurity states possible. A simple calculation has shown that an insulator-metal transition (Mott-Hubbard-Anderson) should occur in uniaxially stressed Ge having a copper concentration in the 10^{15} cm^{-3} range. These results provide a first explanation for the performance of uniaxially stressed, copper-diffused Ge:Ga detectors which have a high conductivity in the absence of a photon signal and consequently have poor sensitivity. Clearly, copper contamination can have seriously adverse effects on the performance of stress Ge detectors.

6. Future Work

The results presented in this thesis have provided new insight into the electronic processes of p-type germanium at low temperature. Uniaxial stress has proven a valuable external perturbation for studying both the similarities and differences between the crystals doped with monovalent and multivalent acceptors. However, much work remains to be accomplished.

Although studied for more than three decades, the non-radiative capture of holes by ionized acceptors is by no means a resolved issue. Capture by monovalent acceptors appears to be well understood; however, the same cannot be said for multivalent acceptors. The results obtained for the Be-doped Ge system strongly suggest the occurrence of a combination of capture processes at low temperatures. One of these is hole capture by neutral acceptors. Further work on other dopants including Hg should aid the development of a theoretical model that can explain the stress as well as temperature dependence of the capture cross section.

At the outset of this work, it was hoped that measurements on uniaxially stressed copper-doped germanium crystal would provide key information about hole capture. Instead, these measurements produced new phenomena, some of which have been explained in this thesis. Questions remain regarding the interpretation of some of these phenomena. The behavior of the Hall mobility, the onset of impurity conduction in relatively low-doped Ge:Cu, the occurrence of electric field-induced effects, these are all issues that may be challenging to be addressed experimentally and/or theoretically and that can further the understanding of electronic processes in semiconductors.

7. Appendices

Appendix A: Hall and photo-Hall effect measurements

A.1 Hall effect and photo-Hall effect

This section briefly reviews the basics of the Hall effect. More elaborate presentations on the subject may be found elsewhere.[103,104] In the presence of a magnetic field **B**, a moving charge experiences a Lorentz force $\mathbf{F_L}$ defined by

$$\mathbf{F_L} = q(\mathbf{v} \times \mathbf{B}) \tag{A.1}$$

where **v** is the velocity of a carrier of charge q. In 1879 E.H. Hall observed that a metal strip carrying an electrical current I_x and is placed in a magnetic field B_z normal to the current direction exhibited a voltage V_H perpendicular to both I_x and B_z.[105] This is the Hall effect, and V_H is known as the Hall voltage. The Hall effect is a direct manifestation of the production of a Lorentz force in a material by applied fields and the reaction of the material revealed as the Hall voltage. This phenomenon has since been used in the study of the nature and concentration of charge carriers not only in metals but also in other materials including semiconductors.

Figure A.1 shows a bar of material. A current I_x injected in the +x direction results in the motion of mobile, charge carriers along the length of the bar with a drift velocity $v_x = I_x/(nqtw)$ where n is the majority carrier concentration. (It is assumed that minority carriers contribute a negligible amount to electrical conduction.) If a magnetic field B_z is applied in the +z direction, the carriers will be deflected in the -y direction by a Lorentz force of magnitude $F_L = qv_xB_z$. As carriers accumulate on one side of the bar and are depleted on the other side, the redistribution of the mobile charge produces an electric field along the y

direction which prevents further accumulation of carriers. So, the Lorentz force is balanced by a field induced force F_E equal to qE_H. In a homogeneous material under a uniform magnetic field, $E_H = V_H/w$. Thus,

$$qv_xB_z - qE_H = q\left(\frac{I_x}{nqtw}\right)B_z - q\frac{V_H}{w} = 0 \qquad \text{(A.2)}$$

and

$$qn = \frac{I_xB_z}{tV_H} = R_H^{-1} \qquad \text{(A.3)}$$

where R_H is the Hall coefficient. Because I_x, B_z, t and V_H can usually be determined experimentally, the Hall coefficient is readily computed. The sign of R_H indicates whether the mobile charge carriers are holes (positive R_H) or electrons (negative R_H).

The majority carrier concentration is determined from the magnitude of the Hall coefficient ($n=1/R_Hq$). By measuring the Hall coefficient as a function of temperature, one obtains the "freeze-out" curve shown in Figures 2.7 and 4.3. The temperature dependent Hall measurements allow for the determination of the majority and minority impurity concentrations and provide information about the ionization energy of the majority impurity level.

It is found in practice that R_H^{-1} is not exactly equal to the product of the charge and the carrier concentration. In general, $R_H=r_H/qn$ where r_H is called the Hall factor which is a function of the relaxation time . Values for the Hall factor range from 1/2 to 2 and depend on the dominant carrier scattering mechanism(s). However, at high magnetic fields r_H approaches unity. It has been shown that for lightly doped p-type Ge at low temperatures, a magnetic induction of 0.1 Tesla is sufficient to meet the condition $\mu B>1$ (μ is the carrier mobility in m^2/Vs and B is in units of Tesla) resulting in $r_H \approx 1$.[106]

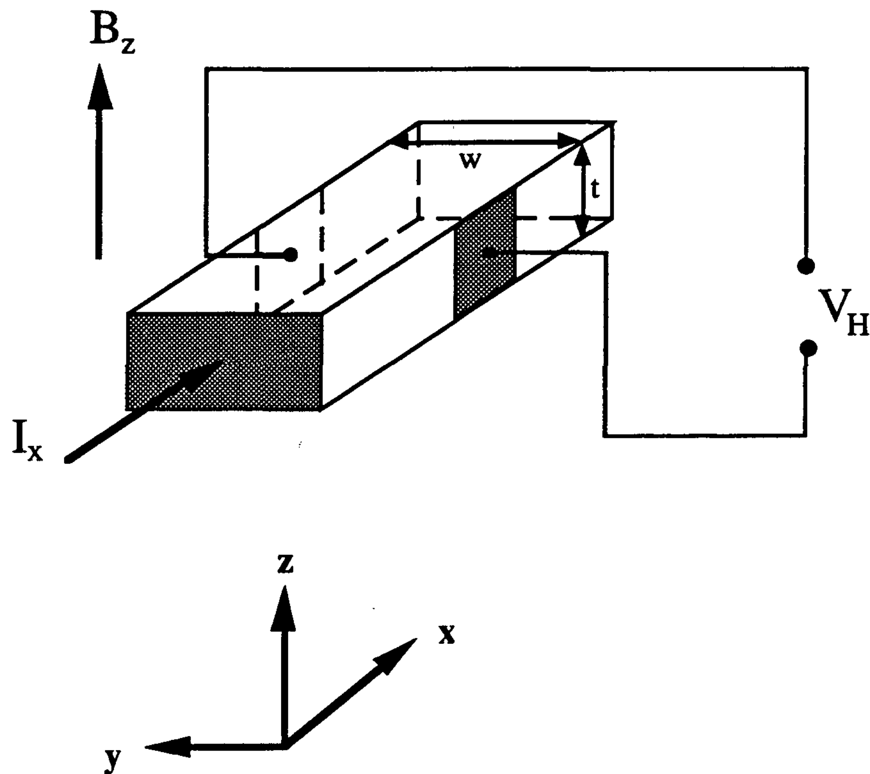

Figure A.1. Schematic arrangement for a Hall measurement.

The photo-Hall effect is very similar to the Hall effect phenomenon described above. The only difference is that carriers are generated optically as well as thermally. The temperature region of interest for determining the carrier lifetime is that in which optical generation dominates. In this case one finds that

$$R_H^{-1} = qn = qg_{ext}\tau_n \,. \qquad \text{(A.4)}$$

Thus, the determination of the Hall coefficient in conjunction with the knowledge of the external (optical) generation rate g_{ext} yields the majority carrier lifetime

(assuming that the photons are of sufficient energy to ionize impurities but not to produce electron-hole pairs due to band to band excitation).

A.2 Hall apparatus and measurement

Three pieces of equipment are needed to perform a Hall effect measurement: a) a voltmeter, b) a current source, and c) a magnet. Fig. A.2 is a schematic of a three component system with the additional features of automation and temperature control. The sample temperature was measured with a LakeShore DRC 80 cryogenic thermometer when the standard coldfinger was used. The stressing coldfinger requires the use of a multimeter in order to read the resistance of a calibrated temperature sensing resistor.

Samples were mounted to a coldfinger attached to a LakeShore CT-310 continuous flow cryostat (Fig. A.3). This allowed for Hall measurements at temperatures ranging from 300 K down to approximately 2.5 K. Appropriate vacuum ($\sim 10^{-5}$ torr) was reached via a diffusion pump system. Sub-liquid He temperatures were achieved by pumping on the He reservoir. Although optical ports are available for external photon sources, photo-Hall measurements were performed using an internal blackbody source as will be described in the following section.

A modified bar configuration was used for measurements of stressed samples as shown in Figure A.4. Current was passed through contacts 1 and 3 in either direction, and all voltages were measured across 2 and 4. The sample's resistivity was determined by two measurements, one with current injected at contact 1 and the other at 3. This provided a measure of the sample resistance ($R_{resist}=0.5V_{24}/I_{13} - 0.5V_{24}/I_{31}$). This resistance was converted to a resistivity by taking into account a geometric factor determined by obtaining the actual resistivity of samples configured in the van der Pauw geometry.[107] This

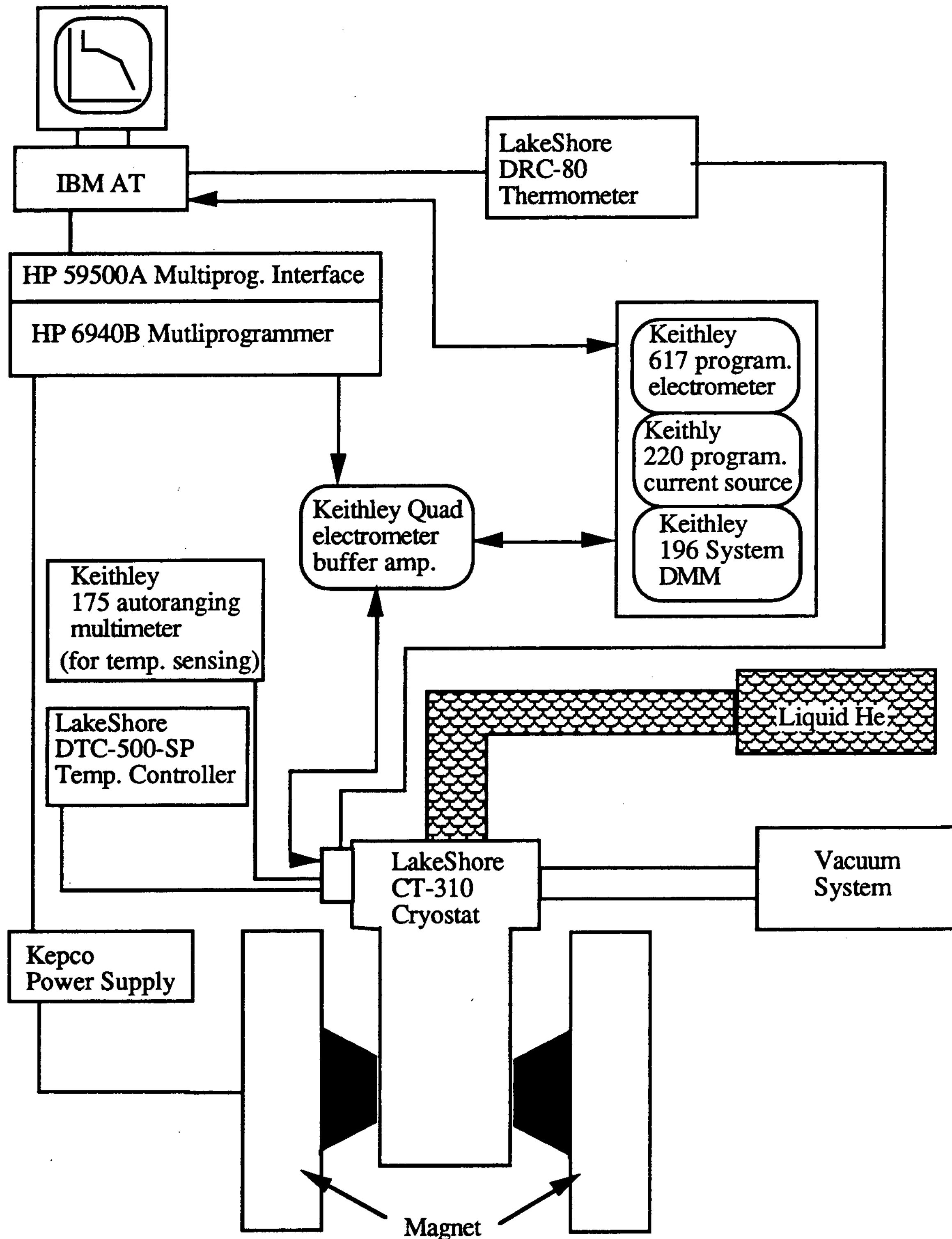

Figure A.2. Schematic of variable temperature Hall effect apparatus.

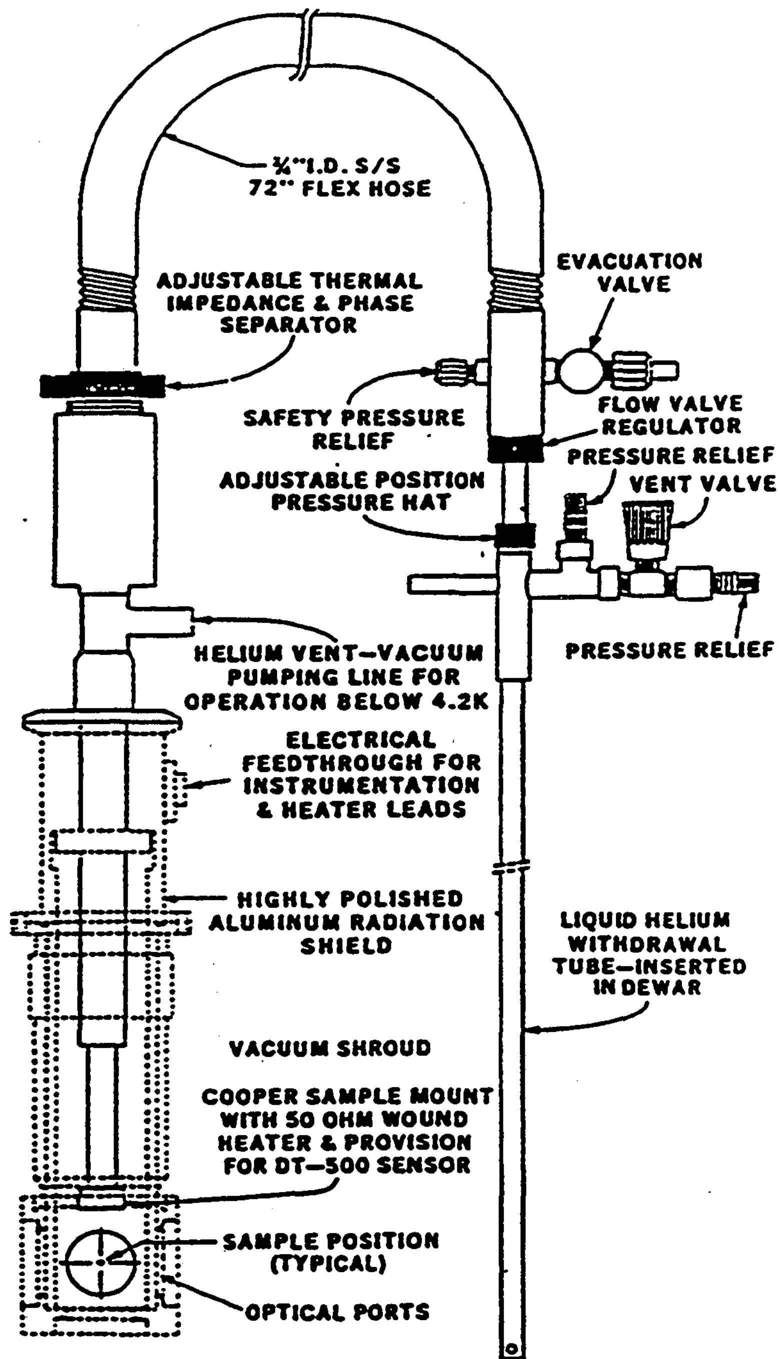

Figure A.3. Schematic of Lake Shore CT-310 continuous flow cryostat.

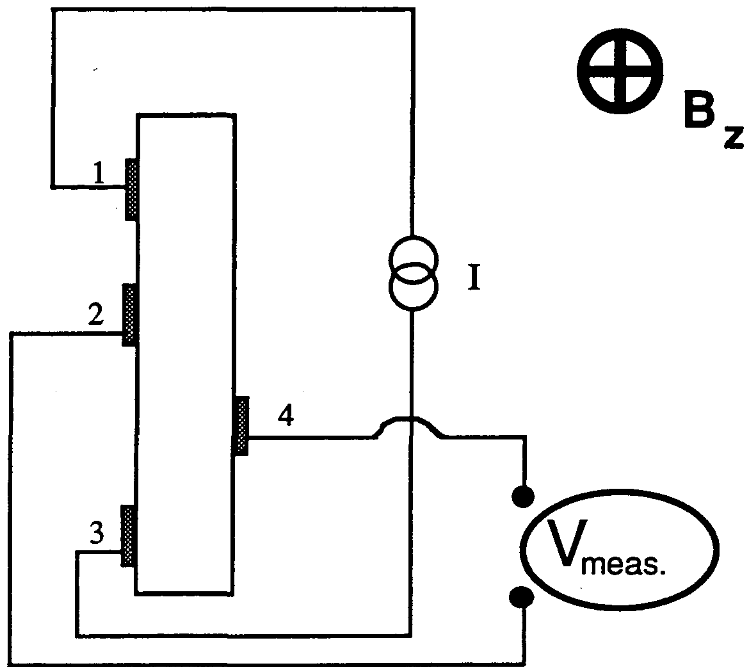

Figure A.4. Sample configuration for dark- and photo-Hall measurements.

geometric factor was calculated at one temperature and applied to other temperatures.

The Hall coefficients for the modified bar samples involved four rather than two measurements. The same arrangement as the one just described was utilized with the additional requirement of a magnetic field. The magnet was set at a magnetic induction of 0.3 Tesla. Two measurements were performed with the field in one direction (normal to both the contactless surfaces and the axis of compression) and repeated with the field changed to the opposite direction—the measurements being averaged. By switching the magnetic field direction, the Hall voltage was obtained from the voltage measurements between contact 2 and 4 (i.e., $R_{resist.}$ was measured in the presence of a magnetic field):

$$V_H/I_x=0.5[R_{resist}]^{+}-0.5[R_{resist}]^{-} \quad (A.5)$$

where the "+" and "–" superscripts indicate the orientation of the field along the z axis (Fig. A.1). The only sample dimension that is necessary to obtain the carrier concentration is the distance between the two contactless surfaces (equivalent to the dimension t in Figure A.1).

A.3 Stressing coldfinger

The characteristics of the stressing coldfinger are most important to the successful performance of standard and photo-Hall measurements of uniaxially stressed samples. Three factors were considered in its design: a) the accurate measure of temperature at low temperatures, b) the ability to apply uniaxial compression to small, bar shaped samples (≈1x1x5 mm^3), and c) the capability of shining light on the sample. The major overall constraint in the design was space (≈1 inch cubed available). In addition, the coldfinger materials had to be of sufficient a) strength to support stresses of up to a few kbar, b) thermal conductivity to minimize thermal time constants and c) non-magnetic behavior so as to not affect the Hall measurement.

A schematic of the stressing coldfinger is provided in Fig. A.5. Its design was based on the stressing devices used successfully for low temperature, far-infrared photoconductor applications.[90] It includes the following components: a) the main body constructed from a solid piece of brass, b) one stainless steel piston and sample set screw, c) one #4-40 screw with which to apply stress, d) one stainless steel fulcrum attachment, e) one calibrated temperature sensing resistor, f) one gold-coated, hemispherical, optical brass cavity, g) one cavity as described in f) and with a blackbody emitter within it, and h) one brass attachment used to connect the coldfinger to the LakeShore cryostat. In

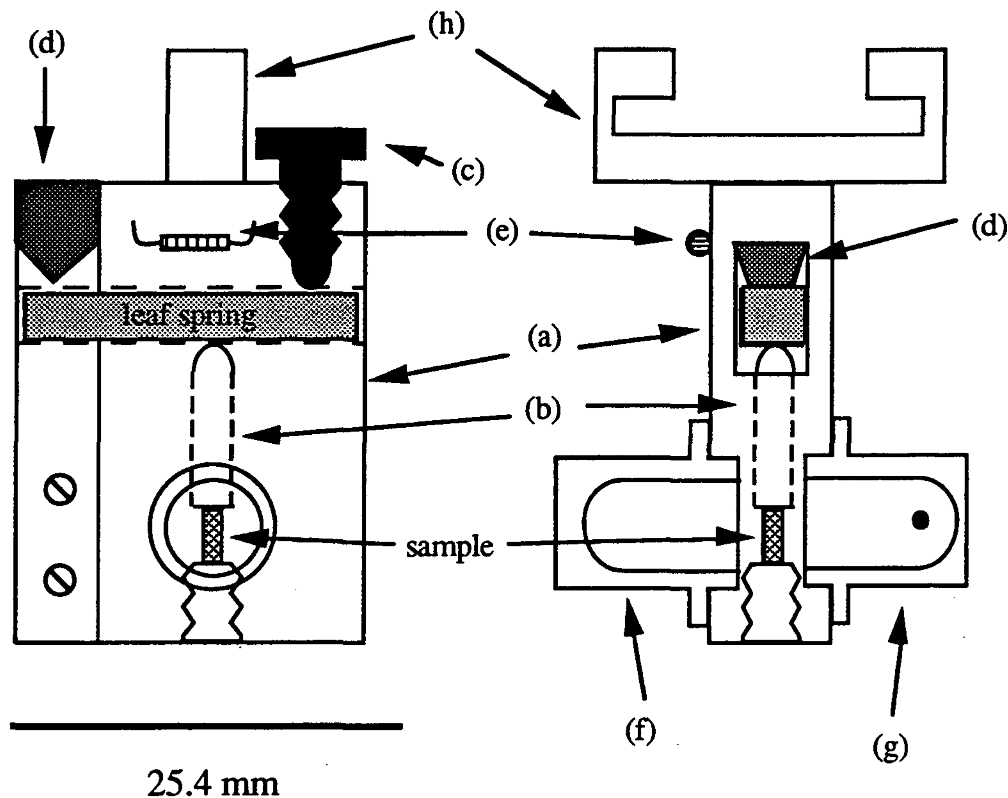

Figure A.5. Drawing of the stressing coldfinger. All labeled components are identified in the text.

addition, stress was applied via phosphor-bronze, leaf springs of various thicknesses.

An Allen-Bradley, 1/8 watt, 1 kΩ, carbon composite resistor was used as the temperature sensor for the stressing coldfinger. After being cycled several times from room temperature to 4.2 K, the resistor was calibrated between 77 K and 4.2 K with respect to the DRC-80 unit. All calibration points involved the measurement of resistance with a Keithley multimeter versus the temperature of the bath into which the resistor was placed. The 77 K and 4.2 K values were obtained with liquid nitrogen and liquid helium baths, respectively, at standard

pressure. Measurements below 4.2 Kelvin were made by evacuating the liquid He space thus reducing the temperature of the bath. The relationship between pressure and liquid helium temperature is well known. This information was used to calibrate the resistor by making resistance versus pressure measurements. All Hall measurements were made with the same multimeter in order to ensure reproducibility of the temperature reading.

For resistors used over a relatively wide temperature range (3-20 K), several empirical formulae to fit the temperature-resistance relation of Allen-Bradley resistors have been proposed.[108] The data in the present case were fit with a fourth order polynomial $y = A+Bx+Cx^2+Dx^3+Ex^4$, where x is the natural logarithm of resistance (in units of ohms) and y is 1000/T (in units of K^{-1}). The values for the constants are given in the table below.

Constant	Value
A	5169.19
B	-2237.89
C	349.817
D	-23.5618
E	0.601

Table A.1. Constants of the fourth order polynomial used to fit the resistance-temperature characteristics of a 1 kΩ, Allen-Bradley resistor.

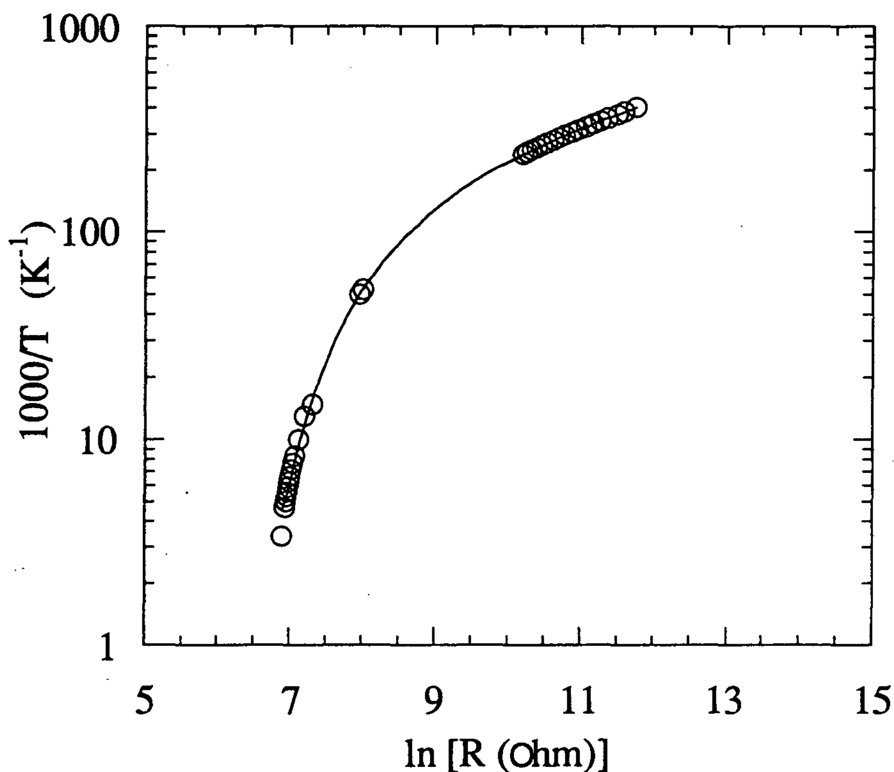

Figure A.6. Fitting of temperature-resistance data of an Allen-Bradley, 1/8 watt, 1 kΩ, carbon composite resistor with a fourth order polynomial and the related constants (Table 3.1).

Figure A.6 is a plot of y versus x. The resistance of the 1 kΩ resistor begins to change significantly at low temperatures (<30 K). Therefore, this calibration allows for temperature measurements to within two or three percent at temperatures below 25 K, the accuracy increasing as the temperature is decreased even further. Subsequent to the calibration process, the resistor was glued with stycast to a small copper plate such that only the leads were exposed in order to minimize the effects of humidity and provide greater

structural integrity. The small copper plate was then mounted directly to the coldfinger.

A knowledge of the carrier generation rate is essential to the determination of the carrier lifetime by the photo-Hall technique. To this end the optical aspects of the stressing coldfinger were designed with two objectives in mind: a) the capability of quantifying the spectrum of photons incident on the sample and b) the ability to determine the number of photons absorbed by the sample. Because shallow impurities in Ge have ionization energies of ~11 meV (or ~110 μm), a far-infrared photon source was required. And because samples were measured under stress, the ionization energies were shifted to lower energies requiring either a tunable or broad bandwidth source.

In the case where a broad bandwidth source is considered, it is necessary to know the absorption cross section of each impurity type as a function of photon energy. One can then compute the rate of photon absorption and, hence, the rate of carrier generation assuming that only one center is ionized per photon absorbed. This is not a bad assumption if the majority of photons are of low enough energy so as to not cause, for example, highly excited free carriers that ionize other centers.

These experimental challenges were met by the design of a closed cavity containing both the sample and a blackbody emitter (Figure A.5). Two hemisphere-like cavities were machined from brass and their interiors were sputter-coated with gold. The emitter is constructed from a ~1 kΩ NiCr square chip one milimeter on the side. The leads are made of 25.4 μm brass and are attached to the chip via silver epoxy. Once the leads were attached, the chip was painted with stycast epoxy such that an approximately spherical shape (diameter ~1.4 mm) was achieved. The leads run out of one of the cavities through small diameter teflon tubing. The tubing was mounted through a small

hole on the side of the cavity and secured with stycast outside the cavity and silver epoxy inside the cavity.

Photo-Hall measurements were typically made below 20 K. At these temperatures a fraction of the emitter's power was dissipated radiatively when current was injected through it. The temperature of the emitter was raised above that of its surrounding. It has been assumed that at the wavelengths of interest (> 30 μm) the emitter behaved as a blackbody. The photons radiated follow a Planck distribution which only depends on the blackbody's temperature and for a 1.4 mm diameter sphere is given by

$$P = \frac{1.16\mathrm{x}10^{4}}{\lambda^{4}\left[\exp\left(\frac{1.44\mathrm{x}10^{-2}}{\lambda T}\right)-1\right]} \quad \text{(photons/m-s)} \qquad \text{(A.6)}$$

where λ is in units of meters and T is in units of Kelvin. Therefore, it was very important to know with some accuracy the temperature of the emitter. This was determined for three different currents and was measured with a half mil, Type K thermocouple and an HP3478A multimeter. The thermocouple was placed in contact with the emitter through a very small amount of GE varnish. Thus the light source was calibrated for three temperatures 77 K, 99 K, and 122 K.

The goal of constructing and calibrating the emitter was to provide the best possible quantification of the photon spectrum impingent on the sample, (i.e., the first objective). Using the two cavities to enclose both the sample and the emitter would facilitate quantifying the photon absorption rate by establishing conditions which would best arrive at a quantum efficiency near unity.

The optical generation rate is equal to the number of photons absorbed by the sample per unit volume per unit time and is given by[41,109]

$$g_{opt} = \frac{\int (\text{photon flux}) \frac{A_{sample}\, \alpha_{sample}}{\sum_i A_i \alpha_i} d\lambda}{[\text{sample volume}]} \tag{A7}$$

where the photon flux (photons per unit time per unit photon wavelength) is approximated by the Planck spectral distribution, A_i is the area of an absorbing surface within the sample cavity (e.g., the emitter and sample surfaces), and α_i is the corresponding absorptivity. The absorptivity of the sample α_{sample} is given by its quantum efficiency and is approximately equal to

$$\alpha_{sample} = \frac{0.64[1\text{-}\exp(-\alpha^* d)]}{1\text{-}0.36\exp(-\alpha^* d)} \tag{A.8}$$

where d is the sample thickness and α^* is the wavelength-dependent absorption coefficient due to the acceptors. This quantity has been measured in the case of unstressed and stressed Ge:Ga, and the numerator in Eq. A.7 can be integrated in the spectral range over which the acceptors are optically active. For an emitter temperature of 77 K, the generation rate for Ge:Ga samples (stressed and unstressed) is $(4.4\text{-}5.4)\times10^{16}$ $cm^{-3}s^{-1}$ in the absence of optical filters. For Ge:Be the calculated generation rates are 5.4×10^{16} $cm^{-3}s^{-1}$ and 7.8×10^{16} $cm^{-3}s^{-1}$ for unstressed and stressed states, respectively.

A.4 Aspects of the stressing configuration

Beyond having an optical cavity and a built-in emitter, the main feature of the coldfinger is the capability of applying uniaxial compression to bar shaped samples. The uniaxial compression of a sample is achieved by turning the #4-40 screw shown in Fig. A.5 in the clockwise direction. The rounded tip of the screw exerts a force on the leaf spring. Because the leaf spring is supported by the stainless steel fulcrum, the force applied by the screw results in a force on

the sample via the stainless steel piston. The applied pressure was determined for each run by comparing the measured binding energy with the published data relating the binding energy to the applied pressure (e.g., Figure 2.2).

Appendix B: Aspects of photoconductivity measurements and IR spectroscopy

Photoconductivity spectroscopy and responsivity measurements were performed on samples using an Infrared Laboratories (Model HD3) cryostat designed for low-background testing (10^6-10^{10} photons/s).[23,57] Operating temperatures ranged between 4.2 K and 1.3 K. In order to achieve a low-photon background, the sample and other optical components (e.g., optical filters and mirrors) were placed in a copper box that is mounted onto a thick copper plate in contact with a liquid helium reservoir. In addition, the interior of the copper box is coated with 3M flat black paint. Attached to one of the walls of the box is a shutter aperture system having three externally adjustable positions: 1 mm, 2 mm, and closed. This provides optical access to the sample as the exciting radiation is produced from outside the cryostat.

The signal resulting from optical excitation was measured with a transimpedance amplifier (TIA) circuit shown in Figure B.1. The input stage consists of two matched JFET's that are mounted adjacent to the sample box in a light-tight copper box on the thick, copper plate. These are operated at a temperature of approximately 70 K. The typical value of the feedback resistor (R_f) between the output and the JFET gate is 2.5×10^{10} Ohm at liquid helium temperatures. Feedback resistors of smaller resistance were used for measurements of samples having low impedance ($<10^6$ Ohm). For a given bias an output voltage is produced, and the signal current is obtained by dividing the output voltage by R_f (Fig. 1.3).

For the responsivity measurements the light signal consisted of photons from alternately chopped 300 K and 77 K blackbody radiation. The total radiant emittance of a blackbody at temperature T is proportional to T^4. The

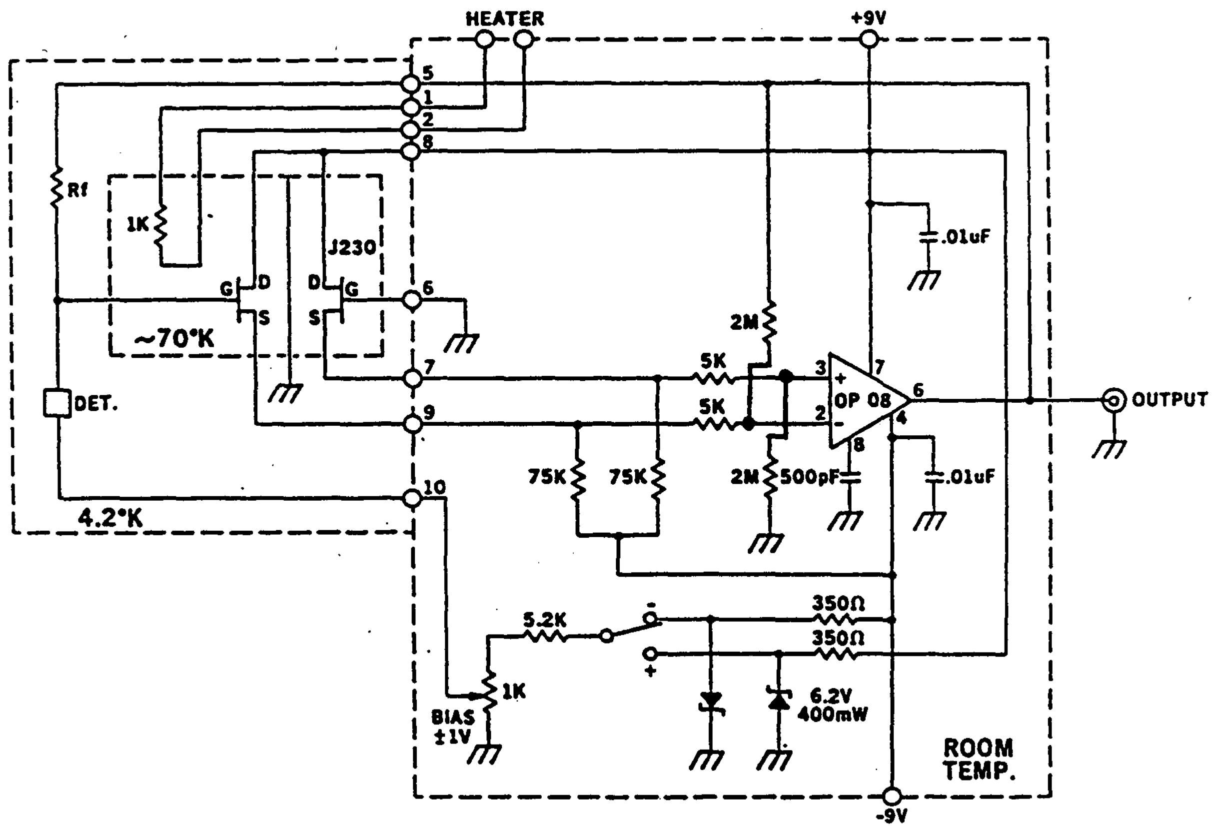

Figure B.1. Schematic of transimpedance amplifier of the HD3 cryostat.

proportionality factor is called the Stefan-Boltzmann constant and has a value of 5.6705×10^{-8} $Wm^{-2}K^{-4}$. The radiation was chopped at a frequency of 23 Hz, and the rms value of the output voltage was measured with a Hewlett-Packard 3582A spectrum analyzer. Dark currents were measured with the aperture in the closed position or with a light tight dewar and integrating amplifier (J-F 4 integrating amplifier, Infrared Laboratories) when the sample impedance was greater that 10^{10} Ohm.

A Fourier transform spectrometer was used to evaluate the photoconductivity response of the germanium crystals.[50,110] It includes a far-infrared Micheleson interferometer shown schematically in Figure B.2. Its major components include a mercury arc lamp (L), a beam splitter (B), a fixed mirror (FM), and a moving mirror (MM), all of which are contained in a vacuum enclosure in order to minimize absorption of the infrared radiation by water vapor. The beam splitter used is made of a thin mylar sheet (either 3.2 μm or 6.4 μm, depending on the sample). Due to the thickness uniformity of the mylar, Fabry-Perot interference reduces the transmission of IR radiation through the beam splitter. For example, the 6.4 μm-thick beam splitter shows close to zero transmission at 500 cm^{-1} with a maximum at 250 cm^{-1} while the thinner one shows nearly zero and maximum transmission at 1000 cm^{-1} and 500 cm^{-1}, respectively. Therefore, the 6.4 μm beam splitter is desirable if the spectral features of interest lie near 250 cm^{-1} and not 500 cm^{-1}.

Photoconductivity spectra were obtained by measuring the sample signal voltage as a function of the moving-mirror position and calculating the Fourier transform of the resulting interference histogram, or interferogram. Broadband radiation from the mercury arc lamp travels via reflectors to the beam splitter where parts of it are transmitted and reflected to the moving and fixed mirrors, respectively. The mirrors reflect the two light beams back to the beam splitter

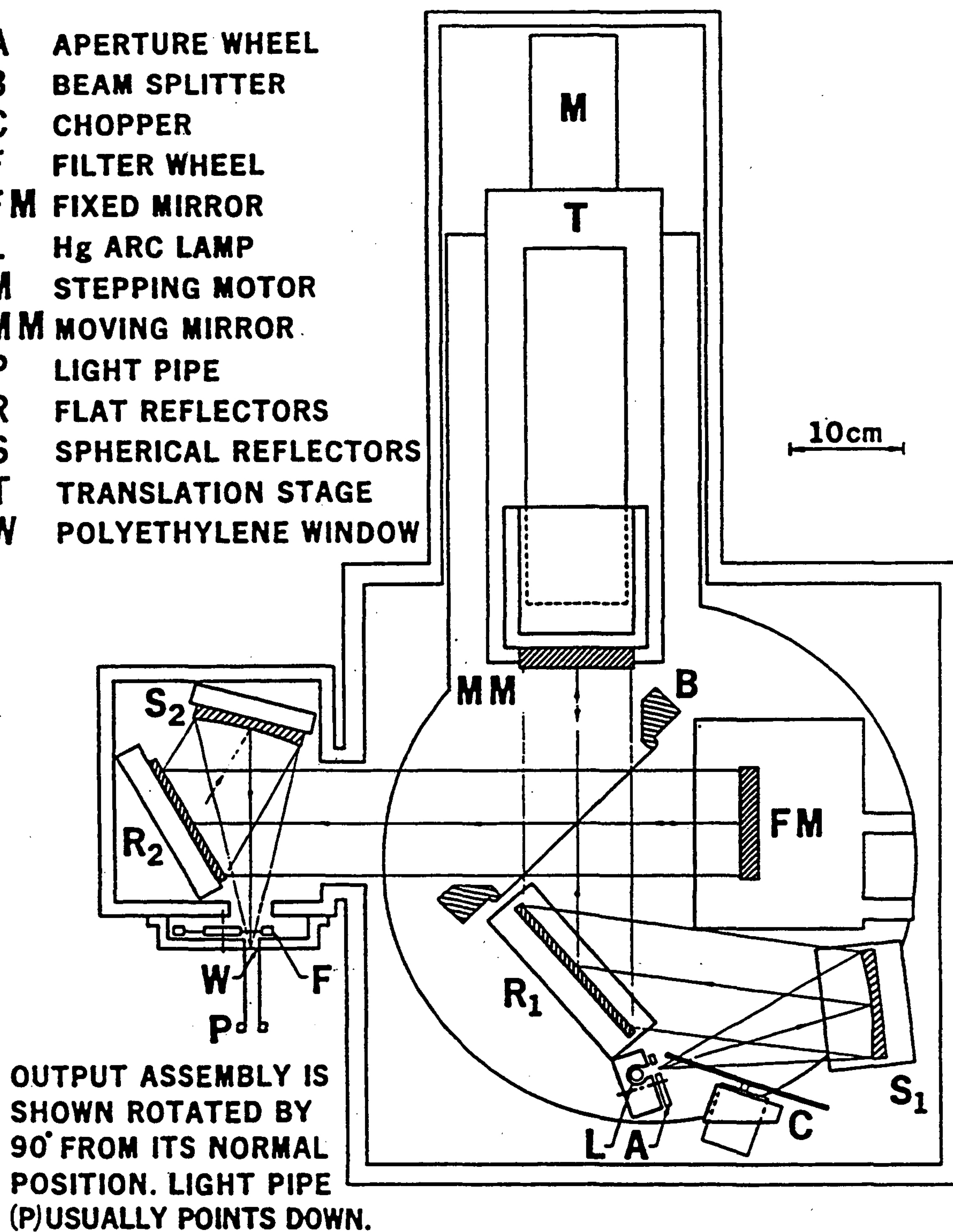

Figure B.2. Optical layout of the FIR Michelson interferometer used in for the studies of this thesis (schematic).

where they interfere with each other and travel to the sample that is optically connected to the output assembly.

The light arriving at the sample changes with the moving mirror position due to the difference in the optical path length which changes the interfered beam that is produced when the two beams recombine at the beam splitter. For each photon frequency of the broadband radiation, the intensity from the sum of the two beams varies with mirror position as $I_0(1+\cos(4\pi \Delta_{mp} x))$, where x is the frequency of light in wavenumber, and Δ_{mp} is the distance the moving mirror has traveled from its zero-path position (where the mirrors are equidistant from the beam splitter and the light intensity at the sample for all photon energies is maximum). The interferogram of a broadband source is then a sum of cosines, and a Fourier transform of it is a collection of delta functions, one for each light frequency. The interferogram obtained from a sample is therefore a sum of cosines associated with those frequencies of light that are absorbed, the Fourier transform revealing the frequencies contributing to the photocurrent in the sample. The spectral resolution is limited by the source size and solid angle and the distance that the moving mirror can travel. The spectral range is determined by the difference in the moving-mirror position between signal measurements. A detailed discussion of Fourier transform spectroscopy and its application has been presented by Bell.[111]

For the spectral response measurements performed on the Hall samples, the stressing coldfinger (including the sample) was placed in the HD3 dewar which was connected to the spectrometer output by a light-pipe/mirror arrangement. The rms signal output from the TIA (Fig. B.1) was measured with a lock-in amplifier and transferred to a computer for subsequent analysis. Pressure-dependent photoconductivity spectra of copper-doped germanium samples (Figure 4.4) were obtained using the liquid helium insert shown

schematically in Figure B.3. In this case the signal voltage was measured with a transconductance amplifier shown in Figure B.4. In this circuit the magnitude of the feedback resistor could be varied from 1 kOhm to 100 MOhm in order to match the sample impedance.

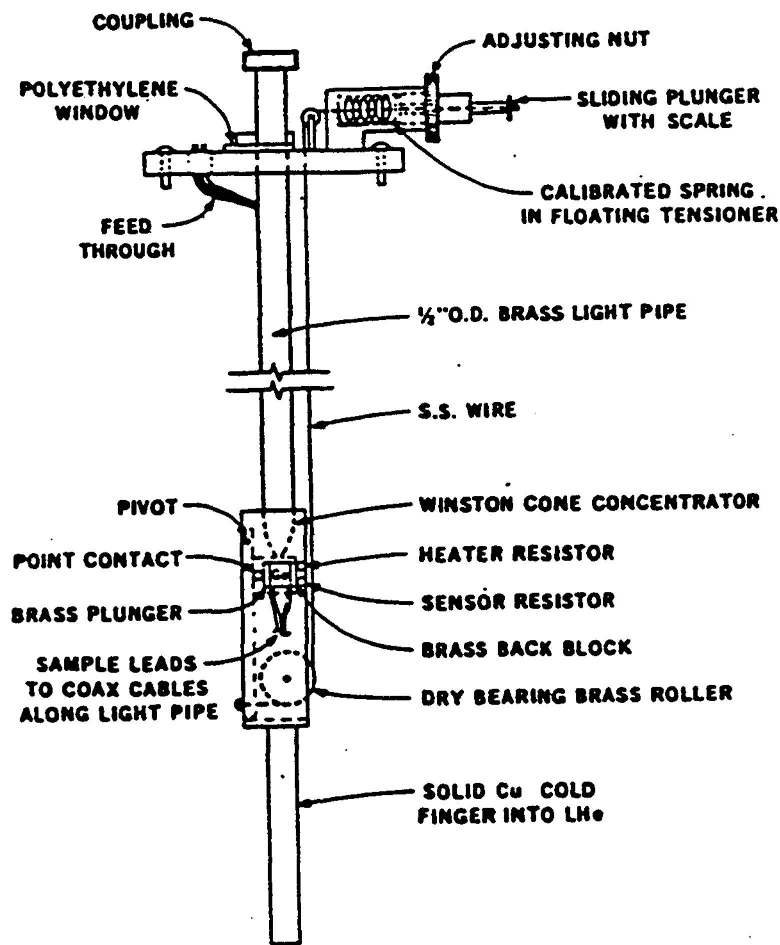

Figure B.3. Stress insert used for the photoconductivity spectroscopy measurements (schematic).

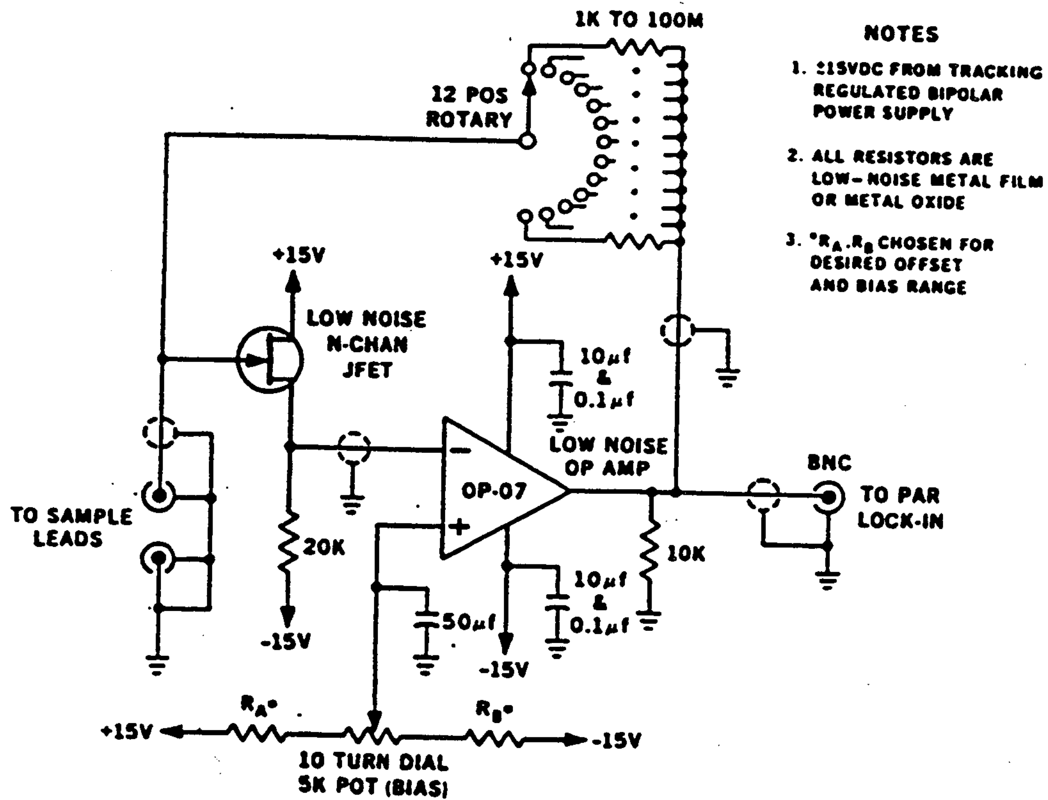

Figure B.4. Transconductance amplifier used with the stress insert in Figure B.3.

Appendix C: Effective mass approximation for Cu impurities in Ge

Because of the degeneracy of the top of the valence band, the triply charged acceptor in semiconductors should assume in the configuration $(1s)^3$, i.e., with occupation of the orbitals $(1s\,\Gamma_8)(1s\,\Gamma_8)(1s\,\Gamma_8)$. The total energy of this state at zero uniaxial stress, in the atomic units system, can be estimated to be[15]

$$E[(1s\,\Gamma_8)(1s\,\Gamma_8)(1s\,\Gamma_8)]=-8.62 \text{ a.u.} \tag{C.1}$$

When uniaxial stress is applied the valence band edge splits into two doubly degenerate bands Γ_7 and Γ_6. The Γ_6 band rises in energy by an amount Δ over the Γ_7 band and, neglecting pressure-induced corrections caused by the slightly varying Coulomb interaction between the electrons and the central-cell correction, the total energy is

$$E[(1s\,\Gamma_7)(1s\,\Gamma_7)(1s\,\Gamma_6), \Delta]=-8.62 \text{ a.u.}+\Delta \tag{C.2}$$

The first ionization potential for this state is obtained by subtracting the energy of the unbound state in which the free carrier is at the bottom of the Γ_7 band, i.e.,

$$E[(1s\,\Gamma_7)(1s\,\Gamma_7)(\text{free }\Gamma_7), \Delta]=E[(1s\,\Gamma_7)(1s\,\Gamma_7)], \tag{C.3}$$

which from Li spectra and from calculations yields

$$E[(1s\,\Gamma_7)(1s\,\Gamma_7)(\text{free }\Gamma_7), \Delta]=-7.29 \text{ a.u.} \tag{C.4}$$

Therefore, the ionization potential (IP) in this case is

$$\begin{aligned} &IP\ [(1s\,\Gamma_7)(1s\,\Gamma_7)(1s\,\Gamma_6), \Delta]= \\ &E[(1s\,\Gamma_7)(1s\,\Gamma_7)(\text{free }\Gamma_6), \Delta]-E[(1s\,\Gamma_7)(1s\,\Gamma_7)(1s\,\Gamma_6), \Delta]= \\ &-7.29 \text{ a.u.}+8.62 \text{ a.u.}-\Delta=1.33 \text{ a.u.}-\Delta. \end{aligned} \tag{C.5}$$

At high enough stresses there is a second state that may compete in energy. This is equivalent to the normal configuration of the Li atoms, i.e., $(1s\,\Gamma_7)(1s\,\Gamma_7)(2s\,\Gamma_7)$. The energy of this state can be easily estimated from the Li spectrum and is equal to the negative of the sum of three ionization potentials: those of Li^0, Li^+ and Li^{++}.[81]

$$E[(1s\,\Gamma_7)(1s\,\Gamma_7)(2s\,\Gamma_7), \Delta]=-[0.20+2.79+4.50] \text{ a.u.}=-7.49 \text{ a.u.} \qquad (C.6)$$

(Since all electrons are in the band Γ_6, there is no explicit dependence on the stress Δ). The ionization potential in this case is

$$IP\,[(1s\,\Gamma_7)(1s\,\Gamma_7)(2s\,\Gamma_7), \Delta]=$$
$$E[(1s\,\Gamma_7)(1s\,\Gamma_7)(\text{free}\,\Gamma_7), \Delta]-E[(1s\,\Gamma_7)(1s\,\Gamma_7)(2s\,\Gamma_7), \Delta]=$$
$$-7.29 \text{ a.u.} + 7.49 \text{ a.u.}=0.20 \text{ a.u.} \qquad (C.7)$$

The ground-state configuration is obtained by comparing the total energies (C.2) and (C.6). Thus, it is

$(1s\,\Gamma_7)(1s\,\Gamma_7)(1s\,\Gamma_6)$ for $\Delta<1.13$ a.u.

$(1s\,\Gamma_7)(1s\,\Gamma_7)(17s\,\Gamma_7)$ for $\Delta>1.13$ a.u.

Finally the ionization potentials to be observed are

$IP\,[(1s\,\Gamma_7)(1s\,\Gamma_7)(1s\,\Gamma_6), \Delta]=1.33 \text{ a.u.}-\Delta$ for $\Delta<1.13$ a.u.;

$IP\,[(1s\,\Gamma_7)(1s\,\Gamma_7)(12s\,\Gamma_7), \Delta]=0.20$ a.u. for $\Delta<1.13$ a.u.

C.1 Bound excited states

Neglecting central-cell corrections (which are definitely large) and details of the changing electron-electron interaction (which is probably small), the discrete lines or resonances to be observed are the following:

a) Optically active lines for $\Delta<1.13$ a.u.

From	To	Energy (a.u.)
$(1s\,\Gamma_7)(1s\,\Gamma_7)(1s\,\Gamma_6)$	$(1s\,\Gamma_7)(1s\,\Gamma_7)(2p\,\Gamma_6)$	
$(1s\,\Gamma_7)(1s\,\Gamma_7)(1s\,\Gamma_6)$	$(1s\,\Gamma_7)(2p\,\Gamma_7)(1s\,\Gamma_6)$	1.20
$(1s\,\Gamma_7)(1s\,\Gamma_7)(1s\,\Gamma_6)$	$(2p\,\Gamma_7)(1s\,\Gamma_7)(1s\,\Gamma_6)$	
$(1s\,\Gamma_7)(1s\,\Gamma_7)(1s\,\Gamma_6)$	$(1s\,\Gamma_7)(1s\,\Gamma_7)(3p\,\Gamma_6)$	
$(1s\,\Gamma_7)(1s\,\Gamma_7)(1s\,\Gamma_6)$	$(1s\,\Gamma_7)(3p\,\Gamma_7)(1s\,\Gamma_6)$	1.27
$(1s\,\Gamma_7)(1s\,\Gamma_7)(1s\,\Gamma_6)$	$(3p\,\Gamma_7)(1s\,\Gamma_7)(1s\,\Gamma_6)$	

$(1s\,\Gamma_7)(1s\,\Gamma_7)(1s\,\Gamma_6)$	$(1s\,\Gamma_7)(1s\,\Gamma_7)(4p\,\Gamma_6)$	
$(1s\,\Gamma_7)(1s\,\Gamma_7)(1s\,\Gamma_6)$	$(1s\,\Gamma_7)(4p\,\Gamma_7)(1s\,\Gamma_6)$	1.30
$(1s\,\Gamma_7)(1s\,\Gamma_7)(1s\,\Gamma_6)$	$(4p\,\Gamma_7)(1s\,\Gamma_7)(1s\,\Gamma_6)$	
$(1s\,\Gamma_7)(1s\,\Gamma_7)(1s\,\Gamma_6)$	$(1s\,\Gamma_7)(1s\,\Gamma_7)(5p\,\Gamma_6)$	
$(1s\,\Gamma_7)(1s\,\Gamma_7)(1s\,\Gamma_6)$	$(1s\,\Gamma_7)(5p\,\Gamma_7)(1s\,\Gamma_6)$	1.31
$(1s\,\Gamma_7)(1s\,\Gamma_7)(1s\,\Gamma_6)$	$(5p\,\Gamma_7)(1s\,\Gamma_7)(1s\,\Gamma_6)$	
$(1s\,\Gamma_7)(1s\,\Gamma_7)(1s\,\Gamma_6)$	$(1s\,\Gamma_7)(1s\,\Gamma_7)(6p\,\Gamma_6)$	
$(1s\,\Gamma_7)(1s\,\Gamma_7)(1s\,\Gamma_6)$	$(1s\,\Gamma_7)(6p\,\Gamma_7)(1s\,\Gamma_6)$	1.31
$(1s\,\Gamma_7)(1s\,\Gamma_7)(1s\,\Gamma_6)$	$(6p\,\Gamma_7)(1s\,\Gamma_7)(1s\,\Gamma_6)$	
$(1s\,\Gamma_7)(1s\,\Gamma_7)(1s\,\Gamma_6)$	$(1s\,\Gamma_7)(1s\,\Gamma_7)(7p\,\Gamma_6)$	
$(1s\,\Gamma_7)(1s\,\Gamma_7)(1s\,\Gamma_6)$	$(1s\,\Gamma_7)(7p\,\Gamma_7)(1s\,\Gamma_6)$	1.32
$(1s\,\Gamma_7)(1s\,\Gamma_7)(1s\,\Gamma_6)$	$(7p\,\Gamma_7)(1s\,\Gamma_7)(1s\,\Gamma_6)$	

(These lines are Fano resonances if their energy is larger than the ionization potential IP=1.33 a.u.-Δ.)

b) Optically active lines for Δ>1.13 a.u.:

From	To	Energy (a.u.)
$(1s\,\Gamma_7)(1s\,\Gamma_7)(2s\,\Gamma_7)$	$(1s\,\Gamma_7)(1s\,\Gamma_7)(2p\,\Gamma_7)$	0.07
$(1s\,\Gamma_7)(1s\,\Gamma_7)(2s\,\Gamma_7)$	$(1s\,\Gamma_7)(1s\,\Gamma_7)(3p\,\Gamma_7)$	0.14
$(1s\,\Gamma_7)(1s\,\Gamma_7)(2s\,\Gamma_7)$	$(1s\,\Gamma_7)(1s\,\Gamma_7)(4p\,\Gamma_7)$	0.17
$(1s\,\Gamma_7)(1s\,\Gamma_7)(2s\,\Gamma_7)$	$(1s\,\Gamma_7)(1s\,\Gamma_7)(5p\,\Gamma_7)$	0.18
$(1s\,\Gamma_7)(1s\,\Gamma_7)(2s\,\Gamma_7)$	$(1s\,\Gamma_7)(1s\,\Gamma_7)(6p\,\Gamma_7)$	0.18
$(1s\,\Gamma_7)(1s\,\Gamma_7)(2s\,\Gamma_7)$	$(1s\,\Gamma_7)(1s\,\Gamma_7)(7p\,\Gamma_7)$	0.19

Some of the lowest energy levels <u>not</u> reachable by optical dipole-active transitions for Δ<1.13 a.u.:

From	To	Energy
$(1s\,\Gamma_7)(1s\,\Gamma_7)(1s\,\Gamma_6)$	$(1s\,\Gamma_7)(1s\,\Gamma_7)(2s\,\Gamma_7)$	
$(1s\,\Gamma_7)(1s\,\Gamma_7)(1s\,\Gamma_6)$	$(1s\,\Gamma_7)(2s\,\Gamma_7)(1s\,\Gamma_7)$	1.13 a.u.-Δ
$(1s\,\Gamma_7)(1s\,\Gamma_7)(1s\,\Gamma_6)$	$(2s\,\Gamma_7)(1s\,\Gamma_7)(1s\,\Gamma_7)$	

$(1s\,\Gamma_7)(1s\,\Gamma_7)(1s\,\Gamma_6)$	$(1s\,\Gamma_7)(1s\,\Gamma_7)(2s\,\Gamma_6)$	
$(1s\,\Gamma_7)(1s\,\Gamma_7)(1s\,\Gamma_6)$	$(1s\,\Gamma_7)(2s\,\Gamma_7)(1s\,\Gamma_6)$	1.13 a.u.
$(1s\,\Gamma_7)(1s\,\Gamma_7)(1s\,\Gamma_6)$	$(2s\,\Gamma_7)(1s\,\Gamma_7)(1s\,\Gamma_6)$	

etc.

Some of the lowest energy levels not reachable by optical dipole-active transitions for Δ>1.13 a.u.:

From	To	Energy
$(1s\,\Gamma_7)(1s\,\Gamma_7)(2s\,\Gamma_7)$	$(1s\,\Gamma_7)(1s\,\Gamma_7)(1s\,\Gamma_6)$	Δ-1.13 a.u.
$(1s\,\Gamma_7)(1s\,\Gamma_7)(2s\,\Gamma_7)$	$(1s\,\Gamma_7)(1s\,\Gamma_7)(3s\,\Gamma_7)$	0.124 a.u.
$(1s\,\Gamma_7)(1s\,\Gamma_7)(2s\,\Gamma_7)$	$(1s\,\Gamma_7)(1s\,\Gamma_7)(2s\,\Gamma_6)$	Δ

etc.

C.2 Central cell correction added

The effective mass approximation in Ge corresponds to an energy scale 1 a.u.=22.4 meV and to a length scale 1 a.u.=4.07 nm=76.9 Bohr radii, and applies to all impurities. This would give for the ground state of unstressed Cu impurities, according to the previous calculation by Wu and Falicov

$$\mathrm{IP}\,[(1s\,\Gamma_8)(1s\,\Gamma_8)(1s\,\Gamma_8)]=1.33\text{ a.u.}=29.8\text{ meV}.$$

The experimental values is 43.2 meV. In other words, the central cell correction is 13.4 meV.

According to the three-exponential approximation (exponents a_1=3.540, a_2=2.086, and a_3=1.486) the value of the central-cell correction for the total energy is

$$W_{ccc}[(1s)^3]=(U/\pi)\,\Sigma(a_i)^3$$

where the a_i are the three exponents. Equivalently the central cell correction for the ionized state is

$$W_{ccc}[(1s)^2]=(U/\pi)\,\Sigma(a_i')^3$$

The experimental value of the ionization potential and the calculated exponents (Wu and Falicov[15]) yields U=0.156 a.u. (energy per length to the third power). A rough calculation for the (1s Γ_7)(1s Γ_7)(2s Γ_7) configuration (simple Hartree approximation), with the (2s Γ_7) envelope function of the form

$$u(r, b, 2s)=(b^3/\pi)^{1/2}(1-br)\exp(-br)$$

yields $a_1=a_2=2.68$ a.u. and b=0.68 a.u. The central cell correction is therefore

$$W_{ccc}[(1s)^2(2s)]=(U/\pi)\{(a_1)^3+(a_2)^3+(b)^3\}.$$

The equivalent approximation for (1s Γ_7)(1s Γ_7)(1s Γ_6) [from Wu and Falicov] is $a_1=a_2=a_3=2.375$ a.u.

With this scaling and since the final state is the same in both cases, one obtains for the correction to the ionization potential caused by the central cell correction

$$\delta[IP]_{ccc}[(1s)^2(2s)]=13.4 \text{ meV } (38.6/40.2)=12.9 \text{ meV}.$$

With these values, and assuming no central cell correction for orbitals other than the (1s) and the (2s), one obtains

$$IP\ [(1s\,\Gamma_7)(1s\,\Gamma_7)(1s\,\Gamma_6),\ \Delta]=43.2 \text{ meV}+\Delta;$$

$$IP[(1s\,\Gamma_7)(1s\,\Gamma_7)(2s\,\Gamma_7),\ \Delta]=17.4 \text{ meV}.$$

The other values are

$$E[(1s\,\Gamma_7)(1s\,\Gamma_7)(1s\,\Gamma_6),\ \Delta]=-5.77 \text{ a.u.}+\Delta=-129.2 \text{ meV}+\Delta;$$

$$E[(1s\,\Gamma_7)(1s\,\Gamma_7)(2s\,\Gamma_7),\ \Delta]=-4.62 \text{ a.u.}+\Delta=-103.4 \text{ meV}.$$

The cross over energy is at $\Delta_{cross\ over}=1.15$ a.u.=25.8 meV.

The optical spectrum is now the following:

a) Optically active lines for $\Delta<25.8$ meV

From	To	Energy(meV)
(1s Γ_7)(1s Γ_7)(1s Γ_6)	(1s Γ_7)(1s Γ_7)(2p Γ_6)	
(1s Γ_7)(1s Γ_7)(1s Γ_6)	(1s Γ_7)(2p Γ_7)(1s Γ_6)	40.3
(1s Γ_7)(1s Γ_7)(1s Γ_6)	(2p Γ_7)(1s Γ_7)(1s Γ_6)	

$(1s\,\Gamma_7)(1s\,\Gamma_7)(1s\,\Gamma_6)$	$(1s\,\Gamma_7)(1s\,\Gamma_7)(3p\,\Gamma_6)$	
$(1s\,\Gamma_7)(1s\,\Gamma_7)(1s\,\Gamma_6)$	$(1s\,\Gamma_7)(3p\,\Gamma_7)(1s\,\Gamma_6)$	41.9
$(1s\,\Gamma_7)(1s\,\Gamma_7)(1s\,\Gamma_6)$	$(3p\,\Gamma_7)(1s\,\Gamma_7)(1s\,\Gamma_6)$	
$(1s\,\Gamma_7)(1s\,\Gamma_7)(1s\,\Gamma_6)$	$(1s\,\Gamma_7)(1s\,\Gamma_7)(4p\,\Gamma_6)$	
$(1s\,\Gamma_7)(1s\,\Gamma_7)(1s\,\Gamma_6)$	$(1s\,\Gamma_7)(4p\,\Gamma_7)(1s\,\Gamma_6)$	42.6
$(1s\,\Gamma_7)(1s\,\Gamma_7)(1s\,\Gamma_6)$	$(4p\,\Gamma_7)(1s\,\Gamma_7)(1s\,\Gamma_6)$	
$(1s\,\Gamma_7)(1s\,\Gamma_7)(1s\,\Gamma_6)$	$(1s\,\Gamma_7)(1s\,\Gamma_7)(5p\,\Gamma_6)$	
$(1s\,\Gamma_7)(1s\,\Gamma_7)(1s\,\Gamma_6)$	$(1s\,\Gamma_7)(5p\,\Gamma_7)(1s\,\Gamma_6)$	43.0
$(1s\,\Gamma_7)(1s\,\Gamma_7)(1s\,\Gamma_6)$	$(5p\,\Gamma_7)(1s\,\Gamma_7)(1s\,\Gamma_6)$	
$(1s\,\Gamma_7)(1s\,\Gamma_7)(1s\,\Gamma_6)$	$(1s\,\Gamma_7)(1s\,\Gamma_7)(6p\,\Gamma_6)$	
$(1s\,\Gamma_7)(1s\,\Gamma_7)(1s\,\Gamma_6)$	$(1s\,\Gamma_7)(6p\,\Gamma_7)(1s\,\Gamma_6)$	43.0
$(1s\,\Gamma_7)(1s\,\Gamma_7)(1s\,\Gamma_6)$	$(6p\,\Gamma_7)(1s\,\Gamma_7)(1s\,\Gamma_6)$	
$(1s\,\Gamma_7)(1s\,\Gamma_7)(1s\,\Gamma_6)$	$(1s\,\Gamma_7)(1s\,\Gamma_7)(7p\,\Gamma_6)$	
$(1s\,\Gamma_7)(1s\,\Gamma_7)(1s\,\Gamma_6)$	$(1s\,\Gamma_7)(7p\,\Gamma_7)(1s\,\Gamma_6)$	43.2
$(1s\,\Gamma_7)(1s\,\Gamma_7)(1s\,\Gamma_6)$	$(7p\,\Gamma_7)(1s\,\Gamma_7)(1s\,\Gamma_6)$	

(These lines are Fano resonances if their energy is larger than the ionization potential IP=43.2 meV-Δ.)

b) Optically active lines for Δ>1.13 a.u.:

From	To	Energy(meV)
$(1s\,\Gamma_7)(1s\,\Gamma_7)(2s\,\Gamma_7)$	$(1s\,\Gamma_7)(1s\,\Gamma_7)(2p\,\Gamma_7)$	14.5
$(1s\,\Gamma_7)(1s\,\Gamma_7)(2s\,\Gamma_7)$	$(1s\,\Gamma_7)(1s\,\Gamma_7)(3p\,\Gamma_7)$	16.1
$(1s\,\Gamma_7)(1s\,\Gamma_7)(2s\,\Gamma_7)$	$(1s\,\Gamma_7)(1s\,\Gamma_7)(4p\,\Gamma_7)$	16.8
$(1s\,\Gamma_7)(1s\,\Gamma_7)(2s\,\Gamma_7)$	$(1s\,\Gamma_7)(1s\,\Gamma_7)(5p\,\Gamma_7)$	17.2
$(1s\,\Gamma_7)(1s\,\Gamma_7)(2s\,\Gamma_7)$	$(1s\,\Gamma_7)(1s\,\Gamma_7)(6p\,\Gamma_7)$	17.2
$(1s\,\Gamma_7)(1s\,\Gamma_7)(2s\,\Gamma_7)$	$(1s\,\Gamma_7)(1s\,\Gamma_7)(7p\,\Gamma_7)$	17.4

Some of the lowest energy levels <u>not</u> reachable by optical dipole-active transitions for Δ<1.13 a.u.:

From	To	Energy(meV)
$(1s\,\Gamma_7)(1s\,\Gamma_7)(1s\,\Gamma_6)$	$(1s\,\Gamma_7)(1s\,\Gamma_7)(2s\,\Gamma_7)$	
$(1s\,\Gamma_7)(1s\,\Gamma_7)(1s\,\Gamma_6)$	$(1s\,\Gamma_7)(2s\,\Gamma_7)(1s\,\Gamma_7)$	25.8-Δ
$(1s\,\Gamma_7)(1s\,\Gamma_7)(1s\,\Gamma_6)$	$(2s\,\Gamma_7)(1s\,\Gamma_7)(1s\,\Gamma_7)$	

$(1s\,\Gamma_7)(1s\,\Gamma_7)(1s\,\Gamma_6)$	$(1s\,\Gamma_7)(1s\,\Gamma_7)(2s\,\Gamma_6)$	
$(1s\,\Gamma_7)(1s\,\Gamma_7)(1s\,\Gamma_6)$	$(1s\,\Gamma_7)(2s\,\Gamma_7)(1s\,\Gamma_6)$	25.8
$(1s\,\Gamma_7)(1s\,\Gamma_7)(1s\,\Gamma_6)$	$(2s\,\Gamma_7)(1s\,\Gamma_7)(1s\,\Gamma_6)$	

etc.

Some of the lowest energy levels <u>not</u> reachable by optical dipole-active transitions for $\Delta>1.13$ a.u.:

From	To	Energy(meV)
$(1s\,\Gamma_7)(1s\,\Gamma_7)(2s\,\Gamma_7)$	$(1s\,\Gamma_7)(1s\,\Gamma_7)(1s\,\Gamma_6)$	Δ-25.8
$(1s\,\Gamma_7)(1s\,\Gamma_7)(2s\,\Gamma_7)$	$(1s\,\Gamma_7)(1s\,\Gamma_7)(2s\,\Gamma_6)$	Δ
$(1s\,\Gamma_7)(1s\,\Gamma_7)(2s\,\Gamma_7)$	$(1s\,\Gamma_7)(1s\,\Gamma_7)(3s\,\Gamma_6)$	2.8

If the $(3s\,\Gamma_7)$ orbital has the same central-cell correction as the $(2s\,\Gamma_7)$ orbital; or

$(1s\,\Gamma_7)(1s\,\Gamma_7)(2s\,\Gamma_7)$	$(1s\,\Gamma_7)(1s\,\Gamma_7)(3s\,\Gamma_6)$	15.7

If the $(3s\,\Gamma_7)$ has exactly zero central-cell correction; or probably a value in between.

etc.

C.3 Ge band-structure corrections

Salib *et al.*[56] showed that for the optical lines in the ordinary Cu triple acceptor in Ge, "the spacings of the excited states of copper and those of the single-hole acceptors are the same" and that "the effective-mass formalism is an adequate description of their excited states of the triple-hole system." They report for the $(1s\,\Gamma_8)(1s\,\Gamma_8)(1s\,\Gamma_8)$ configuration the following lines:

Line	Energy (meV)
G	38.67
D	40.37
C	41.12
B	41.76
A"	42.07
A'	42.27

In that case the same criterion should apply to the $(1s\,\Gamma_7)(1s\,\Gamma_7)(2s\,\Gamma_7)$ configuration in the high-stress regime with the values:

Line	Energy (meV)
G	12.9
D	14.6
C	15.3
B	16.0
A"	16.3
A'	16.5

These lines should be observable, but so far they have not been found experimentally.

8. References

1. W. J. Moore, H. Shenker, *Infrared Phys.* **5**, 99 (1965).

2. H. Shenker, E. M. Swiggard, W. J. Moore, *Trans. Met. Soc. AIME* **239**, 347 (1967).

3. P. R. Bratt, in *Semiconductors and Semimetals* R. K. Willardson, A. C. Beer, Eds. (Academic Press, New York, 1977), vol. 12, pp. 39.

4. E. E. Haller, *Infrared Phys.* **25**, 257 (1985).

5. A. G. Kazanskii, P. L. Richards, E. E. Haller, *Appl. Phys. Lett.* **31**, 496 (1977).

6. E. E. Haller, M. R. Hueschen, P. L. Richards, *Appl. Phys. Lett.* **34**, 495 (1979).

7. G. E. Pikus, G. L. Bir, *Sov. Phys.—Solid State* **1**, 1502 (1959).

8. G. L. Bir, G. E. Pikus, *Symmetry and Strain-Induced Effects in Semiconductors* (John Wiley & Sons, New York, 1974).

9. J. J. Hall, *Phys. Rev.* **128**, 68 (1962).

10. P. J. Price, *Phys. Rev.* **124**, 713 (1961).

11. J.-Q. Wang, P. L. Richards, J. W. Beeman, N. M. Haegel, E. E. Haller, *Appl. Opt.* **25**, 4127 (1986).

12. S. T. Pantelides, *Rev. Mod. Phys.* **50**, 797 (1978).

13. A. K. Ramdas, S. Rodriguez, *Rep. Prog. Phys.* **44**, 1297 (1981).

14. E. E. Haller, R. E. McMurray, Jr., L. M. Falicov, N. M. Haegel, W. L. Hansen, *Phys. Rev. Lett.* **51**, 1089 (1983).

15. Y. Wu, L. M. Falicov, *Phys. Rev. B* **29**, 3671 (1984).

16. Y. Ohmura, *Solid State Comm.* **79**, 1029 (1991).

17. J. S. Blakemore, *Solid State Physics* (Cambridge University Press, Cambridge, 1985).

18. F. J. Morin, J. P. Maita, *Phys. Rev.* **96**, 28 (1954).

19. K. Seeger, *Semiconductor Physics* (Springer-Verlag, Berlin, 1991).

20. K. M. Itoh, et al., *Phys. Rev. B* **50**, 16995 (1994).

21. V. V. Akulinichev, *Sov. Phys.-Semicond.* **16**, 159 (1982).

22. N. M. Haegel, M. R. Hueschen, E. E. Haller, *Infrared Phys.* **25**, 273 (1985).

23. N. M. Haegel, E. E. Haller, P. N. Luke, *Int. J. Infrared and Mil. Waves* **4**, 945 (1983).

24. W. L. Hansen, E. E. Haller, *Mater. Res. Symp. Proc.* **16**, 1 (1983).

25. W. L. Eisenman , J. D. Merriam, R. F. Potter, in *Semiconductors and Semimetals* R. K. Willardson, A. C. Beer, Eds. (Academic Press, New York, 1977), vol. 12, pp. 1.

26. J. D. Vincent, *Fundamentals of Infrared Detector Operation and Testing* (John Wiley &Sons, New York, 1989).

27. D. H. Dickey, J. O. Dimmok, *J. Phys. Chem. Solids* **28**, 529 (1967).

28. R. Buckzko, J. A. Chroboczek, *Phil. Mag. B* **50**, 429 (1984).

29. R. Buczko, *Il Nuovo Cimento* **9**, 669 (1987).

30. J. Broeckx, J. Vennik, *Phys. Rev. B* **12**, 6165 (1987).

31. A. K. Ramdas, S. Rodriguez, in *Progress on Electron Properties of Solids* R. Girlanda, Eds. (Kluwer Academic Publishers, 1989) pp. 65.

32. A. G. Kazanskii, P. L. Richards, E. E. Haller, *Solid State Comm.* **24**, 603 (1977).

33. M. Lax, *Phys. Rev.* **119**, 1502 (1960).

34. A. M. Stoneham, *Theory of Defects in Solids* (Oxford University Press, Oxford, 1975).

35. V. N. Abakumov, V. I. Perel', I. N. Yassievich, *Sov. Phys.—Semicond.* **12**, 1 (1978).

36. V. N. Abakumov, V. I. Perel', I. N. Yassievich, *Nonradiative Recombination in Semiconductors* (North-Holland, Amsterdam, 1991).

37. L. S. Darken, G. E. Jellison Jr., *Appl. Phys. Lett.* **55**, 1424 (1989).

38. L. S. Darken, P. Sangsingkeow, G. E. Jellison, *J. Electron. Mater.* **19**, 105 (1990).

39. L. S. Darken, *Phys. Rev. Lett.* **69**, 2839 (1992).

40. L. S. Darken, C. E. Cox, High-purity germanium technology for gamma-ray and X-ray spectroscopy, R. B. James, T. E. Schlesinger, P. Sifffers, L. Frankss, Eds., Semiconductors for Room-Temperature Radiation Detector Applications Symposium (Mater. Res. Soc., San Francisco, 1993), pp. 31.

41. K. Geim, G. Pensl, M. Schulz, *Appl. Phys. A* **27**, 71 (1982).

42. J. S. Blakemore, *Semiconductor Statistics* (Dover, New York, 1987).

43. V. A. Besfamil'naya, V. V. Ostroborodova, *Sov. Phys.-Solid State* **6**, 3015 (1964).

44. V. A. Besfamil'naya, V. V. Ostroborodova, L. M. Shlita, *Sov. Phys.—Semicond.* **2**, 888 (1969).

45. V. A. Besfamil'naya, V. V. Ostroborodova, *Sov. Phys.-Semicond.* **3**, 15 (1969).

46. J. W. Cross, L. T. Ho, A. K. Ramdas, R. Sauer, E. E. Haller, *Phys. Rev. B* **28**, 6953 (1983).

47. D. Labrie, I. J. Booth, M. L. W. Thewalt, E. E. Haller, *Phys. Rev. B* **38**, 5504 (1988).

48. J. W. Cross, C. R. LaBrec, S. Rodriguez, A. K. Ramdas, E. E. Haller, *Phys. Rev. B* **32**, 7992 (1985).

49. E. I. Gershenzon, G. N. Gol'tsman, A. P. Mel'nikov, *JETP Lett.* **14**, 185 (1971).

50. R. E. McMurray, Jr., Ph.D., University of California, Berkeley (1984).

51. N. M. Haegel, J. W. Beeman, P. N. Luke, E. E. Haller, *Phys. Rev. B* **39**, 3677 (1989).

52. R. E. McMurray Jr., *Solid State Comm.* **53**, 1127 (1985).

53. N. M. Haegel, E. E. Haller, *Infrared Phys.* **26**, 247 (1986).

54. N. M. Haegel, Ph.D., University of California, Berkeley (1985).

55. R. J. Collins, H. Y. Fan, *Phys. Rev.* **93**, 674 (1954).

56. E. H. Salib, P. Fisher, P. E. Simmonds, *Phys. Rev. B* **32**, 2424 (1985).

57. N. M. Haegel, M. S., University of California, Berkeley (1983).

58. N. M. Haegel, E. E. Haller, *SPIE* **659**, 188 (1986).

59. T. A. Germer, N. M. Haegel, E. E. Haller, *J. Appl. Phys.* **60**, 1055 (1986).

60. R. E. McMurray, Jr., N. M. Haegel, J. M. Kahn, E. E. Haller, *Solid State Comm.* **61**, 27 (1987).

61. R. N. Hall, J. H. Racette, *J. Appl. Phys.* **35**, 379 (1964).

62. E. E. Godik, Y. A. Kuritsyn, V. P. Sinis, *Sov. Phys.-Semicond.* **8**, 1373 (1975).

63. P. Norton, *J. Appl. Phys.* **47**, 308 (1976).

64. T. Sanada, K. Matsushita, T. Ohyama, E. Otsuka, *J. Phys. Soc. Japan* **45**, 501 (1978).

65. E. E. Haller, R. E. McMurray, Jr., N. M. Haegel, L. M. Falicov, Positively charged acceptors with (1s)3 and (1s)4 configurations, J. D. Chadi, W. A. Harrisons, Eds., Proc. 17th Int. Conf. Phys. Semicond. (Springer-Verlag, 1984), pp. 679.

66. E. R. Weber, *Appl. Phys.* **A30**, 1 (1983).

67. A. Fazzio, M. J. Caldas, A. Zunger, *Phys. Rev. B* **32**, 934 (1985).

68. J. M. Kahn, L. M. Falicov, E. E. Haller, *Phys. Rev. Lett.* **57**, 2077 (1986).

69. J. M. Kahn, R. E. McMurray, E. E. Haller, L. M. Falicov, *Phys. Rev. B* **36**, 8001 (1987).

70. G. Sirmain, O. D. Dubon, W. L. Hansen, C. S. Olsen, E. E. Haller, *J. Appl. Phys.* **79**, 209 (1996).

71. H. H. Woodbury, W. W. Tyler, *Phys. Rev.* **105**, 84 (1957).

72. N. A. Stolwijk, W. Frank, J. Hölzl, S. J. Pearton, E. E. Haller, *J. Appl. Phys.* **57**, 5211 (1985).

73. E. E. Haller, W. L. Hansen, F. S. Goulding, *Advan. Phys.* **30**, 93 (1981).

74. E. E. Haller, F. S. Goulding, in *Handbook on Semiconductors* C. Hilsum, Eds. (North-Holland, Amsterdam, 1993), vol. 41, pp. 939.

75. J. I. Pankove, N. M. Johnson, Eds., *Semiconductors and Semimetals* , vol. 34 (Academic, San Diego, 1991).

76. F. C. Frank, D. Turnbull, *Phys. Rev.* **104**, 617 (1956).

77. J. W. Beeman and E. E. Haller, unpublished.

78. E. H. Salib, K. J. Duff, *Phys. Rev. B* **33**, 1275 (1986).

79. V. A. Karasyuk, E. C. Lightowlers, *Mater. Sci. Forum* **65-66**, 211 (1990).

80. V. A. Karasyuk, E. C. Lightowlers, *Phys. Rev. B* **45**, 3319 (1992).

81. C. E. Moore, *Atomic Energy Levels*, Natl. Bur. Stand. (U. S.) Circular No. 467 (U. S. GPO, Washington D. C., 1949), Vol. I, pp. 8, 10, and 11.

82. I. Balslev, *Solid State Comm.* **5**, 315 (1967).

83. M. E. Fine, *J. Appl. Phys.* **26**, 862 (1955).

84. H. Fritzsche, *J. Phys. Chem. Solids* **6**, 69 (1958).

85. H. Kamimura, H. Aoki, *The Physics of Interacting Electrons in Disordered Systems* (Clarendon Press, Oxford, 1989).

86. H. Fritzsche, M. Cuevas, *Phys. Rev.* **119**, 1238 (1960).

87. B. I. Shklovskii, *Sov. Phys.-Semicond.* **6**, 1053 (1973).

88. B. I. Shklovskii, A. L. Efros, *Electronic Properties of Doped Semiconductors* (Springer-Verlag, Berlin, 1984).

89. S. N. Mott, *Metal-Insulator Transitions* (Taylor & Francis Ltd., London, 1974).

90. J.-Q. Wang, P. L. Richards, J. W. Beeman, *Appl. Opt.* **26**, 4767 (1987).

91. B. K. Ridley, *Quantum Processes in Semiconductors* (Clarendon Press, Oxford, 1988).

92. B. V. Rollin, J. P. Russell, *Proc. Phys. Soc.* **81**, 571 (1963).

93. N. F. Mott, *Proc. Phys. Soc.* **A 62**, 416 (1949).

94. J. Hubbard, *Proc. Roy. Soc. A* **281**, 401 (1964).

95. N. F. Mott, *Conduction in Non-Crystalline Materials* (Clarendon Press, Oxford, 1993).

96. P. P. Edwards, M. J. Sienko, *Phys. Rev. B* **17**, 2575 (1978).

97. N. F. Mott, M. Kaveh, *Advan. Phys.* **34**, 329 (1985).

98. P. W. Anderson, *Phys. Rev.* **109**, 1492 (1958).

99. N. A. Mora, S. Bermon, F. H. Pollack, *Phys. Rev. Lett.* **28**, 225 (1972).

100. J. C. Slater, *Quantum Theory of Atomic Structure, Volume I* (McGraw-Hill Book Company, Inc., New York, 1960).

101. L. Pfeiffer, K. W. West, H. L. Störmer, K. W. Baldwin, *Appl. Phys. Lett.* **55**, 1888 (1989).

102. T. Saku, Y. Kirayama, Y. Horikoshi, *Jap. J. Appl. Phys.* **30**, 902 (1991).

103. E. H. Putley, *The Hall Effect and Related Phenomena* (Butterworths, London, 1960).

104. A. C. Beer, in *The Hall Effect and its Applications* C. L. Chien, C. R. Westgate, Eds. (Plenum Press, New York, 1980) pp. 299.

105. E. H. Hall, *Amer. J. Maths.* **2**, 287 (1879).

106. A. C. Beer, R. K. Willardson, *Phys. Rev.* **110**, 1286 (1958).

107. L. J. van der Pauw, *Philips Res. Rep.* **13**, 1 (1958).

108. H. Weinstock, J. Parpia, in *Temperature, Its Measurement and Control in Science and Industry* H. H. Plumb, Eds. (Instrument Society of America, Pittsburgh, 1971), vol. 4, pp. 785.

109. W. E. Lamb, Jr., *Phys. Rev.* **70**, 308 (1946).

110. J. M. Kahn, Ph.D., University of California, Berkeley (1986).

111. R. J. Bell, *Introductory Fourier Transform Spectroscopy* (Academic Press, New York, 1972).

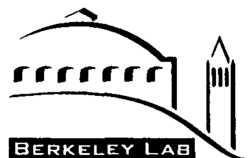

ERNEST ORLANDO LAWRENCE BERKELEY NATIONAL LABORATORY
TECHNICAL AND ELECTRONIC INFORMATION DEPARTMENT
UNIVERSITY OF CALIFORNIA | BERKELEY, CALIFORNIA 94720